Upconversion and Anti-Stokes Processes with f and d Ions in Solids

François Auzel

GOTR, UMR 7574-CNRS, 1, Place A-Briand, 92195 Meudon Cedex, France

Received February 25, 2003

Contents

1. Introduction and Historical Background

Before the 1960s, all anti-Stokes emissions, which were known to exist, involved emission energies in excess of excitation energies by only a few kT. They were linked to thermal population of energy states above excitation states by such an energy amount. It was the well-known case of anti-Stokes emission for the so-called thermal bands or in the Raman effect for the well-known anti-Stokes sidebands. Thermoluminescence, where traps are emptied by excitation energies of the order of kT, also constituted a field of anti-Stokes emission of its own. Superexcitation, i.e., raising an already excited electron to an even higher level by excited-state absorption (ESA), was also known but with very weak emissions. These types of well-known anti-Stokes processes have been reviewed in classical textbooks on luminescence.[1]

All fluorescence light emitters usually follow the well-known principle of the Stokes law which simply states that excitation photons are at a higher energy than emitted ones or, in other words, that output photon energy is weaker than input photon energy. This, in a sense, is an indirect statement that efficiency cannot be larger than 1. This principle is

10.1021/cr020357g CCC: $48.50
Published on Web 11/18/2003

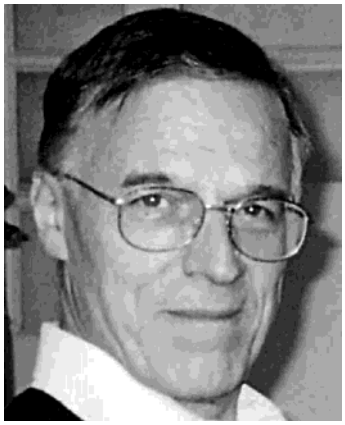

Francois Auzel, born July 5, 1938 in Roanne (France), graduated as both an engineer from ISEP (Institut Supereur d'Electronique de Paris) in 1961 and a "Licencié-es Sciences Physique" in 1962 from the University of Paris. He was with France-Telecom Research Center (CNET) from 1961 to 1999. There, in 1961, he started working on Nd-doped phosphate glasses. In 1968, he received his Ph.D. degree from the University of Paris on "Erbium doped glasses for laser" under the guidance of Professor Otto Deutschbein and with Professor Alfred Kastler as adviser; as an outcome of this work, he proposed rare-earth-doped fluorophosphate glasses as laser materials with weak OH interactions. During his thesis work he demonstrated the possibility of upgoing sequential energy transfers (ETU) giving rise to upconversion of infrared to visible light, using Yb–Er (green emission) and Yb–Tm (blue emission) couples. In 1973, he received the Foucault prize from the "Societé Française de Physique" for his discovery of upconversion processes by energy transfers (APTE effect)(1965–1966). In 1989, the French Academy of Science granted him the "Prix Winter-Klein" for his pioneer work on the spectroscopy of erbium-doped glasses (1965–1968). Other advances have been the experimental demonstration of the existence of Stokes and anti-Stokes multiphonon sidebands for trivalent lanthanides (1976), the proposal of a scalar crystal field parameter proportional to the maximum splitting of a *J* term (1979), the first observation of superradiance emission of a lanthanide (Er ions at 2.7 μm at 10 K in weakly doped YLF crystals) (1986), the room-temperature avalanche effect of Er-doped glasses and crystals (1993), and the saturation effect of multiphonon decays in glasses (1996). He has been a part-time Professor at Ecole Centrale des Arts et Manufactures (1971–99) and at Orsay University (DEA Ecole Polytechnique-Lab. Aime Cotton) (1990–99). He created and headed the "Groupe d'Optique des Terres Rares", a team belonging to both CNRS and CNET, until his retirement from CNET in 1999. He is currently a voluntary researcher at CNRS and a consultant for active optical materials.

valid, of course, only when one excited ion system is considered.

In this review we will discuss anti-Stokes emissions or upconversion processes for which emission is found to exceed excitation energies by 10−100 times kT, which is violating Stokes law in its basic statement.

It will be shown that coupled lanthanide and uranide f ions and transition-metal d ions, when embedded in solids, may deviate rather easily from the above principle, producing upconversion emissions of the anti-Stokes types under moderate to strong excitation density.

A number of different mechanisms have been recognized to be involved in upconversion either alone or in combination.

Besides multistep excitation due to classical excited-state absorption (ESA), there is the very efficient process of upconversion by sequential energy transfers which has been named by Auzel APTE effect (for addition de photon par transferts d'energie;[2] this effect was also later termed ETU for energy transfer upconversion.[3] This last phenomenon has to be distinguished from a third process, namely, cooperative upconversion either between two ions or between a pair of ions and a third one. Though some aspects of its theoretical behavior are rather analogous with upconversion by energy transfers, its efficiency is usually much weaker. This is because it involves quasi-virtual pair levels between which transitions have to be described in a higher order of perturbation due to their double-operator nature.

A fourth process will also be considered: the photon avalanche effect, also based on sequential energy transfers but of the downconversion type (usually called cross-relaxation), whereas the upconversion step itself is due to ESA.

The various experimental techniques, which allow distinctions between the behaviors of these various processes, will be analyzed taking examples from the literature.

With the advent of high energy density laser sources, these processes have been observed in various types of ion-doped solids such as crystals and glasses in bulk, fiber, or waveguide form; the recent advances will be encompassed and described thereafter.

The whole field of upconversion in ion-doped systems can be traced back to an idea of Bloembergen in 1959,[4] proposing that infrared (IR) photons could be detected and counted through sequential absorption (ESA) within the levels of a given ion in a solid, that is using superexcitation as a detector. This was a short proposal for a detector called an infrared quantum counter (IRQC). In fact, because there was little chance with incoherent pumping that the same single doping ion would receive two photons in sequence at its given position during the first excited-state lifetime, the experimental demonstration of this effect had to wait for laser excitations and fiber local confinement. Some of the first experiments[5] have been proved later to be due to energy diffusion through energy transfers between identical ions.[6]

The role of energy transfers in upconversion processes was not recognized until 1966, when it was suggested by Auzel that energy transfers between RE ions could take place between two ions, both of them being in an excited state at the energy transfer initial step.[7] Until then, all energy transfers were assumed to take place from a first ion in an excited state to a second one in its ground state.[8] Because upconversion by sequential energy transfers or APTE effect is so efficient, it could initially be obtained through blackbody excitation or spontaneous diode emission even before laser sources became commonly available.[2]

Principles and applications of such upconversion phosphors have already been presented in several reviews up to the 1970s by Auzel,[2] Mita and Nagazawa,[9] Garlick,[10] and Wright.[3] Since then, laser excitation in the IR and/or the use of fibers have become so easy that upconversion has become a pervading effect in all RE-doped materials under high-density IR excitation. Also, another type of upconversion, namely, the photon avalanche process,[11,12] has been widely investigated in recent years.

Limited aspects of recent progress have partially been reviewed through the 1980s and 1990s,[13−18] but

the general field has recently evolved from the rare-earth (4f) consideration toward the use of actinide (5f) and transition-metal (3d, 4d, 5d) ions with a systematic use of laser excitation at precisely defined wavelengths.

This evolution justifies the present review.

Because it appears that the language in the upconversion field is still not completely fixed, possibly inducing misinterpretation, the basic processes of energy transfers, cooperative processes, and their application to upconversion together with their more recent evolutions and selected examples of applications will be presented in reference to the accepted vocabulary proposed by the pioneers. Some of the original papers in this field were reprinted in 1998 in a collective edition.[19]

2. Energy Transfers between RE Ions: Role of Energy Diffusion in Up- and Downconversion

In the following, the mutual interactions between ions are the key feature.

When the concentration of active ions is increased, long before the appearance of new lines due to pairs or modifications in radiative transition probabilities, a migration of energy between the centers is found. We are going to study this now, assuming that multiphonon decays and the radiative transitions remain one-center processes.

As single f and d ions properties are supposed to be known, multiion processes, namely, energy transfers, are now dealt with. Energy transfer occurs in a system where absorption and emission do not take place within the same center. It may occur without any charge transport. Then one may distinguish between radiative and nonradiative, resonant, and phonon-assisted energy transfer. Theoretical approaches start from a microscopic point of view with a macroscopic result averaged over all the centers in the sample. In fact, an energy transfer between two given ions cannot by itself increase efficiency; it can only provide a new excitation wavelength range with a reduced efficiency since it consists of the product of two processes with intrinsic efficiency less than or equal to 1. Overall efficiency improvement by energy transfers is gained only from the spatial averaging due to the macroscopic process of diffusion.

2.1. Recall of Basics of Energy Transfer with Activator in Its Ground State[20,21]

In a schematic way, the different microscopic energy transfer processes between two ions can be presented as in Figure 1. Following the traditional vocabulary of the phosphor field, the ion being first directly excited is called a senzitizer (S); some people would call it a donor, but because f and d ions may also be imbedded in semiconductors, such vocabulary leads to confusion and is not retained here. The ion to which energy is transferred and which emits the output photon is called an activator; in a synonymous manner, it is some times termed an acceptor. To avoid any ambiguity with the semiconductor field, this vocabulary is not retained in the following.

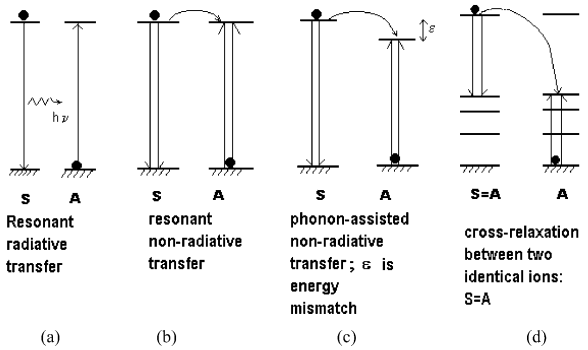

Figure 1. Various basic energy transfer processes between two ions considered before 1966: note that activator ion (A) receiving the energy from the sensitizer (S) is initially in its ground state. Cross-relaxation is the special case where S is identical to A. Doubled arrows symbolize the Coulombic interaction: (a) radiative resonant transfer; (b) resonant nonradiative transfer; (c) phonon-assisted nonradiative transfer; (d) cross-relaxation special case of nonradiative transfer.

One usually distinguishes radiative transfer (Figure 1a), nonradiative energy transfer (Figure 1b), and multiphonon-assisted energy transfer (Figure 1c). S and A may also be identical ions, and nonradiative transfer may give rise to self-quenching by cross-relaxation (Figure 1d).

When energy transfer is radiative (Figure 1a), real photons are emitted by the sensitizer ions (S) and are then absorbed by any activator ions (A) within a photon travel distance. As a consequence, such transfer depends on the shape of the sample.

Moreover, according to the degree of overlap between the emission spectrum of the sensitizer (S) and the absorption spectrum of the activator (A), the structure of the emission spectrum of the sensitizer will change with activator concentration. Since photons are emitted anyway, the sensitizer lifetime is independent of the activator concentration. These three facts are the criteria used to distinguish between radiative and nonradiative resonant energy transfer.

Probability for such transfer between two ions at a sufficiently large distance R is found to be[20]

$$p_{SA}(R) = \frac{\sigma_A}{4\pi R^2 \tau_S} \frac{1}{\int g_S(\nu) g_A(\nu)\, d\nu} \qquad (1)$$

where τ_S is the sensitizer lifetime and σ_A the absorption-integrated cross section. The integral represents the spectral overlap between A and S. It should be noted that the distance dependence goes as R^{-2}. Such resonant radiative transfer may permit long-range energy diffusion between identical ions and gives rise to photon-trapping effects of the same type as the ones observed a long time ago in gases.[22] Trapping effects increase the apparent experimental lifetime, and τ_S has to be measured on thin and lightly doped samples. These effects are particularly strong in Cr^{3+} and Yb^{3+}.[23−25]

Let us consider the simple case of two ions, each with one excitable electronic state separated from its electronic ground state by nearly equal energy; it is the case described in Figure 1b. With suitable

interaction between the two electronic systems, which is the case for nonradiative energy transfer, the excitation will jump from one ion to the other before one is able to emit a quantum of fluorescence. The mutual interactions are Coulomb interactions of the van der Waals type between the two ions. Förster,[26] who first treated such a case theoretically by quantum-mechanical theory, considered the dipole−dipole interaction. He assumed that the interaction is strongest if for both transitions electric−dipole transitions are allowed.[26] The interaction energy is then proportional to the inverse of the third power of the interionic distance and the transfer probability is given by

$$p_{SA} = \frac{2\pi}{h}|\langle S^*A^0|H_{SA}|S^0A^*\rangle|^2\rho_E \qquad (2)$$

H_{SA} = electric dipole−dipole interaction Hamiltonian, proportional to the inverse third power of ion separation,

ρ_E = density of states provided by the vibrational motion contributing to the line broadening of the transition,

p_{SA} is proportional to the inverse sixth power of the ion separation. The wave functions to be considered for the matrix element describe an initial state of the system with the sensitizer in its excited state and the activator in its ground state, the final state having the sensitizer in its ground state and the activator in its excited state.

Therefore, the transfer probability can be written as

$$p_{SA} = \frac{1}{\tau_S}\left(\frac{R_0}{R}\right)^6 \qquad (3)$$

where τ_S is the actual lifetime of the sensitizer excited state, including multiphonon radiative decay, and R_0 is the critical transfer distance for which excitation transfer and spontaneous deactivation of the sensitizer have equal probability.

However, Dexter pointed out[27] that this theory should be extended to include higher multipole and exchange interactions. In fact, for an isolated atom, one can consider the transition probability as decreasing as $(a_0/\lambda)^{2n}$, where a_0 is the Bohr radius, λ the wavelength, and n an integer. However, in an energy transfer process with a dependence on near-zone interactions, the transition probabilities drop off as $(a_0/\rho)^{2n}$, where ρ is the separation of the interacting ions. ρ can be as much as 3 orders of magnitude smaller than λ, so that the energy transfer effect tends to be more pronounced in systems with forbidden transitions.[27] This holds true for ions for which transitions to first order are forbidden, such as transition-metal and lanthanide ions.

The energy transfer probability for electric multipolar interactions can be more generally written as[27]

$$p_{SA} = \frac{(R_0/R)^s}{\tau_S} \qquad (4)$$

where s is a positive integer taking the following values:

$s = 6$ for dipole−dipole interactions,

$s = 8$ for dipole−quadrupole interactions,

$s = 10$ for quadrupole−quadrupole interactions.

It should be noted that for dipole−dipole interactions, the difference between radiative and nonradiative resonant transfer lies essentially in the fact that for radiative transfer there is no critical R_0 depending only upon concentration. The variation goes as R^{-2} instead of R^{-6}, and the sensitizer lifetime does not depend on the distance R.

Now, to be able to calculate effectively $p_{SA}(R)$, eq 4 is not very useful because R_0 cannot be easily obtained theoretically. Applying Racah's tensorial methods at the beginning of the calculation of Dexter, eq 2, allows development of calculations analogous to Judd's theory for radiative transitions. The case of the multipolar interactions was treated in this way by Kushida[28] and extended by Pouradier and Auzel[29] to magnetostatic and exchange interactions, showing that a single general formula could be used for all types of energy transfers.

The general form obtained is then

$$p_{SA}(R) = \frac{2\pi}{\hbar}\frac{I}{g_{S^*}g_{A^0}}\sum_{l_1l_2}|C_{l_1l_2}\langle S^*||U^{(l_1)}||S^0\rangle \times \langle A^0||U^{(l_2)}||A^*\rangle|^2 \qquad (5)$$

with

$$I = \int \gamma_S(E)\Gamma_A(E)\,dE \qquad (6)$$

where $g_{S^*}(g_{A^0})$ is the degeneracy of the $S^*(A^0)$ level, $\gamma_S(E)(\Gamma_A(E))$ is the normalized line shape function of emission (absorption) spectrum, $U^{(l)}$ are the tensorial operators already seen for Judd's theory. $|C_{l_1l_2}|^2$ can be considered as a parameter analogous to Judd T_λ (Ω_λ) for oscillator strength.

This expression of the transfer probability has the following advantages.

(1) Radial and orbital parts have been separated.

(2) Only a few reduced matrix elements need be calculated. They are the same for the three interactions we consider (for any interaction leaving spins unchanged).

(3) Comparison between two different interactions can be made through comparison of $C_{l_1l_2}$ coefficients. They are independent of the states involved in the transfer, and we call them $E_{l_1l_2}$, $M_{l_1l_2}$, and $X_{l_1l_2}$ for electrostatic, magnetostatic, and exchange interactions, respectively.

(4) Forced electric−dipole transitions, as calculated by Judd's method, can be included in eq 5.

(5) This expression also gives a single mathematical form regardless of the interaction, which is a convenient result. The somewhat complicated expressions for the different $C_{l_1l_2}$ of 4f electrons are given in ref 29. However. we can note the following.

(a) For electrostatic interaction $E_{l_1l_2}$, the $l_1 = 1$ and $l_2 = 1$ term, corresponding to dipolar−dipolar interaction, is zero in first order, which makes the introduction of Judd's T_λ parameters necessary. The $E_{l_1l_2}$ values are typically between $E_{22} \approx 30$ cm^{-1} for

quadrupole−quadrupole intensities and $E_{66} \approx 3 \times 10^{-1}$ cm^{-1}, but all contain some dipole−dipole part due to the T_λ.

(b) For magnetostatic interactions ($M_{l_1 l_2}$), only terms with $l_i = 1$, 3, and 5 are nonzero. They have the order of magnitude $M_{11} \approx 1$ cm^{-1} and $M_{55} \approx 2 \times 10^{-7}$ cm^{-1}.

(c) For exchange interactions ($X_{l_1 l_2}$), we have $1 \leq l_1 \leq 6$, giving estimates of $1-10^{-1}$ cm^{-1} for the coefficients.

These results show that exchange or magnetostatic interactions can be found in cases of small dipole−dipole and quadrupole electrostatic interactions if the matrix elements allow them.

If now we consider two ions with excited states of different energies (Figure 1c), the probability for energy transfer should drop to zero when the overlap integral $\int g_S(\nu) g_A(\nu)\, d\nu$ vanishes. However, it has been experimentally found that energy transfer can take place without phonon-broadened electronic overlap provided that the overall energy conservation is maintained by production or annihilation of phonons with energies approaching $k\Theta_d$, where Θ_d is the Debye temperature of the host matrix.[30] Then for small energy mismatches (100 cm^{-1}), energy transfer assisted by one or two phonons can take place.[31] However, for energy transfers between rare earths, energy mismatches as high as several thousand reciprocal centimeters are encountered. This is much higher than the Debye cutoff frequency found in normally encountered hosts, so multiphonon phenomena have to be considered here.

Miyakawa and Dexter[32] showed that it is still legitimate to write the probability of energy transfer in the form of eq 2, where $\rho(E)$ is taken as S_{SA}, the overlap of the line shape functions for emission by ion S and absorption by ion A, including the phonon sidebands in the line shape. It is necessary to consider each partial overlap between the m-phonon emission line shape of ion S and the n-phonon absorption line shape of ion A. A physical meaning to this mathematical assumption, criticized in ref 31, has been given by Auzel's experimental demonstration[33] of the existence of multiphonon sidebands for trivalent rare-earth ions. Their existence could be revealed by laser excitation spectroscopy even though they had not been seen by usual absorption spectroscopy because of their very small electron−phonon coupling.

Along the same lines as for vibronic sideband studies, S_{SA} can be expressed as follows

$$S_{SA} = \sum_N e^{-(S_{OS} + S_{OA})} \frac{(S_{OS} + S_{OA})^N}{N!} \times \sigma_{SA}(0,0;E)\delta(N, \Delta E/\hbar\omega) \quad (7)$$

where S_{0S} and S_{0A} are the respective lattice coupling constants for the ions S and A, N is the order of the multiphonon process with $N = \Delta E/\hbar\omega_m$, ΔE is the energy mismatch between both ions, and $\hbar\omega_m$ is the phonon cutoff frequency. σ_{SA} (0,0;E) is the zero-phonon overlap integral between S and A. Equation 7 contains a Pekar function of the Poisson type.[20]

The expression for S_{SA} with an energy mismatch of ΔE for small S_0 constants and for an occupation number $\bar{n} = (\exp(\hbar\omega/kT) - 1)^{-1}$, not exceeding 1 at the operating temperature, can be approximated with Stirling's formula by

$$S_{SA}(\Delta E) = S_{SA}(0) e^{-\beta \Delta E} \quad (8)$$

where $S_{SA}(0)$ is the zero-phonon overlap between S and A in the case where there is no energy mismatch between the two ions. β is given by

$$\beta = (\hbar\omega)^{-1} \log N/S_0(\bar{n} + 1) - \log\left(1 + \frac{S_{OA}}{S_{OS}}\right) \cong \alpha_S - \gamma \approx \alpha_S - \log 2 \quad (9)$$

involving α_S the nonradiative decay parameters and assuming identical electron−phonon coupling for ions A and S. This exponential dependence on energy mismatch is well substantiated by experiments.[34]

Up to this point we have been dealing with the microscopic case of two ions interacting with one another. To discuss the case of real macroscopic samples with many ions and to obtain a link with experimental facts, a statistical analysis of the energy transfer is necessary.

We have then to think about the overlap integrals that arise in all transfers between two ions as already seen. In the microscopic case we are sure that the involved line shapes can be only due to some homogeneous broadening even for transfer between two identical ions in different lattices sites.

In the macroscopic case, we can measure absorption and emission spectra taking into account all broadening processes averaged over the whole sample; for instance, the inhomogeneous broadening process due to emission and absorption at centers in different lattice sites. Then the overlap integral measured experimentally from the usual spectra is a measure in excess of the real overlap since we take into account emission and absorption of centers at any distances, even those which cannot interact. The error is the largest for the processes occurring at shortest interacting distances (exchange) and a contrario is certainly negligible for radiative transfer, since photons can travel a much larger distance than the spread of the spatial disorder. The error is also smaller for systems with small inhomogeneous broadening and having centers in only one type of lattice site, that is, without disorder.

Fluorescence line-narrowing techniques (FLN) could give some idea about the homogeneous part of an emission line, but the statistical analysis for the whole sample should still be performed. Supposing only a sensitizer−activator interaction, an averaged transfer efficiency can be calculated.[27] This has been studied in some detail by Inokuti and Hirayama.[35] They considered the number of activators located at random in a sphere around a sensitizer in such a way that the activator concentration is constant when the volume of the sphere and the number of activator ions considered goes to infinity. Then the averaged prob-

ability for transfer from one sensitizer to any acceptor is

$$W_{SA} = N_A \int_{R_{min}}^{\infty} p_{SA}(R) 4\pi R^2 \, dR \quad (10)$$

Introducing eq 1 into the expression for the intensity emitted by all sensitizers, each with different activator neighborhood, they obtained the following relation for the intensity decay of the emission of the sensitizer surrounded by many activators

$$I(t) = \exp - \frac{t}{\tau_{SO}} - \Gamma\left(1 - \frac{3}{S}\right)\frac{C}{C_0}\left(\frac{t}{\tau_{SO}}\right)3/S \quad (11)$$

where τ_{SO} is the decay constant of the sensitizer in the absence of activators; C is the activator concentration; C_0 is the critical activator concentration, and s is the parameter of the multipolar interaction. The comparison between experimental decay and this theoretical expression has been widely used to determine the index of the multipolar interaction involved. However, because it is difficult to avoid diffusion between sensitizers, fits of experimental results using eq 11 have to be taken with great care. For example, values of s larger than 10 have been found and it has been shown that for large s values the multipolar result has the same limit as the exponential behavior of an exchange process.[24] Yet, one cannot infer, as is sometimes done, that exchange coupling[36] is more likely than multipolar coupling. In fact, eq 11 is valid only at the microscopic level when there is neither sensitizer-to-sensitizer transfer nor activator-to-activator transfer. This formulation, therefore, has to be modified for high concentrations of sensitizers and activators. Then, due to the perfect resonance conditions in such cases, rapid energy migration between sensitizers or between activators is possible. The general result is complicated,[37] but Weber has shown that for large t, $I(t)$ decays exponentially[38]

$$I(t) = \exp\left(-\frac{t}{\tau_S} - \frac{t}{\tau_D}\right) \quad (12)$$

Then, two cases can be distinguished.

(i) In one case, spontaneous decay of excited sensitizers, diffusion among sensitizers, and energy transfer between sensitizers and activators are of about the same order of magnitude.

For sufficiently long times and dipole−dipole interactions one has[38]

$$\tau_D^{-1} = V N_S N_A \quad (13)$$

where $V = 8\pi C^{1/4} C_{SS}^{3/4}$, N_S is the sensitizer concentration, N_A is the activator concentration, C is the sensitizer−activator energy transfer constant, such that $C = (R_0)^s/R$, and C_{SS} is the sensitizer−sensitizer transfer constant.

(ii) For high sensitizer concentration, the diffusion rate can be faster than spontaneous sensitizer decay or sensitizer−activator energy transfer. The limiting step is no longer diffusion, and D appears to saturate with increased donor concentration; each activator experiences the same excited sensitizer neighborhood. R is taken as the minimum distance between sensitizers as permitted by the lattice ($R = R_{min}$). One has

$$\tau_D^{-1} = U N_A \quad (14)$$

with U being a constant depending on the type of interaction as discussed earlier in this section through eq 5.

Another approach to the macroscopic case is the use of the well-known rate equations that deal with the population of ions in a given state. This was used as a phenomenological approach in studies of lasers. The applicability of those equations in relation to the Inokuti and Hirayama statistics has been discussed by Grant.[39] The basic result of Grant is that the energy transfer probability is proportional to the activator concentration

$$W_t = U N_A \quad (15)$$

This result is the same as that obtained in fast-diffusion studies (eq 14). The practical interest in considering diffusion is that the decays are again exponential, as when ions are not interacting. This validates the use of rate equations.

Cross-relaxation terminology usually refers to all types of downconversion energy transfers occurring between identical ions. In such a case the same kind of ion is both sensitizer and activator.

As shown in Figure 1d, cross-relaxation may give rise to the diffusion process already considered between sensitizers when the involved levels are identical or self-quenching when they are different. In the first case there is no loss of energy, whereas in the second case there is a loss or a change in the energy of the emitted photons.

Theoretically, the same treatment is valid as in the more general case of energy transfer. However, it may be more difficult experimentally to distinguish between sensitizers and activators. Thus, any of the microscopic processes discussed above may happen with a maximum overlap when an identical couple of levels are involved. From the macroscopic point of view, the diffusion-limited case predicts from eq 13

$$\tau_D^{-1} = V N^2 \quad (16)$$

for $N_S = N_A = N$, and in the fast-diffusion case

$$\tau_D^{-1} = U N \quad (17)$$

A typical illustration of this is found for the self-quenching behavior of $Nd^{3+}(^4F_{3/2})$. In weak quenching materials, such as $La_{1-x}Nd_xP_5O_{14}$, self-quenching is found to behave linearly with ion concentration, whereas for strong quenching ones, such as YAG, a quadratic behavior is obtained. This, respectively, reflects the fast diffusion before the quenching step in the first type of materials and the limited diffusion before quenching in the second type of materials.[20,40]

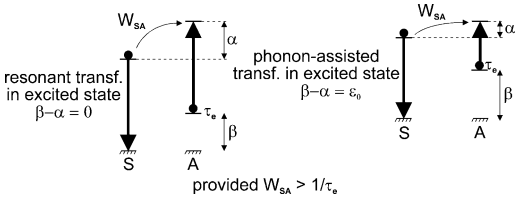

Figure 2. APTE basic step: energy transfer toward an ion already in an excited state. Nonradiative energy transfer is either resonant or phonon-assisted with energy mismatch $\epsilon_0 \neq 0$.

2.2. Upconversion Processes by Sequential Energy Transfers (APTE or ETU Process): Comparison with ESA and Typical Examples

As said in the Introduction, up to 1966 all identified energy transfers between rare-earth ions were of the types summarized in Figure 1, that is the activator ion receiving the energy from a nearby sensitizer (S) was in its *ground state*. Then Auzel proposed to consider cases where activators (A) were already in an *excited state*[7] as shown in Figure 2. Because activator ions usually have several (n) excited states but a single ground state, one can understand why n-photons may be summed up through this new consideration. This becomes obvious when one realizes that only energy differences and not absolute energy can be exchanged between ions.

The reason for proposing such upgoing transfer was to point out that energy transfers then used[41] to improve the laser action of $Er^{3+}$by pumping Yb^{3+}in a glass matrix could also have the detrimental effect of increasing reabsorption.[7,24] The simple proof of such an effect was to look for an upconverted green emission (from $^4S_{3/2}$ of Er^{3+}) while pumping Yb^{3+} ($^2F_{7/2}-^2F_{5/2}$) transition, which was effectively observed.[7,42] Of course, the situation in Figure 2 could repeat itself several times at the activator. This meant that n-photon upconversion by energy transfer was possible as demonstrated by the three-photon upconversion of 0.97 μm into blue light (0.475 μm) in the $Yb^{3+}-Tm^{3+}$ couple.[7] Independently this IR to blue upconversion was interpreted by Ovsyankin and Feofilov[43] as a two-photon effect connected with two excited Yb^{3+} ions and a cooperative sensitization of Tm^{3+} initially in its ground state. This interpretation originated from the law for output versus excitation, which was quadratic instead of cubic as found in ref 7 and because energy transfers between excited states were only being recognized independently at the time.[7] The experimental discrepancy aroused probably from a saturation in an intermediate step in the APTE process.[44]

Recently a systematic analysis of the power law governing the APTE (or ETU) process has been performed by Pollnau,[45] generalizing by rate equations what had been discussed for the Yb−Tm couple:[2] a P^n law can be found for an n-photon process when W_{APTE}, the APTE (ETU) upconversion probability, is weak, whereas a P^1 law can be asymptotically obtained when W_{APTE} is large in front of other processes depopulating the metastable state.

To make the terminology clearer, a schematic comparison between the APTE (ETU) effect and other

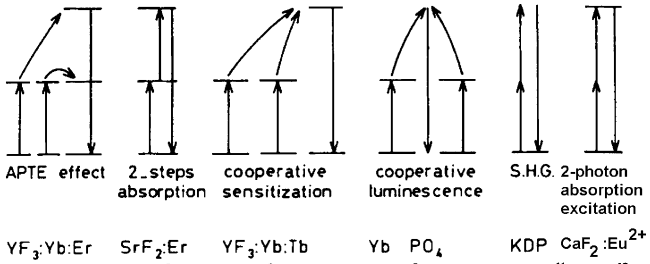

Figure 3. Various two-photon upconversion processes with their relative efficiency in considered materials.

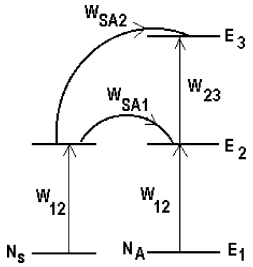

Figure 4. Simplified energy level scheme and symbols used in eqs 18−22.

two-photon upconversion processes, namely, two-step absorption, cooperative sensitization, cooperative luminescence, second-harmonic generation (SHG), and two-photon absorption excitation, is presented in Figure 3 together with their respective typical efficiency.

Since we are dealing with nonlinear processes, usual efficiency, as defined in percent, has no meaning because it depends linearly on excitation intensity. Values are then normalized for incident flux and given in cm^2/W units for a two-photon process. More generally, for an n-photon process it should be in $(cm^2/W)^{n-1}$.

A simple review of the energy schemes shows that they differ at first sight by the resonances involved for in- and outgoing photons: for highest efficiency, photons have to interact with the medium a longer time, which is practically obtained by the existence of resonances. As shown, the APTE (ETU) effect is the most efficient because it is closest to the full resonance case.

However, reality is sometimes not so simple, and different upconversion processes may exist simultaneously or their effects can be tentatively made to reinforce each other. For instance, a combination of two-photon absorption and cooperative absorption has been theoretically investigated.[46] Also, SHG and cooperative luminescence have been considered simultaneously in order to increase SHG by the partial resonance of cooperative luminescence.[47,48]

Let us consider now the role of macroscopic energy diffusion in both APTE (ETU) and ESA upconversion second-order processes.

The probability for ESA in a two-step absorption (W_{13}) connecting a state E_1 to E_3 by the intermediate state E_2 is just given by the product of the probabilities for each step (Figure 4)

$$W_{13} = W_{12} \cdot W_{23} \tag{18}$$

To obtain the same result by an APTE effect, we also have to consider the product of two energy transfer probabilities and calculate the equivalent rate for populating E_3 by APTE (ETU); we get (Figure 4)

$$N_A W_{13} \equiv (N_A N_S^* W_{SA1}) N_S^* W_{SA2} \qquad (19)$$

or

$$W_{13} \equiv N_S^* W_{SA1} W_{SA2} \qquad (20)$$

where W_{SA} are the energy transfers probabilities for each step and N_s^* is the concentration of excited sensitizers which is given by

$$N_S^* = N_S W_{12}$$

Assuming all W_{ij} have the same magnitude and all W_{SA} also, as is typical for rare-earth ions, we have to compare

$$W_{13} \approx W_{12}^2 \qquad \text{for single-ion ESA} \qquad (21)$$

with

$$W_{13} \approx N_S^{*2} W_{SA}^2 = N_S^2 W_{12}^2 W_{SA}^2 \qquad \text{for two-ion APTE} \qquad (22)$$

Clearly, the APTE (ETU) gain over one ion ESA comes from the product $N_S^2 W_{SA}^2$, which has to be as large as possible. However, this simple quadratic behavior with sensitizer concentration for a two-photon upconversion though observed in the past[2] can be questioned in some practical case as recently shown by Mita;[49] for Yb−Tm:BaY_2F_8, a quadratic behavior is first observed for a three-photon case and then a linear one (probability is constant) at Yb concentration above about 10%.

In any case, this points to an increase in sensitizer concentration (N_S) which leads to fast diffusion[38] and allows the use of rate equations in such multiion systems.[39] This validates a posteriori the implicite use of the rate equation for establishing eqs 18−22. Now the behavior is different for certain hosts where ions are clustered into pairs even at low average concentration. This has been shown by Pellé and Goldner[50] for $CsCdBr_3$:Yb, Er for which an Yb optimum concentration of 1% has been demonstrated, a significant difference with the usual 15% for other materials.[51]

Besides nonradiative diffusion at the sensitizer level, it has been observed that radiative diffusion plays also a role in APTE (ETU) upconversion. The measured time constants for the Er^{3+} or Tm^{3+} emission have been observed to be correlatively lengthened by the photon-trapping lengthening of the Yb^{3+} lifetime, reflecting the radiative diffusion at the sensitizer level.[52] Also, reducing single crystals doped with Yb−Er or Tm to powder form usually produces an intensity reduction when the grain size is less than 100 μm. This shows that the effective radiative diffusion length is of this order of magnitude in this experiment. Recently, studies on nanometric size upconversion phosphors with crystallites of Y_20_3:Yb,-Er, ranging from 75 to 200 nm in grains between 600 and 800 nm have shown that the maximum intensity for the blue and green emission under 632.8 nm excitation is obtained for the maximum size of 800 nm.[53,54] This effect is also most probably in connection with diffusion within Yb ions which, though not being directly excited, plays a role in an intermediate relay step of the APTE (ETU) process.

Many times in the literature, when ESA is not advocated, upconversion involving coupled ions is referred to as cooperative effects or cooperative energy transfers without proof when in fact APTE (ETU) effects are involved as can be guessed from their relative efficiencies and from the provided description. The fact that the APTE (ETU) effect and cooperative ones are often mistaken is due to a number of common properties.[2] For instance, for two-photon upconversion, both processes show quadratic increases on excitation and on absorber concentrations; both show an emission lifetime equal to one-half the absorber lifetime. However, they show different rise times; cooperative rise time is instantaneous as for ESA or any absorption, whereas APTE (ETU) rise time reflects the population accumulation at the sensitizer excited state. However, as shown below, the difference is more basic, though sometimes difficult to establish experimentally except in special cases where single-ion resonances clearly do not exist or where diffusion between ions is prohibited by a too small concentration with still an interaction as in clusters.

The basic distinction between both upconversion processes (ETU or ESA) within a single-ion state description and cooperative pair states is the purpose of the next section.

3. Upconversion in a Single-Ion Level Description for APTE (ETU) or ESA and in a Pair-Level One (Cooperative Effects): Theoretical and Experimental Discrimination

Because in the field of upconversion pair states or more recently dimer states are advocated to explain some of the observed processes, it is felt appropriate here to precisely define the vocabulary, which is done in the next subsection.

3.1. Three Different Kinds of Pair States

In fact, when active ion concentration is increased, besides the occurrence, at first, of changes in probabilities for lower concentration as already pointed above, its value may reach a point where clusters may be formed and new levels may be experimentally observed. We think it is useful to distinguish between three types of pair levels, according to their different origin and shift from their parent single-ion level. When two resonant systems are coupled, it is a basic physical phenomenon that their degeneracy is removed. This may be called a dynamic shift, and for rare-earth ions it is typically 0.5 cm^{-1} [55] up to a maximum of a few cm^{-1}; it is 2.7 cm^{-1} for Nd^{3+} in CdF_2[56] and 3 cm^{-1} in the stoichiometric compound $Cs_2Yb_2Br_9$ with built-in pairs with a distance of 3.9 Å.[57] In a stoichiometric material this would give rise

to a Frenkel excitonic band, though for rare-earth ions it has been shown to be rather limited by the weakness of the interaction.[58] Now in divalent materials or even in trivalent hosts,[59] when the active trivalent ion concentration is increased, one may understand that the local static crystal field is modified by the replacement of a divalent cation with a trivalent one or even by the ion size modification. This gives rise to a spectral shift on the considered single-ion levels when its concentration is increased. Such a shift may reach up to 10 cm^{-1}. Though still often called a pair level,[59] this new single-ion level is of completely different origin from the previous one; it is sometimes also called a new site or a static pair state due to the active ion concentration increase.[59] It must be stressed here that one-center operators just as for transitions between single-ion states govern any transitions between such pair states.

Now, the third type of pair levels coming from what are called cooperative processes are very different from the two previous types because, as we are going to see, they involve two-center operators and are second order with respect to the transitions between pair levels of the two previous types. As we will see, the shift from the single parent states is the sum of the energy of the parent states; it is several hundreds or thousands of cm^{-1},[60] which does not represent the interaction strength inside the pair. The cooperative pair levels will be dealt with in more detail below (sections 3.2 and 3.3).

3.2. Fundamental Difference for Transitions between Single-Ion States, Dynamical and Static Pair States, and Cooperative Pair States

When active ions are situated at sufficiently short distances for interactions between them to take place, two types of upconversion processes may occur: summation of photon energy through energy transfers[2] (APTE (ETU) effect) and/or cooperative effects either by sensitization[43] or emission as found by Nakazawa and Shionoya.[61] Both APTE (ETU) effects and cooperative ones are often mistaken for the one another because both present several similarities and may simultaneously occur in a given system for a given excitation. In particular, both processes reflect the *n*-photon order versus excitation density and sensitizer concentration in the same manner.

As seen in the Introduction, upconversion by energy transfer is a generalization of Dexter's energy transfer[27] to the case where the activator is in a metastable state instead of being in its ground state; this requires the interaction between S and A (H_{SA}) to be smaller than the vibronic interaction of S and A, so that both ions can be described by single-ion levels coupled to the lattice. It is generally the case since for fully concentrated rare-earth crystals or for clusters, pair level splitting is of the order of 0.5 cm^{-1};[55,62] in host with smaller concentrations, this interaction can be even weaker, whereas one-phonon or multiphonon sidebands may modulate the level positions by several hundreds of cm^{-1}. Further, upconversion requires the transfer probability for the second step (W_{SA}) to be faster than radiative and nonradiative decay from the metastable level, that is $W_{SA} > \tau^{-1}$ with τ measured intermediate state lifetime for ion A. W_{SA} is obtained from

$$W_{SA} = \frac{2\pi}{\hbar}|<\Psi_S{}^e\Psi_A{}^0|H_{SA}|\Psi_S{}^0\Psi_A{}^e>|^2\rho(E) \quad (23)$$

where the wave functions are simple products of single-ion wave functions; ρ(E) describes the dissipative density of states due to the coupling with the lattice. H_{SA} is the interaction Hamiltonian, the origin of which may be multipolar or exchange interactions as discussed above in section 2.1.

All cooperative processes, including the simple cooperative absorption in $PrCl_3$ first observed by Varsanyi and Dieke[63] and the cooperative Stokes emission as observed by Van der Ziel and Van Uitert in $EuAlO_3:Cr^{3+}$ [64] from pair states and called exciton-(Eu) sidebands of localized excitons(Cr) or cooperative upconversion emission,[61] have to be considered as two-operator transitions between pair levels for both ions as a whole. A one-center dipolar electric transition would be strictly forbidden for a two-center transition, and as a difference with energy transfers for which plain product wave functions are used, one needs product wave functions *corrected to first order* to account for interaction between electrons of different centers[65]

$$\Psi_{pair} = \Psi^0(S)\Psi^0(A) - \sum_{s''\neq 0}\sum_{a\neq 0}\frac{\langle s''a''|H_{SA}|00\rangle}{\delta_{s''} - 0 + \epsilon_{a''} - 0}\Psi_{s''}(S)\Psi_{a''}(A) \quad (24)$$

as given, for example, for the ground state; s″, a″ denote intermediate states for S and A and δ_s,ϵ_a denote their corresponding energies. Then any one-photon transition in the cooperative description involves already four terms in the matrix element, which cannot be reduced to eq 5 that contains only single-ion wave functions and not pair wave functions as in eq 24:

APTE (ETU) upconversion or ESA, even between static or dynamic pair levels, corresponds to a lower order of perturbation than cooperative processes, which involve cooperative pair states; the latter have to be considered practically only when the first type cannot take place.

Such is the case when real single-ion levels do not exist to allow energy transfer; it is the case for Yb^{3+}–Tb^{3+} upconversion[55,66,67] or when the concentration is too small to allow efficient transfer by energy diffusion between sensitizers. Then cooperative upconversion is likely within clusters.[59,68] One may also look for crystal structures where the pair clustering is built-in.[57,62,69]

Because cooperative transitions are of second order with respect to transitions between other pair states or single-ion states, they are very weak, about 3–4 orders of magnitude less than one-center transitions, and consequently they can usually be observed on small samples only in excitation and emission spectra. For example, a direct absorption spectra for a cooperative process between Yb and an allowed OH transition has only been observed on very long samples of about 5 cm and high Yb concentration

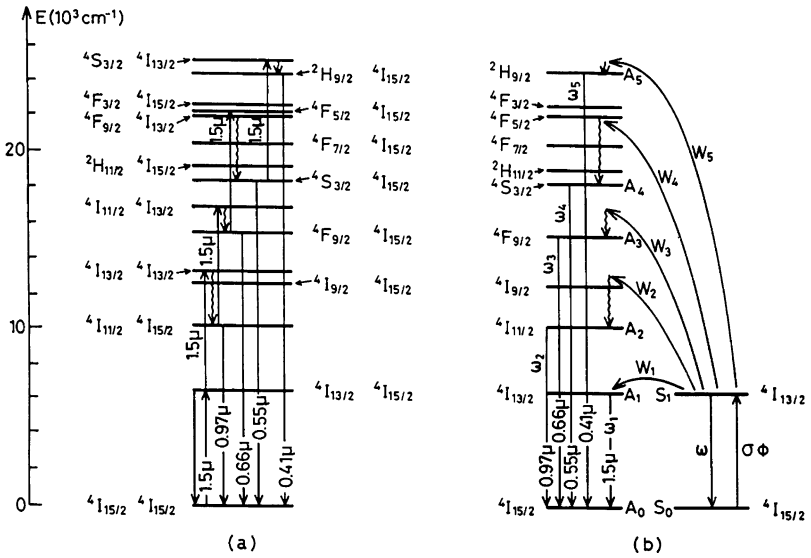

Figure 5. Cooperative (a) and APTE (b) energy scheme for *n*-photon ($n = 1-5$) upconversion in Er^{3+}-doped hosts.

(from 1.6×10^{22} to 4.3×10^{23} cm^{-3})[60] with an intensity ratio to single-ion transition of about 10^{-3}. Very recently similar results have been obtained for cooperative Yb−Yb pairs on 1−12 cm long Yb-doped laser crystals.[70] The intensity was found to be 1.3×10^{-5} of the single-ion one for a 1 cm long crystal of Y_2O_3:Yb(10%), that is with a concentration of $2.8 \times 10^{21}cm^{-3}$. Such very weak ratios demonstrate the role of the double-operator nature of the transition. The 2 orders of magnitude difference, in both ratios given above, reflect in part the fact that Yb−Yb pairs are forbidden−forbidden pairs whereas Yb−OH are forbidden−allowed pairs.

Generally, experimental discrimination between APTE (ETU) and cooperative processes is not straightforward apart from the trivial cases where no real intermediate energy level exists for the APTE (ETU) effect to take place, even from unwanted impurities. The weak ion concentration level alone is not a good argument to eliminate APTE (ETU) upconversion, knowing that RE ion clusters may exist, for instance, in glasses, even at a doping level as low as 70 ppm.[71]

To illustrate the experimental difference between APTE (ETU) and cooperative upconversion, we will discuss an example of excitation line-narrowing effect in *n*-photon summation as a mean to distinguish between both processes.[72,73] Irradiating Er^{3+}-doped samples with IR radiation at 1.5 μm leads to various visible emissions.

Room-temperature IR F-center laser excitation between 1.4 and 1.6 μm of 10% Er^{3+}-doped vitroceramics and of YF_3:Er leads to emission bands from the near-IR to the UV. Such emission may be ascribed to multiphoton excitation, respectively, of order 1 to 5, either of the APTE (ETU) or of the cooperative type as depicted, respectively, with energy levels of single-ion (APTE) or cooperative pair levels (Figure 5).[72,73]

Successive absorptions in Figure 5a involve a combination of several *J* states. APTE (ETU) effect, because of self-matching by multiphonon processes, involves (Figure 5b) only $J = 15/2$ and 13/2 states.[72]

Excitation spectra in Figure 6 show a striking behavior: each spectrum presents the same spectral

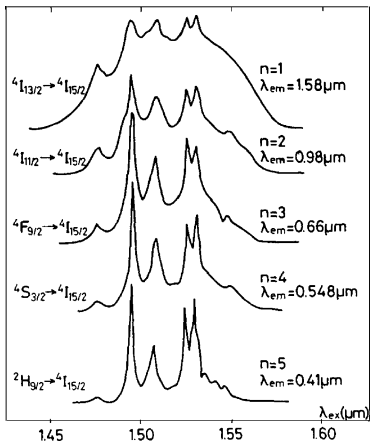

Figure 6. Excitation spectra for *n*-photon ($n = 1-5$) upconversion in Er-doped YF_3.

structure with clearly an increasing narrowing with process order. The structure reproduces the Stark structure of the $^4I_{15/2}-{}^4I_{13/2}$ first excited terms as can be obtained by a diffuse reflectance spectrum.

The spectral narrowing can be understood by a rate equation treatment where higher excited populations are neglected in front of the lower ones in order to obtain a tractable development (weak excitation assumption).

The emitted power from an *n*-photon summation is then given by

$$P_n(\lambda) = \frac{W_n \cdots W_2}{(\omega_{(n-1)} \cdots \omega_2)} P_1{}^n(\lambda) \qquad (25)$$

with symbols of Figure 5b and $P_1(\lambda)$ the line shape of $^4I_{15/2}-{}^4I_{13/2}$ absorption.[72]

The obtained excitation spectra are direct proof of the validity of the APTE (ETU) explanation, since a cooperative effect should show the convolution of all *J* states involved in the multiple absorption between pair levels.[72]

Until the 1980s, few unquestionable experimental examples of cooperative upconversion were demonstrated besides the Yb−Tb cooperative sensitization

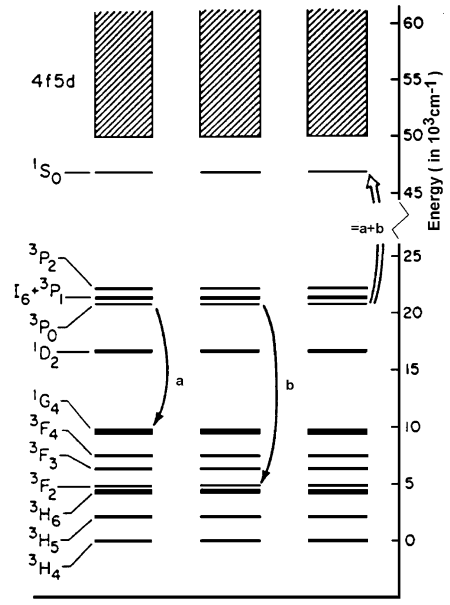

Figure 7. Cooperative luminescence and APTE (activator ion already in an excited state) cooperative sensitization in LaF_3:Pr^{3+} system. (Reprinted with permission from ref 75. Copyright 1984 American Physical Society.)

quoted above and the cooperative luminescence in Yb^{3+} described in detail below.[61] Since then, many more cases have been described:

The cooperative luminescence in the UV (from 405 to 270 nm) comes from two ($^2P_0$)Pr^{3+} excited ions in PrF_3[74] and LaF_3:Pr^{3+}; the APTE (ETU) cooperative sensitization of the $^1S_0$ state of one Pr^{3+} ion is *already in its excited state* ($^3P_0$) from the energy annihilation of two other Pr^{3+} ions also in their $^2P_0$ excited state as for the cooperative luminescence case.[75] Overall, this is a three-ion, three-photon effect which, from 477 nm blue excitation, gives an upconversion in the UV region (400−250 nm). Figure 7 describes the energy schemes and mechanisms for both processes. However, for some unknown reason, the cubic law which should be present for emission intensity versus excitation is not observed for the $^1S_0$ level emission[74] and a quadratic law is obtained as for the cooperative luminescence case. The cooperative effects were clearly discriminated from other processes through excitation spectra investigations.

Very recently, Valiente et al. obtained upconversion from near-IR Yb^{3+} excitation with visible emission from Mn^{2+} ions in stoichiometric materials, $CsMnCl_3$, $RbMnCl_3$, $CsMnBr_3$, and Rb_2MnCl_4, respectively at 690, 630, 680, and 625 nm.[76−79] Explanations were based on sequential absorption between dimer states built from Yb and Mn single-ion states which are in fact the cooperative pair states discussed above and shown, for instance, for Er^{3+} in Figure 6a in a cooperative hypothesis. This explanation is coming from the fact that emission of Mn^{2+} is instantaneous, as it would be for ESA between the dimer states, which have to be considered since both ions are involved. Along the same lines, the Yb−Tb case has been reconsidered in $SrCl_2$ and $Cs_2Tb_2Br_9$:Yb(1%),[80,81] and the cooperative effect is found to be ESA between cooperative pairs states and Yb cooperative luminescence with 10^{-6} efficiency[81] (at 5.6 kW/cm^2 excitation) for T < 100 K instead of the usual cooperative sensitization as in ref 66 found at larger T. As rarely given, efficiency for the cooperative sensitization process has been determined to be 10^{-4} under 2.4 10^4 W/cm^2 at 300 K for $SrCl_2$,[80] that is 4.2 × 10^{-9} at a normalized excitation level of 1 W/cm^2 for comparison, see Figure 3 and Table 1, with the values for cooperative sensitization of 10^{-6} in Yb,Tb:YF_3 and of 10^{-8} for cooperative luminescence in $YbPO_4$.

The Yb−Tb cooperative effect has also been revisited by Strek's group in $KYb(WO_4)_2$:Tb.[82] Besides the cooperative upconversion process itself, the interesting feature of a lifetime depending on the excitation level has been observed. It has been attributed to the inverse of cooperative sensitization, first predicted a long time ago by Dexter[83] and only recently identified experimentally for the first time by Basiev et al.[84] in $La_{1-x}Ce_xF_3$. This is different from quantum cutting,

Table 1. Available Measured Normalized Absolute Efficiencies for Various Upconversion Processes

matrix	ions	process	order n	temp (K)	efficiency (cm^2/W)$^{n-1}$	ref
YF_3	Yb^{3+}−Er^{3+}	APTE (ETU)	2	300	≅10^{-3}	2
SrF_2	Er^{3+}	ESA	2	300	≅10^{-5}	2
YF_3	Yb^{3+}−Tb^{3+}	coop. sensitiz.	2	300	≅10^{-6}	2
$YbPO_4$	Yb^{3+}	coop. lumin.	2	300	≅10^{-8}	13,61
KDP		SHG	2	300	≅10^{-11}	2
CaF_2	Eu^{2+}	two-phot. absorpt.	2	300	≅10^{-13}	2
YF_3	Yb^{3+}−Er^{3+}	APTE (ETU)	2	300	2.8 × 10^{-1}	201
vitroceramics	Yb^{3+}−Er^{3+}	APTE (ETU)	2	300	2.8 × 10^{-1}	51
$NaYF_4$	Yb^{3+}−Tm^{3+}	APTE (ETU)	3	300	3.4 × 10^{-2}	158
YF_3	Yb^{3+}−Tm^{3+}	APTE (ETU)	3	300	4.25 × 10^{-2}	158
vitroceramics	Yb^{3+}−Tm^{3+}	APTE (ETU)	3	300	8.5 × 10^{-2}	158
$NaYF_4$, $Na_2Y_3F_{11}$	Yb^{3+}−Er^{3+}	APTE (ETU)	2	300	10^{-2} to 2 × 10^{-4}	191
$NaYF_4$	Yb^{3+}−Er^{3+}	APTE (ETU)	2	300	2.5 × 10^{-4}	16
$NaYF_4$	Yb^{3+}−Tm^{3+}	APTE (ETU)	3	300	5.5 × 10^{-2}	191
$NaYF_4$	Yb^{3+}−Tm^{3+}	APTE (ETU)	3	300	3 × 10^{-7}	16
fluorohafnate glass	Yb^{3+}−Tm^{3+}	APTE (ETU)	2	300	6.4 × 10^{-3}	129
fluorohafnate glass	Yb^{3+}−Ho^{3+}	APTE (ETU)	2	300	8.4 × 10^{-4}	129
vitroceramics	Yb^{3+}−Tm^{3+}	APTE (ETU)	2	300	3.5 × 10^{-1}	157
vitroceramics	Yb^{3+}−Tm^{3+}	APTE (ETU)	3	300	3.6 × 10^{-3}	157
$ThBr_4$	U^{4+}	ESA	2	300	2 × 10^{-6}	161
$SrCl_2$	Yb^{3+}−Yb^{3+}	coop. lumin.	2	100	1.7 × 10^{-10}	80
$SrCl_2$	Yb^{3+}−Tb^{3+}	coop. sensitiz.	2	300	8 × 10^{-8}	80
$SrCl_2$	Yb^{3+}−Tb^{3+}	coop. sensitiz.	2	100	1.8 × 10^{-8}	80

considered by Wegh et al.,[85−89] which is just the reverse of the APTE effect. Both quantum cutting and cooperative quenching can produce quantum efficiency larger than 1 but not with the same energy efficiency.

Along analogous lines, cooperative upconversion and downconversion processes mixed with multiphonon processes have been investigated in KYb$(WO_4)_2$:Eu,Tb[90] and in $KYb_{0.8}Eu_{0.2}(WO_4)_2$.[91]

A more complicated case of cooperative explanation has been given by Orlovskii et al.[56,92] for Nd^{3+} in CaF_2, CdF_2, and SrF_2 at 4.2 K. There the three kinds of pair states discussed in section 3.1 are simultaneously involved in a qualitative description through both APTE (ETU) and ESA processes. Unfortunately no quantitative analysis with respect to the mixing of first-order and second-order transitions has been given.

3.3. Application of Cooperative Luminescence; Theory, and Examples

Because cooperative processes are less effective than APTE (ETU) ones by 4−5 orders of magnitude, very few applications of such processes exist except, as we will see, the detection of RE ion clusters. We proposed that the simplest cooperative process, the cooperative luminescence of Yb^{3+},[61] be used as a probe of the existence of Yb^{3+} ions clusters in glasses.[68]

Cooperative luminescence (or its opposite cooperative absorption) is the simplest cooperative phenomenon, and the corresponding two-center matrix element is

$$\langle \Psi_{pair}{}^{g} | D_1{}^{(1)} + D_2{}^{(1)} | \Psi_{pair}{}^{e} \rangle \qquad (26)$$

where the operator is the sum of the electric dipole operators for ion 1 and ion 2. The wave functions for both ions in their excited state $\Psi_{pair}{}^{e}$ and in their ground state $\Psi_{pair}{}^{g}$ are derived from expressions given by eq 24. The calculation of eq 26 gives four terms that are represented in Figure 8; terms III and IV provide the cooperative emission at twice the energy of the single-ion excited state.

Since along the RE series nearest neighbor ions have analogous chemical properties, we assumed that Yb^{3+} would chemically behave for the clustering process ion the same way as for Er^{3+}, the ion generally used in optical amplifiers. Because Yb^{3+} ions have only two spin−orbit states, they are good examples of the simple situation schematized in Figure 8. This is one of the reasons for its use as a cluster probe. The other reason is as follows:

In optical amplifier applications, the basic limitation linked with the existence of the so-called clustering of RE ions was addressed. Clusters of RE dopant, as found in the literature from direct fiber amplification experiments,[71,93,94] are related to what could be called interaction clusters which are much larger than chemical clusters. Because of spatial diffusion as shown in section 2.1, such interaction clusters could have a spatial extension of more than 20−100 Å for nonradiative interaction clusters and up to 100 μm for radiative ones. Clearly, such clusters have

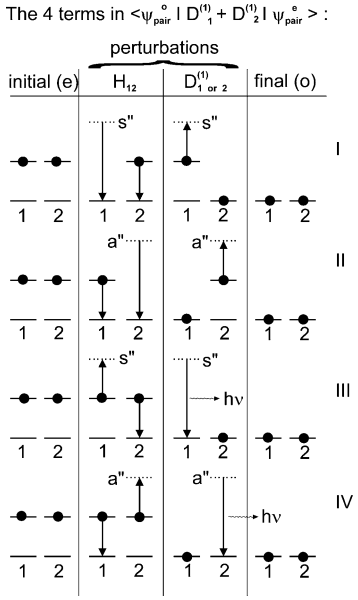

Figure 8. Four terms for cooperative luminescence in a two-level ion system (the Yb^{3+} case).

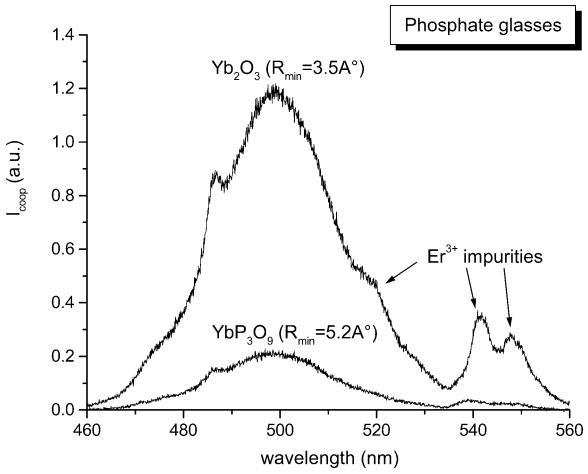

Figure 9. Normalized cooperative emission spectra for Yb^{3+} in a phosphate glass for two doping precursors with different Yb−Yb shortest distance R_{min}.

nothing to do with chemical clusters, which depend only on the chemical processes of the glass preparation. The existence of chemical clusters of spatial extension of a few Angstroms would increase tremendously ion−ion interactions of any kind. One need to obtain a signature of such clusters that is the only one that chemistry could eventually modify. Cooperative luminescence of Yb^{3+} has been proposed as a signature of the existence of chemical clusters in glasses.[68]

Cooperative luminescence[68,95−97] is a phenomenon which, requiring very close proximity of interacting RE ions in order to be seen in experiments, is a very good signature of clusters constituted by ions at distances of less than about 5 Å. Such distances, or shorter ones, between interacting ions are also the order of magnitude of the size of chemical clusters. Figure 9 presents the cooperative luminescence of Yb^{3+} in a phosphate glass doped with Yb^{3+} introduced through various precursors with different Yb−Yb shortest distances.[98] It has been shown that the normalized cooperative intensities depend on such

distances. Also, it can be noted that unwanted impurities (Er^{3+}, Tm^{3+}) introduced with Yb^{3+} oxide are revealed at ppm level by the much more efficient APTE (ETU) effect.[99]

4. Experimental Results and Their Implications in Various Fields

4.1. Recent Upconversion Studies in Lanthanide (4f) and Actinide (5f) Ion-Doped Solids with APTE (ETU) and ESA Processes

(Cooperative processes have been discussed in sections 3.2 and 3.3 above.)

Most of the more recent published results on upconversion under various laser pumpings have aimed, besides cooperative effects already discussed, at distinguishing the processes involved and mainly at separating APTE (ETU) from plain ESA. Most of the examples treat cases of upconversion in the now classical 4f ion-doped solids and few in the 5f ones.

4.1.1. Pr^{3+} ($4f^2$) Ion

When doping fluoride glasses of the ZBLAN type in either fiber or bulk form, Pr^{3+} shows blue upconversion both of the ESA (two photon) and APTE (ETU) (three photon) types from the $^3P_0$ state when pumping into the $^1G_4(^1D_2)$ state.[100] Analogous results are obtained for $LiKY_{1-x}Pr_xF_5$ crystals,[101] but the process is mainly APTE (ETU). Identifying the process is based on the presence of an excitation delay.

Germanate of general formula $60GeO_2 \cdot 25PbO \cdot 15NbO_5$ as well as chalcogenide glasses of general formula $50GeS_2 \cdot 25Ga_2S_3 \cdot 25CsX$ with X = Cl, Br, and I,[102] doped with Pr^{3+} have been investigated. IR to blue upconversion is obtained under both ESA and APTE (ETU) processes as revealed by the absence or the presence of an excitation delay. The excitation sequence is $^3H_4$ to $^1G_4$ then $^1G_4$ to $^3P_0$ (ESA) or/and $^1D_2$ (ETU). $^3P_0$ gives the blue emission and $^1D_2$ the orange one. In $Bi_4Ge_3O_{12}:Pr^{3+}$ crystal red, green, and blue upconversion is obtained with mainly ESA and a less important APTE (ETU) process.[103] From a dynamic study of a Pr^{3+}-doped tellurite glass, ESA is proposed to explain the $^3H_4$ to $^1D_2$ followed by a multiphonon process connected to a $^3H_6$ to $^3P_1$ sequence.[104] An analogous process is proposed for $LiYF_4:Pr^{3+}$,[105] whereas a two-photon absorption is proposed for an IR to blue upconversion in a $60ZrF_4 \cdot 33BaF_3 \cdot 7LaF_3$ glass doped with Pr^{3+};[106] however, because a two-photon process is likely to be less probable than a sideband absorption,[33] this explanation may be questioned.[105]

In $KYb(WO_4)_2:Pr(0.42\%)$,[107] blue upconversion under red and IR excitation is obtained along now classical APTE (ETU) schemes.

4.1.2. Nd^{3+} ($4f^3$) Ion

Probably due to the availability of Nd^{3+}-doped materials for laser research, many investigations in Fernandez's group with Nd^{3+} in various kinds of hosts have been recently performed. In germanate glasses of composition $60GeO_2 \cdot 25PbO \cdot 15NbO_5$ doped with Nd^{3+},[108] the APTE (ETU) process has been observed under CW IR excitation in the $^4I_{9/2}$ to $^4F_{5/2}$ absorption. Green, red, orange emissions have been detected from $^4G_{7/2}$ due to the following upconversion energy transfer ($^4F_{3/2}$, $^4F_{3/2}$ gives $^4G_{7/2}$, $^4I_{13/2}$). ESA has also been observed with the sequence $^4I_{9/2}$ to $^4F_{5/2}$, nonradiative decay to $^4F_{3/2}$, followed by ESA to $^2P_{1/2}$ decaying to $^4G_{7/2}$. In a fluoride glass of composition $25CdF_2 \cdot 13.5CdCl_2 \cdot 30NaF \cdot 20BaF_2 \cdot 1.5BaCl_2$ doped with $0.5\%Nd^{3+}$,[109] mostly APTE (ETU) is observed as revealed by the delay in the emission wavelengths ranging from red to UV and the analogy between the absorption and their excitation spectra. The output slope for P^n with $n = 1.7$ indicates a two-photon process.

In fluoroarsenate,[110] fluoroindate,[111] and in chalcogenide glasses,[112] upconversion by Nd^{3+} ions has been studied too, taking advantage of the weak energy phonons of such glasses. It is mostly APTE (ETU), with some ESA for the $^4G_{7/2}$ emission, that have been observed from $^2P_{1/2}$ as shown by the similar spectral features in the excitation and absorption spectra for two-photon processes.

In $Pb_5Al_3F_{19}:Nd^{3+}$ crystals,[113] at 300 and 4.2 K, APTE (ETU) is observed for visible (from $^4G_{7/2}$, with $n = 1.5$) and UV emission (from $^2P_{3/2}$, with $n = 2.2$) as indicated by similar excitation and absorption spectra.

In the stoichiometric laser material $K_5Nd(MO_4)_4$, IR to visible, blue (from $^4G_{7/2}$ with $n = 1.6$), and UV (from $^2P_{3/2}$ with $n = 2.4$) emissions have been studied with the very high Nd concentration of 2.37×10^{21} cm^{-3}.[114] The studies, conducted in or outside the IR lasing phases, show that the laser metastable state is depopulated during the lasing phase as shown by the stronger blue and orange emission. Again, upconversion is essentially of the APTE (ETU) type as shown by comparing excitation and absorption spectra.

In $LiYF_4:Nd(0.1-3\%)$,[115] upconversion is found to be due to ESA, the first step being a one-phonon sideband absorption situated at $16563-15919 = 644$ cm^{-1} above the $^2H_{11/2}$ state followed by the ESA step populating $^4D_{3/2}$. In the same type of fluoride crystal as well as in YAG, the following APTE (ETU) steps have been observed: ($^4F_{3/2}$, $^4F_{3/2}$) giving ($^4I_{15/2}$, $^4G_{5/2}$); ($^4F_{3/2}$, $^4F_{3/2}$) giving ($^4I_{13/2}$, $^4G_{7/2}$), and ($^4F_{3/2}$, $^4F_{3/2}$) giving ($^4I_{11/2}$, $^2G_{9/2}$)[116,117] to some extent similar with the high-intensity quenching of the $^4F_{3/2}$ state.[118] $BaLu_2F_8:Nd^{3+}(0.6\%)$ crystals have also been studied.[119] Yellow to blue and green upconversion has been observed due to ESA, whereas under IR excitation, green upconversion is due to APTE (ETU) when site selection is involved at low temperature. Also, $KLiYF_5:Nd^{3+}$ has been investigated, and upconversion through ESA from $^4F_{3/2}$ has been observed.[120] With CaF_2 thin films on LaF_3 crystalline sample in waveguide form, three-photon APTE upconversion ($n = 2.9$) can be easily observed through pumping confinement.[121] Very interestingly, emission at 381 nm in the UV from $^4D_{3/2}$ ends on $^4I_{11/2}$, thus providing good hope for a UV four-level scheme laser.

4.1.3. Gd^{3+} ($4f^7$) Ion

Due to the fact that its lowest excited state ($^6P_{7/2}$) is at very high energy (32 000cm^{-1}), this ion is mainly considered for downconversion studies and is involved in fewer upconversion studies than the two previous ones. However, upconversion has been considered in the stoichiometric material with centrosymmetric sites $Cs_2NaGdCl_6$.[122] ESA has been advocated (maybe with some direct two-photon allowed absorption) for the emissions between excited states from the 5d to ^6I_J and ^6P_J bands at 578 and 755 nm under excimer laser excitation into the ^6P_J lines. Another stoichiometric material, K_2GdF_3, has also been investigated in upconversion.[123] Pumping is into the $^6P_{1/2}$ state at 312 nm. Three anti-Stokes emissions attributed to $^6G_{7/2}$ and $^6I_{7/2}$ down to the ground state $^8S_{7/2}$ at 204.7, 242.0, and 2798 nm have been observed and attributed to an APTE (ETU) process.

4.1.4. Dy^{3+} ($4f^9$) Ion

This ion had the reputation of being a poisonous center even at trace levels for APTE (ETU) in usual Yb−Er and Yb−Tm or Ho upconversion matrices.[2] For this reason it was banished from the laboratory. This could explain why so few studies exist about the upconversion properties of this ion. It is probably also because the proximity of the lower excited states requires low-energy phonon matrices. The level structure is also somewhat analogous to the situation for Eu and Tb for which essentially cooperative upconversions have been observed (see section 3.2). Yet recently $CsCdBr_3$:Dy^{3+} (0.2%) has been studied in upconversion.[124] Both APTE (ETU) and ESA processes have been observed at 10 K. Near-IR excitation is by absorption into $^6F_{5/2}$ at 12 338 cm^{-1} and into $^6F_{3/2}$ at 13 200 cm^{-1}. Emission is from $^4F_{9/2}$ to $^6H_{13/2}$ at 17 341 cm^{-1}. Two APTE (ETU) schemes are likely, the more probable being ($^6F_{5/2}$, $^6F_{5/2}$) giving ($^4F_{9/2}$, $^6H_{13/2}$). At higher temperature (295 K) and large concentration, ESA is operative from $^6F_{9/2}$ to $^4F_{9/2}$. At lower concentration, ESA appears to be from $^6F_{5/2}$ to $^4I_{13/2}$.

4.1.5. Ho^{3+} ($4f^{10}$) Ion

Though this ion is among the first studied in upconversion[2] with Yb codoping, it has later been studied alone. First, some years ago,[125] red to blue upconversion was observed as well as a red (He−Ne laser) pumped IRQC for 2 μm detection at 300 K was demonstrated in $Ho_xY_{1-x}F_3$ (x from 0.005% to 1). An APTE (ETU) process, ($^5F_5$, $^5I_7$) giving ($^5F_3$, $^5I_8$), provides the $^5F_3$ emission at 485 nm. Much more recently, $CsCdBr_3$:Ho^{3+}(0.035% and 2.25%)[126] has been studied, this host differing from the previous one by its lower phonon maximum energy (163 versus 560 cm^{-1}) and its pair building ability. A two-photon process has also been found for the blue emission from $^5F_3$ with slope $n = 1.8$. ESA is advocated at a higher temperature (T > 100K), whereas APTE (ETU) is found at T < 100K. Comparison of excitation spectra with absorption and delay in the emission help to separate the processes. Ho^{3+} has also been excited in the red at 647 nm from a gas Kr laser in $LiTaO_3$:Ho(0.3%).[127] At 15 K, a green emission with $n = 2$ is observed; it is attributed to the $^5S_2$ to $^5I_8$ transition excited by an ESA process. In a more classical experiment, Ho is excited via Yb in YVO_4:Yb,Ho.[128] The near-IR excitation at 1 μm provides both a red emission from $^5F_5$ by an ESA process (n = 1.6) and a faint green one from $^5S_2$ (n = 1.6) attributed to an APTE (ETU) process. Interestingly and along the same lines in Yb, Ho-doped fluorohafnate glasses,[129] APTE (ETU) IR to green upconversion has been measured to give an absolute efficiency of 8.4 × 10^{-4} cm^2/W, a value directly comparable to the one of Figure 3 and Table 1, with 10^{-3} cm^2/W for YF_3:Yb,Er.

4.1.6. Er^{3+} ($4f^{11}$) Ion

(See also section 4.2.)

Er^{3+} was the first ion showing upconversion,[2] and it seems that the numerous previous studies have not exhausted its upconversion properties. It still appears as the most studied ion in recent times, as will be shown in the following.

With the availability, in the 1980s, of efficient laser diodes (LD) and tunable Ti−sapphire lasers in the 800−1100 nm range, the field of upconversion studies with Er^{3+} has been renewed. In particular, Er^{3+} has demonstrated its capacity as a laser ion just as Nd^{3+} did a long time ago, and consequently, all kinds of upconversion emissions have been observed and studied. The role of upconversion on the CW functioning of the $LiYF_4$:Er and ZBLAN fiber lasers at 2.7 μm[130−132] has recently been confirmed,[133] and a cascade laser at 1.72 and 2.7 μm laser have been optimized, in particular, in a ZBLAN glass doped with Er(0.25−8.75%) alone or with Pr(0.25−1.65%)−Er[134] using the APTE (ETU) process for optimizing the $^4I_{11/2}$ and $^4I_{13/2}$ lifetimes. Even classical laser hosts have been investigated: YAG:Er,[135] YSGG:Er,[136] and $YAlO_3$[137] for which either ESA or APTE (ETU) have been observed.

In a more fundamental approach, $Cs_3Lu_2Cl_9$, $Cs_3Lu_2Br_9$, and $Cs_2Lu_2I_9$ doped with Er^{3+}(1%) as well as the stoichiometric material $Cs_3Er_2X_9$ (X = Cl, Br, I) have been investigated[138,139] under 1.5 μm excitation. As in ref 72, an APTE (ETU) process describes the observed four-photon upconversion process at higher Er concentration, though the process is called cooperative energy transfer.[139]

In $BaLu_2F_8$:Er(1%; 4.5%), IR (0.97 μm) to green upconversion from $^4S_{3/2}$ is observed.[140] Both APTE (at all temperature) and ESA at lower temperature from $^4I_{11/2}$ and $^4I_{9/2}$ are identified by the transients of the upconversion emission. Ba_2YCl_7:Er (1−100%) has been studied[141] under 800 nm excitation of the $^4I_{9/2}$ state. Depending on excitation energy and concentration, both APTE (ETU) (for Ba_2ErCl_7) and ESA are observed. In $RbGd_2Br_7$:Er (1%),[142] under 980 nm excitation of $^4I_{11/2}$, both APTE (ETU) and ESA, discriminated by the excitation transients, are observed with a ratio depending on excitation energy and temperature. Besides the above studies, the Güdel's group in a systematic manner also studied BaY_2F_8:Er and $Cs_3Er_2Br_9$[143] in order to compare the

upconversion properties from near-IR to green in two hosts differing by their highest phonon energy, respectively, 415 and 190 cm^{-1}. In $Cs_3Lu_2Br_9$:Er-(1%),[144] a lattice with built-in pair structure, both ESA and APTE (ETU) processes are observed but mostly ESA when exact matching between levels and laser excitation is obtained. Energy migration is noted even at the relatively low 1% doping.

Similar studies have been performed in $Ca_3Al_2Ge_3O_{12}$:Er, where both ESA and APTE are observed depending on the excitation wavelength.[143] In $LiYF_4$:Er(3%), Yb(20%),[146] five-photon near-IR to UV has been observed with APTE (ETU) processes similarly to[72] for Er alone.

A rather original and interesting result in a classical Yb(0.5%)−Er(0.1%) system is the optical amplification in an upconversion-pumped chalcogenide glass ($70Ga_2S_3-30La_2O_3$).[147] Pumping is at 1.06 μm in an anti-Stokes two-phonon sideband at 2 times 425 cm^{-1} from the YAG:Nd laser photon energy. Amplification, which is maximum at 165 °C is at 555 nm with a gain factor of 10. This corresponds to an amplification efficiency of 0.012 dB/mW in the bulk glass sample without optical confinement. Also, in the same aim of amplification in the green spectral region with near-IR pumping, $LiYF_4$:Er has been studied in detail under an InGaAs LD pumping.[148] $LiNbO_3$:Ti,-Er waveguides[149] have been studied for upconversion-pumped laser either at 550 nm or 2.7 μm. Both APTE (ETU) and ESA are observed. For a 550 nm laser, APTE (ETU) is necessary and can be obtained essentially in Er clusters which have to be increased at Li^+ and Nb^{5+} sites. Here Er clusters are looked for, in contrast to the situation in Er-doped optical fibers for 1.55 μm amplification, see section 3.3. $LiNbO_3$:Er waveguides, carefully pumped in a site-selective manner[150] have shown ESA and APTE (ETU) upconversion according to the pumping photon energy. When weaker than 12450 cm^{-1}, ESA is observed; otherwise APTE (ETU) is obtained. A two-photon process exists in both cases as shown by the observed $n = 1.92$ value. Pumping is into $^4I_{9/2}$ at 800 nm, and emission is from $^4S_{3/2}$. ESA is from $^4I_{13/2}$ to $^2H_{11/2}$ with some involved nonradiative decays. For APTE (ETU), after a nonradiative decay to $^4I_{11/2}$, the following takes place: ($^4I_{9/2}$, $^4I_{11/2}$) gives ($^4I_{15/2}$, $^4F_{3/2}$) providing the $^4S_{3/2}$ excitation reached by a nonradiative decay from $^4F_{3/2}$. In the same kind of waveguide, traces of avalanche (see section 4) have been identified.[151]

4.1.7. Tm^{3+} ($4f^{12}$) Ion

Tm^{3+} is known to be one of the first ions having shown upconversion either alone or with the help of Yb^{3+}.[2] As for other ions, the advent of lasers has renewed its interest. Also, research of upconversion-pumped lasers has also been an impulse to the research. $LiYF_4$:Tm has been studied from its spectroscopic parameter point of view for laser applications[123] with codoping with Pr^{3+} as well.[152] After a $^3H_6$ to $^3H_4$ excitation at 12 643 cm^{-1} (791 nm) in the Tm^{3+} ion, a double excitation, $^3H_6$ to $^1G_4$ then to $^3P_2$ by an APTE (ETU) process in the Pr^{3+} ion, as revealed by a delay in the built-up transient, allows emission from $^3P_0$ to $^3H_6$ (600 nm) and $^3H_4$ (490 nm) in the Pr^{3+} ion.

Upconversion has been studied in the stoichiometric crystal TmP_5O_{14} as well as in the amorphous $Tm_{0.1}La_{0.9}P_5O_{14}$,.[153] Under red pumping, UV and blue emission are observed from $^1D_2$ with $n = 2$, respectively, to $^3H_6$ (360 nm) and $^3F_4$ (450 nm). $^1G_4$ emission at 480 nm is quenched at a concentration of 100% down to 10%. Comparing excitation spectra, stepwise APTE (ETU) and ESA are conjectured. The amorphous sample provides the largest intensity at 450 nm. An emission at 347 nm from $^5I_6$ to $^3F_4$ can be observed with $n = 2.5$.

In garnets $Y_3Sc_2Ga_3O_{12}$, $Gd_3Ga_5O_{12}$ and in $GdAlO_3$ doped with Yb(10%) and Tm(0.1%),[154] upconversion to 460−500 nm can be observed under Ti−sapphire excitation at 790 nm corresponding to the $^3H_6$ to $^3H_4$ transition in Tm^{3+}. Then a back transfer to Yb allows the $^2F_{5/2}$ Yb^{3+} population and the subsequent APTE (ETU) process from $^3H_4$ to $^1G_4$. This behavior is different from the classical Yb−Tm case under a first Yb excitation.

In $Cs_3Yb_2Cl_9$:Tm, a matrix with low-energy phonons (<280 cm^{-1}), up to five-photon APTE (ETU) process is observed with a scheme analogous to the one of Figure 6b, however, with a nonradiative step replaced by an internal APTE (ETU) step within the Tm^{3+} itself.[155] The slopes, respectively, observed are $n =$ 1.4, 2.0, 2.6, and 3.4 for emissions from $^3H_4$, $^3F_3$, $^1G_4$, and $^1D_2$. The respective excitation spectra are the Yb absorption narrowed by the power law as shown in Figure 7 for the Er case, also proving the APTE (ETU) process. The difference here is that because of the internal APTE (ETU) process in Tm^{3+}, the power law to be considered for $^1G_4$ and $^1D_2$ are here, respectively, 3/2 and 4/2, as already explained for the $n = 3/2$ slope mentioned in one of the red upconversion processes of Yb−Er[2].

Fluorohafnate glasses doped classically with Yb and Tm have been investigated,[129] and absolute efficiency has been shown to be 6.4×10^{-3} cm^2/W for the 804 nm emission. This two-photon upconversion efficiency is similar to the one given for Yb−Er, see Figure 3 and Table 1.

In a silica fiber 3.5 m in length doped with Tm alone, visible and UV upconversions at 650, 470, and 366 nm all with a slope of $n = 3$ have been analyzed.[156] Absorption is at 8300 cm^{-1} in the $^3H_6$ to $^3H_5$ transition. Upconversion is thought to be enhanced by the first and second Raman transitions observed at 1120 and 1180 nm. Above a threshold at 10 mW, line narrowing is observed and is considered as an indication of superluminescence.

Along the same directions as in ref 51, lead germanate vitroceramics doped with Yb(15%)−Tm(0.1%) have shown APTE (ETU) upconversion with a two-photon process at 779 and 698 nm, a three-photon process at 478 nm($^1G_4$), and a four-photon one at 363 nm($^1D_2$).[157] Measured absolute efficiencies were 5.8×10^{-3} at 779 nm and 10^{-6} at 478 nm under a 16.5 mW/cm^2 excitation. In normalized units it gives respectively for the two-photon and the three-photon processes 3.5×10^{-1} cm^2/W and 3.6×10^{-3} $(cm^2/W)^2$.

Interestingly this IR to IR two-photon process is much more efficient than the IR to green process in Yb−Er. On the other hand, the IR to blue transition is about 20 times less efficient than the efficiency obtained in the first Yb−Tm-doped vitroceramics (8.5×10^{-2} $(cm^2/W)^2$,[158] see Table 1). In the fluoride glass BiGaZYbTZr:Tm^{3+},[159] a crossover from cooperative sensitization to APTE (ETU) is concluded from the time behavior changes with pulse excitation length.

4.1.8. Tm^{2+} ($4f^{13}$) Ion

This ion is considered for the first time in upconversion. It is isoelectronic with Yb^{3+} and as such has the same level structure: two spin−orbit states $^2F_{7/2}$ and $^2F_{5/2}$ separated by about 8840 cm^{-1} and parity-allowed 4f−5d bands above 15 000cm^{-1}. The presence of Tm^{2+} is not common due to its propensity to oxidation, but here due to the considered $SrCl_2$ divalent host, 2% of Tm^{2+} has been successfully introduced[160] without the presence of any Tm^{3+}. The level structure is such that the 4f−5d bands are at about twice the energy of the first $^2F_{5/2}$ excited state and has prompted Güdel's group to investigate this new ion for upconversion at 15 K under a filtered 80 W lamp excitation at 8840 cm^{-1} and with a pulsed Nd:YAG laser for the transient study. The absence of delay in the upconversion signal indicates an ESA process.

4.1.9. U^{4+} ($5f^2$) Ion

This is the first 5f ion in which upconversion has been observed[161] in $ThCl_4$ and $ThBr_4$:U^{4+} (0.05%). The first observation was fortuitously found at CNET on a supposedly undoped $ThBr_4$ sample. Under a Nd:YAG pulsed excitation, a green SHG signal at 532 nm was looked for in order to detect the crystal eventual noncentrosymmetry. In fact, instead of the green spectrally narrow signal at 532 nm, we essentially observed a broad red one at a luminescence emission wavelength known for U^{4+}. This observation indicated that upconversion was active in U^{4+} at very weak concentration levels. A derived conclusion was that the oscillator strengths were very large and probably the energy transfers too. This induced the first determination of U^{4+} oscillator strengths that showed values of $\cong 10^{-4}$ [162] about 2 orders of magnitude larger than for Ln^{3+} and one order larger than then known values for U^{3+}. Recent results for U^{3+}, introduced for the first time by a pure chemical way in a $ZnCl_2$-based glass, indicate values of $\cong 10^{-6}$ which is about the same as that for Ln^{3+} [163] and 2 orders of magnitude less than that for U^{4+}.

With the 1 KW tungsten iode filtered lamp experiment already used for the first Yb−Er and Yb−Tm investigations (see Figure 17 in section 4.2), several emission lines in the red and green have been attributed to ESA either for excitation at 950 and 1170 nm separately or for excitation at 950 plus 1170 nm.[161] The involved levels are connected by absorption from the ground-state $^3H_4$ to $^3H_6$, $^3F_3$, and $^3H_5$ and then ESA from these states to $^3P_0$, $^3P_1$, and $^1I_6$, see Figure 10. The linear behavior with concentration showed that upconversions were not due to APTE

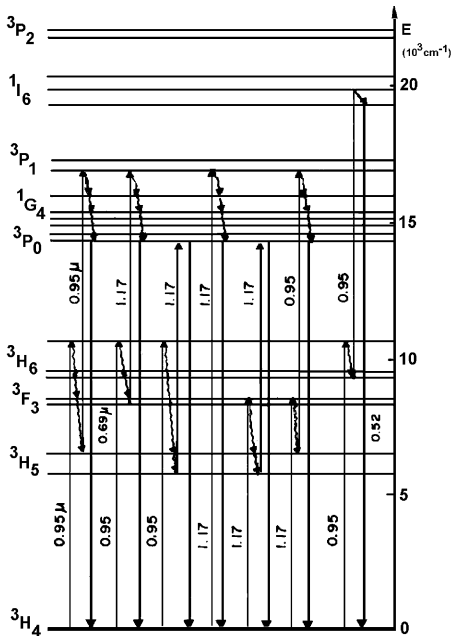

Figure 10. Energy scheme for various ESA upconversions involved in $ThBr_4$:U^{4+}.

(ETU) processes. On the other hand, as shown for Yb−Er and Yb−Tm,[51] photon trapping was present as indicated by the grain size effect on lifetimes and on the upconversion efficiencies. It shows that radiative diffusion plays an important role also in ESA upconversion. Normalized efficiency is found to be 2×10^{-6} cm^2/W, see Table 1, for $ThBr_4$ grains doped with 0.05% U^{4+} and of 0.2−0.3 mm optimized size.[161]

4.1.10. U^{3+} ($5f^5$) Ion

Though there has been one publication on the upconversion properties in trihalide-doped Cm^{3+},[164] most of the upconversion studies with trivalent actinides are with U^{3+} from Strek's group. In $LaCl_3$:U^{3+} and $LaCl_3$:U^{3+}, Pr^{3+},[165] under Nd:YAG laser excitation, ESA is found to give the $^2K_{15/2}$ to $^4I_{9/2}$ green emission in U^{3+} alone. When coupled to Pr^{3+}, a cross-relaxation process allows a second ESA within the Pr^{3+} ion giving its $^3P_0$ excitation. A refined study indicates a more complex upconversion process with back transfer to U^{3+} and APTE (ETU) process within U^{3+}.[166] Under red laser pumping in the $^4I_{9/2}$ to $^2K_{13/2}$ transition, green emission from $^2K_{15/2}$ to $^4I_{9/2}$ can be observed. This upconversion is attributed to two processes:[167] (i) a sequential absorption within one U^{3+} ion where the second photon populates the $5f^5$−6d bands and thus the energy is transferred to the $^2K_{15/2}$ emitting state and (ii) an APTE (ETU) process within an U^{3+} pair of ions following the sequence ($^4F_{9/2}$, $^4F_{9/2}$) $\Rightarrow$ ($^2H_{9/2}$, $^2H_{11/2}$) -35 cm^{-1} (a weak phonon energy). Other paths for excitation have also been investigated in $LaCl_3$:U^{3+},[168] and green and red emissions have been obtained with slopes, respectively, equal to $n = 1.97-2.5$ and $1.7-1.85$, according to the precise excitation wavelength.

In centrosymmetric elpasolites Cs_2NaYBr_6 and in Cs_2NaYCl_6 doped with U^{3+},[169] due to multiphonon quenching, ESA upconversion has been observed only in the bromide type.

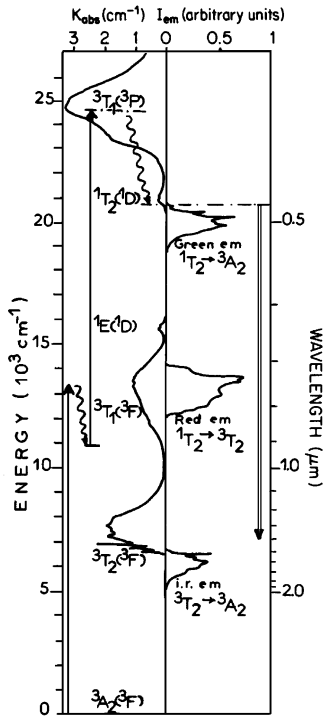

Figure 11. Energy scheme for ESA upconversion in MgF_2:Ni^{2+}.

4.2. Recent Upconversion Studies in Transition-Metal (3d, 4d, 5d) Ion-Doped Solids with APTE (ETU), ESA, or Cooperative Processes

The first consideration of d ions in upconversion can be found in the work of Cresswell et al.[170] in 1978, where in Cs_2NaYCl_6 they considered Re^{4+}, a $5d^3$ ion, as a replacement for Yb in the IR to blue upconversion in Yb−Tm systems, with the idea of having an APTE (ETU) two-photon process instead of a three-photon one. This was supposed to improve overall efficiency in diode-pumped anti-Stokes visible light sources. Unfortunately this system proved itself to be surprisingly inefficient. The second example was obtained in Auzel's group at CNET in the tunable laser material MgF_2:Ni^{2+}.[171] Due to the strong Stokes shift experienced by d ions in solids caused by a medium crystal field strength inducing itself medium electron−phonon couplings, resonant diffusion is not as effective as in lanthanides. Under a krypton gas laser excitation at 752.5 nm, green upconversion at 80 K was observed at 500 nm coming from the $^1T_2$-(^1D) to $^3A_2$(^3F) transition, see Figure 11. It was attributed to the $^3T_1$(^3F) to $^3T_1$(^3P) ESA transition. A cross-relaxation, ($^1T_2$, $^3A_2$) giving ($^3T_2$, $^3T_1$), was observed to self-quench the green emission. The determined microparameter values for this energy transfer were consistent with an exchange interaction. This upconversion was not studied in order to improve upconversion itself but because it was seen as a drawback to be reduced in the IR laser functioning of Ni^{2+}.

Following these two pioneering works one can say that the field of upconversion in d ion-doped solids has been developed by the systematic work of Güdel's group in recent years. Presentation of this field is the subject of the following paragraphs.

4.2.1. Ti^{2+} ($3d^2$) Ion

In NaCl- and $MgCl_2$-doped (0.1−0.2%)Ti^{2+} crystals, the near-IR (9400 cm^{-1}) to visible upconversion is analyzed at 15 K in these two hosts.[172] Spectral analysis of these two crystals reveals that NaCl and $MgCl_2$ have crystal field strength on both sides of the spin crossover point for the first excited metastable state. For NaCl it is $^3T_2$ with the same spin as the ground-state $^3T_1$, whereas for $MgCl_2$ it is $^1T_2$, i.e., it gives a spin-forbidden transition to the ground state. This dramatically changes the metastable state radiative lifetime from, respectively, 1.4 to 109 ms and consequently the relative efficiencies of the ESA processes observed in both crystals.

4.2.2. Cr^{3+} ($3d^3$) Ion

In YAG[173] and YGG ($Y_3Ga_5O_{12}$)[174,175] codoped with (2%)Cr^{3+} and (1%)Yb^{3+}, upconversion of Cr^{3+} through a near-IR pumping of Yb^{3+} is observed at 10 K with an efficiency of 6% under 150 mW of excitation[173−175] but at undefined energy density. The presence of a delay in the transient of the emitted signal indicates the presence of an energy transfer. Because there is no metastable level below the ^2E Cr^{3+} emitting state, a cooperative sensitization process can only explain the whole process. Further, the cooperative luminescence of Yb^{3+} is simultaneously observed. The role of the efficient diffusion of energy among the Yb^{3+} ions is stressed as is generally the case with this ion.

Even three ion systems have been studied one of them being Cr^{3+} in YAG: (5.76%)Tm^{3+}, (0.36%)Ho^{3+}, and (1%)Cr^{3+},[176] a well-known 2.1 μm laser material. Under near-IR (720−790 nm) and red excitation (610−660 nm), a blue emission from $^1G_4$ (Tm) at 486 nm and from $^5F_3$ (Ho) at 486, 489, and 497 nm can be seen; an upconverted emission is obtained also from the ^2E (Cr^{3+}) level at 688.7 and 687.6 nm, the R_1 and R_2 lines. All such emissions are losses for the laser process. They come from cross energy transfers between the three ions and ESA excitation.

4.2.3. Ni^{2+} ($3d^8$) and Mn^{2+} ($3d^5$) Ions

Besides Ni^{2+} in MgF_2,[171] already mentioned, Ni^{2+}-(0.1−10%) has been investigated as an upconversion ion either alone in $RbCdCl_3$,[177] $CsCdCl_3$,[178] and Rb_2CdCl_4,[179]or coupled with Mn^{2+} in $RbMnCl_3$,[180] $CsMnCl_3$, and $RbMnCl_3$,[178] and in Rb_2 $MnCl_4$.[179]

Under near-IR excitation at 15 K, Ni^{2+} alone is found to produce a green upconversion by an ESA process as explained above for MgF_2:Ni^{2+} [171] but with different level attributions, maybe due to the fact that crystal field strengths are different and that zero-phonon lines have not been considered. Here, the ground-state absorption is from $^3A_2$ to ^1E and ESA from $^3T_2$ to $^1T_2$; emission is the same transition $^1T_2$ to $^3A_2$. In $RbCdCl_3$, a pressure study modifying the crystal field strength shows an increase in upconversion due an increase in the spectral overlap between ground-state absorption and ESA.

With the Mn^{2+} presence, a strong increase in upconversion is observed, though Mn^{2+} has no metastable level below $^1T_2$ (Ni^{2+}). On the contrary, the metastable state $^4T_1$ of Mn^{2+} is in resonance with $^1T_2$

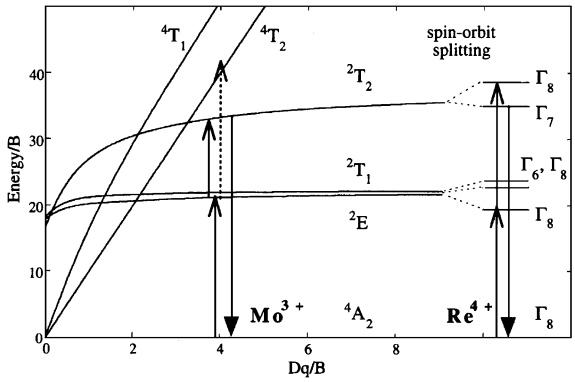

Figure 12. Tanabe and Sugano diagram for the d^3 configuration of Cr^{3+} and corresponding energy schemes involved in upconversion by ESA processes for Mo^{3+} and Re^{4+}. (Reprinted with permission from ref 181. Copyright 1998 American Chemical Society.)

(Ni^{2+}) and in $CsMnCl_3$ is found to emit slightly at the expense of $^1T_2$, which is then slightly quenched. An explanation is given by a strong enhancement of the ^1E absorption intensity due to a stronger spin−orbit interaction linked to the proximity of the $^3T_1$ and ^1E state. The upconversion enhancement also found in $RbMnCl_3$ cannot be of this type because this proximity does not exist. It is attributed to a strong exchange coupling[178] between Ni^{2+} and Mn^{2+}, removing the spin selection rule for the $^3A_2$ to ^1E absorption from $\Delta S = 1$ to 0, and coming from the mixing of both Ni^{2+} considered states with the Mn^{2+} $^6A_1$ ground state.

4.2.4. Mo^{3+} ($4d^3$) Ion

This ion has been studied in Cs_2NaYCl_6 and Cs_2NaYBr_6[181,182] at 2% doping concentration. Under near-IR excitation from a Ti−sapphire laser, red upconversion is observed from 10 to 150 K. Under one-wavelength excitation, both ESA and APTE are observed. Under two-wavelength excitation, essentially ESA provides upconversion with a better efficiency. ESA upconversion implies a $^2T_1/^2E$ to $^4T_2$ absorption preceded by a $^4A_2$ to $^2T_1/^2E$ from the ground state, see Figure 12. APTE is provided by the ($^2T_1/^2E$, $^2T_1/^2E$) to ($^4A_2$,$^4T_2$) energy transfer, giving the emission from $^4T_2$. In the chloride host, the ratios for upconversion processes are estimated to be APTE (15%) and ESA (85%). For the bromide, it is, respectively, 35% and 65%. This ion is characterized by a very long lifetime of 67.5 ms coming from the relatively weak oscillator strengths; it can be noted that electron−phonon parameters are weak (S = 0.05) for the intermediate states $^2E/^2T_1$ and strong (S = 4.5−5.7) for the final excited state very near the emitting state (S = 0.05). This explains the necessity of the low temperature for the upconversion emission.

4.2.5. Re^{4+} ($5d^3$) Ion

This ion, also being a d^3 configuration ion, has roughly the same Tanabe and Sugano energy diagram[183] as other better known transition metals (TM) such as Cr^{3+} and Mo^{3+}. It has been studied in Cs_2ZrCl_6[181,184] and Cs_2GeF_6.[185] Though Re^{4+} has the same level structure as Cr^{3+} and Mo^{3+}, as shown in Figure 12, it has been the first TM ion to show upconversion at room temperature.[181,184] Contrary to other TM ions, Re^{4+} shows an efficient APTE (ETU) process because selection rules on spin are relaxed by a larger spin−orbit coupling. The main difference with Mo^{3+} can be traced back to the larger oscillator strength for the $^4A_2(\Gamma_8)$ to $^2T_1$ (Γ_8) by a factor 10^2 with respect to $^4A_2$ to $^2T_1/^2E$ in Mo^{3+}. The upconversion energy transfer involved being ($^2E/^2T_1(\Gamma_8)$, $^2E/^2T_1(\Gamma_8)$) gives ($^4A_2(\Gamma_8)$, $^2T_2(\Gamma_8)$). Thus, excitation into $^2T_1(\Gamma_8)$ at about 1.1 μm (Nd:$LiYF_4$ laser at 1.047 μm) provides a red emission at about 725 nm.

In a solution-grown Cs_2GeF_6:(2%)Re^{4+} crystal,[185] the upconversion luminescence decreases down to 2% when temperature is increased from 15 to 300 K. This is explained only partially by the larger maximum phonon energy, 600 versus 350 cm^{-1} in chlorides and 220 cm^{-1} in bromides, which increases nonradiative transitions, and mainly by a decreasing absorption cross section at the laser excitation wavelength. Upconversion is here also mainly an APTE (ETU) process as shown by the time transient measurements.

4.2.6. Os^{4+} ($5d^4$) Ion

This 5d TM ion has been found to have also the right sequence of levels to show upconversion, see Figure 12. An APTE (ETU) effect is observed in Cs_2ZrCl_6:Os^{4+}(1%)[186,187] below 80 K; in Cs_2ZrBr_6:Os^{4+} two ESA processes lead to upconversion;[187] and in Cs_2GeF_6:Os^{4+}, no upconversion is detected.[187] Such differences are traced back, in the fluoride host, to the strong nonradiative decay from the $^1A_1(\Gamma_1)$ state, which would emit the visible light at about twice the excitation energy. In the bromide[188] and chloride[189] the level sequences allow both resonant and out of resonance ground-state absorption, which contribute to APTE (ETU), ESA, and avalanche upconversion (see section 4).

In the double-doped Cs_2NaYCl_6:Os^{4+}, Er^{3+},[190] upconversion is observed under a scheme similar to the pioneer work[170] involving a TM ion for absorption and a lanthanide for emission. The green emission from $^4S_{3/2}(Er^{3+})$ has been found to be both of the APTE (ETU) and ESA types (though called cooperative) with some back-transfer from Er^{3+} to Os^{4+}.

4.3. APTE (ETU) for Display and IR Detection Applications

In display technology the light-emitting material is always in powder form, traditionally called a phosphor. Because of various inclinations of the crystallite external surfaces reducing total internal reflection, more light output is extracted in a wider view angle from crystallites than from the equivalent single crystal. The upconversion phosphor field has recently been reinvestigated[191−195] for the now well-known two-photon and three-photon phosphors based, respectively, on Er−Yb and Tm−Yb codoped materials. Beyond the older light-emitting incoherent sources,[2] the renewed interest stems from potential applications ranging from simple handheld devices used to find IR laser beams[196−198] to visible enhanced detection of IR emissions, X-rays reusable memory plates,[199] and 3-D display technologies.[200]

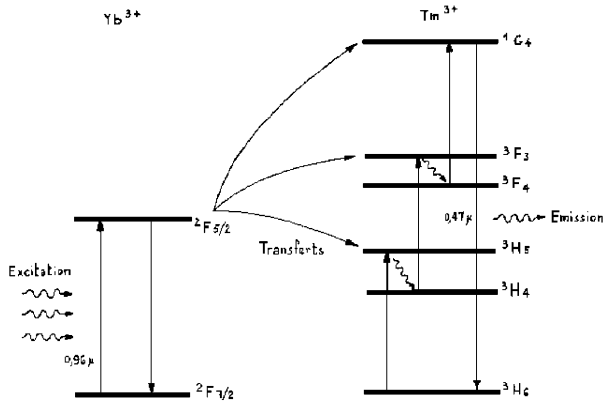

Figure 13. Three-photon APTE upconversion energy scheme in $Yb^{3+}-Tm^{3+}$ couples.

In particular, with now available tunable lasers and fiber beam homogenizers, the various efficiencies have been recently revisited in Krupke's group[191] with more refined experiments than pioneering ones.[158,201,202] Results essentially confirm the previously measured efficiencies below saturation; normalized efficiencies of 10^{-2} and 2×10^{-4} cm^2/W, for two photons, have been obtained, respectively, for the fluoride hosts $NaYF_4$ and $Na_2Y_3F_{11}$, instead of 10^{-3} cm^2/W as shown in Figure 3 and in Table 1 for YF_3. In the case of the Yb−Tm couple, the initial energy level diagram depicting the involved processes, as shown in Figure 13,[7] is confirmed[191] against the cooperative sensitization scheme[43] of Figure 3. In $NaYF_4$, efficiency as high as 2% is reached under pump excitation of 6 W/cm^2 at 960 nm, though a saturation density of 4 W/cm^2 is estimated for the first intermediate step ($^4H_4$). In the Yb−Er case, the saturation is found at about 100 W/cm^2 for fluoride hosts $NaYF_4$ and $Na_2Y_3F_{11}$;[191] observed saturation is explained by an excitation trapping into the long lifetime $^4I_{13/2}$ state. These more recently obtained results actually confirm the theoretical prediction[73,159] that fluorides should be the ideal hosts for green and blue emissions with the Yb−Er and Yb−Tm couples, see Figure 14.

In this respect, Quimby et al. studied heavy-metal fluoride glasses[203] and Auzel et al.[51] proposed and studied particularly efficient composite APTE (ETU) upconversion materials in which the RE ions were substituted into a crystalline matrix (PbF_2) itself embedded into an oxygen-based glass material. By such means, the multiphonon processes were optimized in the fluoride crystals whereas the overall sample was obtained through classical oxygen glass techniques. Silver nanometric particles have been shown to couple to lanthanide in glasses,[204] and such coupling has been used in Er−Yb-doped vitroceramics as a way to study this coupling inside a scattering medium.[205] As expected, it shows a quenching of the APTE process. The vitroceramic pioneering work has recently been extended to transparent glass ceramics by Ohwaki's group.[206] Transparency was obtained by reducing the crystallite ($Pb_{0.0.5}Cd_{0.0.5}F_2$) size down to about 20 nm.

The same group also recently investigated Er^{3+}-doped $BaCl_2$ and ErX_3 (X = Br, I)[207] polycrystalline phosphors for 1.5 μm detection cards,[198] which follow

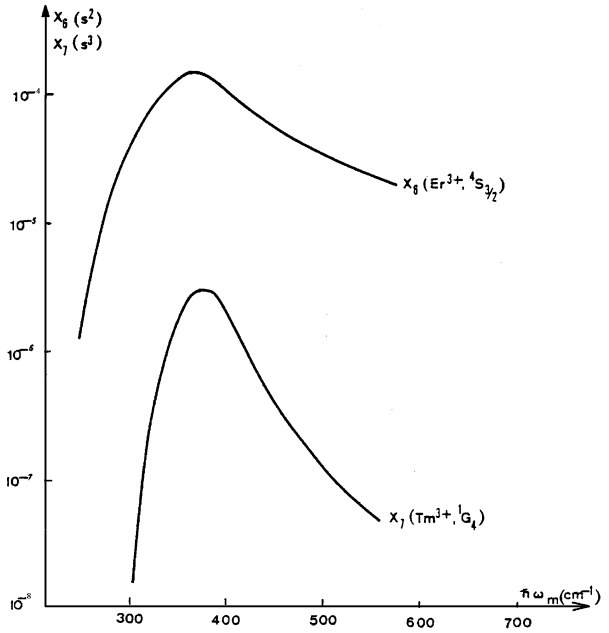

Figure 14. Theoretical effective phonon energy optimization for Yb−Er (green upconversion) and Yb−Tm (blue upconversion).

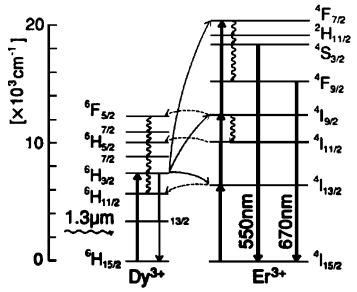

Figure 15. APTE scheme for 1.3 μm to visible upconversion in $Dy^{3+}-Er^{3+}$-doped $BaCL_2$. (Reprinted with permission from ref 208. Copyright 1994 American Physical Society.)

the upconversion processes described in Figure 5b. More recently, they demonstrated[208] a 1.3 μm to visible detection in a $Dy^{3+}-Er^{3+}$ codoped $BaCl_2$ phosphor. The involved APTE (ETU) scheme is given in Figure 15. As can be seen, Dy^{3+} is the sensitizer while Er^{3+} is the activator. It should be noted that some back transfer from Er to Dy is taking place and will be a basic limitation as it has been known for years that Dy^{3+} is a quencher for the Er^{3+} emissions.[2]

Besides equal energy photon summation as just seen, different energy photons may be summed up by APTE (ETU), so producing an effective IRQC with visible-enhanced IR detection.[209] Again, with the Yb−Er couple, embedded in vitroceramics of general composition, $PbF_2-GeO_2-YbF_3-ErF_3$, an IRQC has been obtained for 1.5 μm, using an additive pump flux at 0.96 μm. Final detection at 0.66 μm is obtained by summation as shown in Figure 16a. The experimental test scheme is presented in Figure 16b; the pump flux is produced by an IR GaAs:Si light-emitting diode (Mullard GAL-10); the signal is produced by a filtered tungsten lamp; a GaAs photocathode photomultiplier provides the final detection at 0.66 μm. A noise equivalent power of 10^{-11} WHz$^{-1/2}$ has been obtained for 3 mW of pumping at 0.96 μm and useful

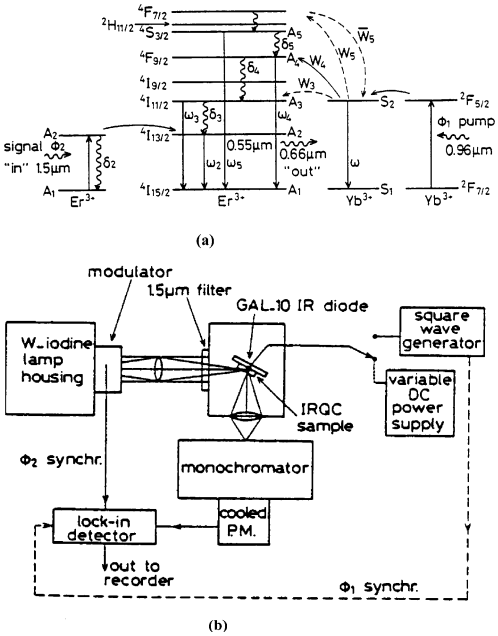

Figure 16. Experimental scheme for a 0.96 μm diode-pumped IRQC at 1.55 μm with energy transfers (a); experimental setup for IRQC detection at 1.55 μm (b).

concentration of 10%(Yb^{3+}) and 5%(Er^{3+}). As always in APTE (ETU) effects, it can be noted that the sensitizer concentration is larger than the activator one, as predicted by eq 22. Of course, if instead of a photomultiplier the detection is made through an electronic image intensifier, an imaging IRQC can be obtained for IR visualization purposes. This approach has recently been systematically considered in Smirnov's group[210] in order to make an IR image converter at wavelengths beyond the usual S1 or GaAS photocathode limits. Here, IR(1.5−1.6 μm) to -IR(0.8−0.9 μm) upconversion phosphors have been developed with the addition of microchannel image intensifiers. On the basis of $Y_{0.85}Er_{0.15}O_2S$ phosphors and an image intensifier with a GaAs photocathode, an IR sensitivity of 10^{-11} W/cm^2 is anticipated for an image converter screen illuminance of 0.1 cd/m^2.[211]

In another direction, reusable X-ray memory detection plates have been made from screens based on the same type of vitroceramics as mentioned above. X-rays are then the source of defect centers, which reduce the Yb lifetime, which in turn reduces the APTE upconversion efficiency. After an X-ray irradiation through the object to be investigated, the X-ray latent image is revealed in the visible spectrum by an IR irradiation at 0.96 μm, the Yb^{3+} excitation wavelength. The sensitivity is increased with the higher order upconversion processes. An image so produced in the blue spectrum is shown in Figure 17 for a three-photon APTE (ETU) process in a Yb−Tm-doped vitroceramic screen revealed under IR after a 90 KV, 5 mA, 1 min 45 s X-ray irradiation.[199] The screen may be reused after a heating procedure, which bleaches the defect centers.

The inherent nonlinearity of the APTE (ETU) process had been considered as an incoherent optical amplifier since the first days of APTE.[7] Its principle, given in Figure 18, is based on a two-beam scheme; one of them, the pump beam, is at broad band and

Figure 17. Latent X-ray image of a tooth in a Yb−Tm-doped vitroceramic, revealed by the blue emission under an IR irradiation at 960 nm.

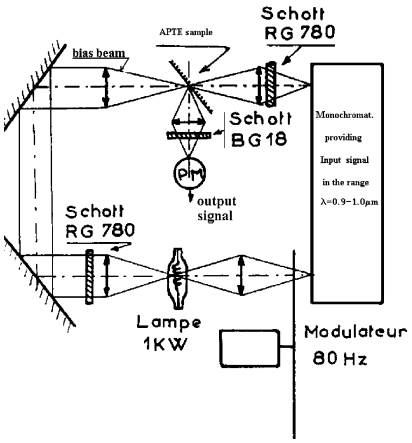

Figure 18. Incoherent amplifier scheme with an APTE sample.

CW; it fixes the bias point of the sample. The other beam (narrow band and modulated) is the signal beam which is tuned through the excitation band to be investigated. Practical gain of a few factors of 10 can be so obtained. This procedure has been effectively used to obtain the excitation spectra for upconversion both in 4f systems[7] and 5f systems (U^{4+} in $ThBr_4$ and $ThCl_4$),[161] in the absence, at the time, of synchronous electronic amplifiers.

The first proposed use of APTE (ETU) phosphors has been the handheld laser mode visualization screen[196] since then proposed again for visualization of both 0.96 and 1.5 μm spectral regions.[197,198]

In ending this section, it may be useful from an applied point of view to summarize in Table 1 the various values for measured normalized efficiencies as they have appeared in the literature. As it may have been noticed, such values are rarely given but are important in showing the relative practical interest of the various proposed upconversion schemes.

4.4. General Negative Roles Brought up by Undesired APTE (ETU) Effects

APTE (ETU) being an anti-Stokes process does induce reabsorption from excited states. Because it is so efficient when concentration and excitation

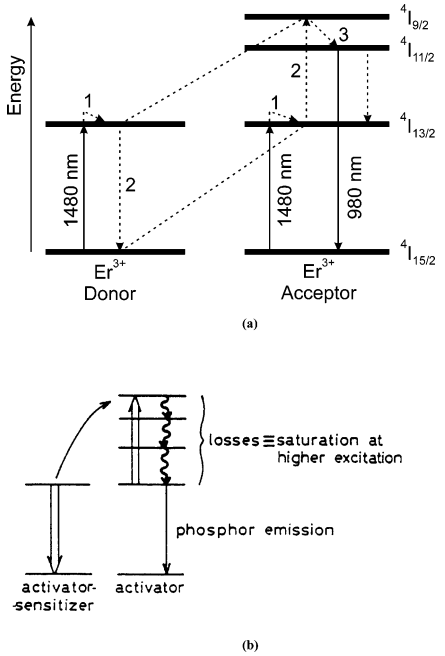

Figure 19. (a) Energy scheme for cluster quenching in an Er-doped amplifier. Reprinted with permission from ref 71. Copyright 1991 Institute of Electrical and Electronic Engineers.) (b) Energy scheme for APTE saturation in a cathode ray tube phosphor, note analogy. (Reprinted with permission from ref 216. Copyright 1983 Elsevier.)

density are high, it is sometimes an undesired pervading effect. Historically this effect takes its roots in a study on reabsorption from a population-inverted state in Yb−Er laser glass studies:[24] all visible light is obtained by upconversion at the expense of the 1.5 μm laser transition. In high-concentration Nd^{3+} laser materials, the so-called stoichiometric lasers, APTE effect may induce reabsorption.[118] Because upconverted energy feeds nonradiative states, this is a direct loss for the laser output. In NdP_5O_{14} such an effect begins when population inversion reaches 10%, whereas in YAG:Nd^{3+} where the concentration of RE ions is much lower, it cannot be seen even at high pumping levels.[212]

This type of APTE effect is also just the process that has been advocated to take place within Er^{3+} clusters and which limits the gain in optical fiber amplifiers,[71,93,94] providing the so-called nonsaturable ground-state absorption (see section 3.1 above). Its involved energy scheme is given in Figure 19a.

In a CW 2.7 μm Er^{3+} laser, it had first been thought that APTE had the positive effect of emptying the final $^4I_{13/2}$ laser state, avoiding a self-terminating or self-saturation behavior[213] due to the long lifetime of this final laser state.[214] An investigation of the various upconverted emission in $LiYF_4$:Er during the laser action at 2.7 μm brought some proof that APTE (ETU) was in fact emptying the laser emitting level $^4I_{11/2}$, thus being a drawback rather than an advantage.[130] Thus, the laser CW action was essentially linked with a direct reabsorption from $^4I_{13/2}$ of the pumping laser toward higher states.

Another important field in the phosphor domain is the availability of a high-intensity projection cathode-ray tube, which is presently universally used for large-screen television displays. At high excita-

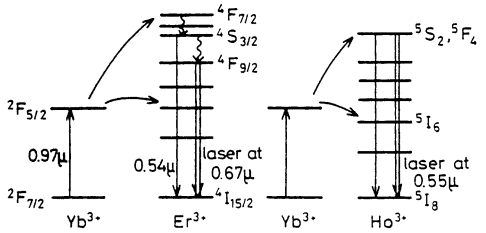

Figure 20. First operating APTE upconversion pulsed laser-pumping schemes in Yb−Ho and Yb−Er couples. (Reprinted with permission from ref 218. Copyright 1971 American Institute of Physics.)

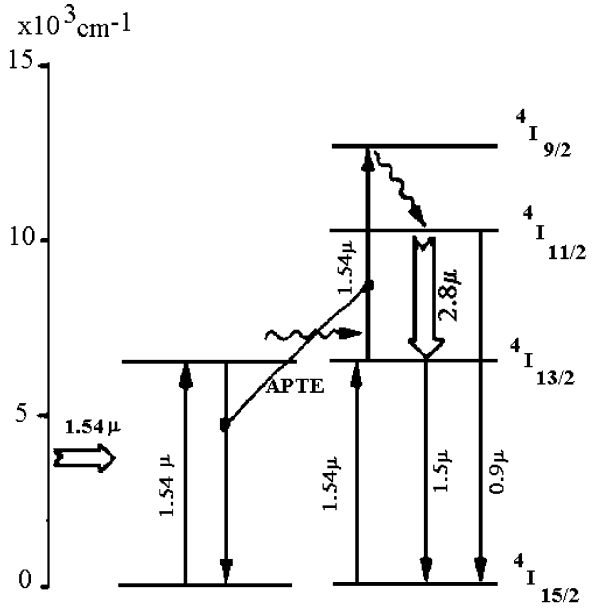

Figure 21. Upconversion APTE pumping in an Er^{3+} laser at 2.8 μm. (Reprinted with permission from ref 219. Copyright 1988 American Institute of Physics.)

tion, density saturation appears that has been partially attributed to APTE (ETU) for higher doping concentration;[215,216] the clear analogy with the cluster role in Er-doped amplifiers is shown in Figure 19b. It has been the explanation for Zn_2SiO_4:Mn, Y_2O_2S:Eu, and YAG:Tb. Furthermore, in electroluminescence phosphors such as ZnS:Mn, upconversion has been proposed to explain saturation.[217]

4.5. APTE (ETU) and ESA Pumped Lasers

Very early, APTE (ETU) effect has been demonstrated to be a new way for laser pumping. For example, in $Ba(Y,Yb)_2F_8$:Er and Ho, even with IR flash pumping,[218] respective pulsed emissions have been obtained at 0.67 and 0.55 μm as shown in Figure 20 in a three-level laser configuration at room temperature. The availability now of powerful CW IR laser diodes has rejuvenated this field. Because powerful blue laser diodes are still lacking for Stokes laser pumping, there are still many openings for APTE (ETU) anti-Stokes pumping.

By using the first two steps described in Figure 21, APTE (ETU) has been used to excite the $^4I_{11/2}$ of Er in CaF_2 to obtain a pulsed laser at 2.8 μm between that level and $^4I_{13/2}$.[219] Shortly afterward and for the first time, a CW upconversion laser in the green for the $^4S_{3/2}-^4I_{15/2}$ transition of Er at 0.551 μm has been

obtained in $LiYF_4$ under laser diode pumping at 0.791 μm at 40 K;[220] this was followed by obtaining the laser blue emission at 0.470 μm with a 10 mW threshold under the same conditions.[221]

Upconversion, attributed to the ESA type, has even provided violet emission at 0.380 μm in LaF_3:Nd^{3+} by summing an IR and a yellow laser pump or two yellow dye laser pumps,[222] however, only at low temperature (at 90 K). Low temperature has been a general drawback for CW upconversion lasers. In solids, a three-level scheme at room temperature generally becomes a quasi-four-level scheme at lower temperature. This explains why the first upconversion lasers were working in a pulsed mode at room temperature and continuous operation could only be obtained at lower temperature. This drawback has recently been overcome by using glass fibers or/and higher density laser pumping, so providing ground-state quasi-saturation. In particular, the versatile tunable Ti−sapphire laser has helped a lot in this matter.

In recent years, Huber's group in Hamburg has obtained many new upconversion laser results. After an initial pulsed laser operation in KYF_4:Er at 0.551 μm at room temperature,[223] the CW functioning has been reached,[224] in both cases with an attributed ESA upconversion pumping by a Ti−sapphire laser; for CW operation, the laser threshold has, however, the large value of 2.2−2.4 W. On the other hand, a very efficient CW laser effect has recently been achieved in a 3 mm long single crystal of $LiYF_4$:Yb(3%)−Er-(1%); the pumping at 0.966 μm at a level of 1.6 W was provided by a Ti−sapphire. An upconversion laser threshold of 418 mW was obtained, and the nature of the pumping was proved to be of the APTE type both by the laser excitation spectrum analysis replicating the Yb absorption spectrum and by a nonlinear narrowing as described in section 3.2. The laser useful output at 0.551 μm is 40 mW with 5% output coupling.[225]

Research on upconversion-pumped laser materials continues to be active, and groups of laboratories have considered $GdAlO_3$, $LiGd(MoO_4)_2$, $Y_3Sc_2Ga_3O_{12}$, and $Gd_3Ga_5O_{12}$, doped with Yb, Tm, not in the usual scheme with Yb pumping, but with Tm excitation by the $^3H_6$ to $^3H_4$ absorption with forth and back transfer with Yb.[154] The conclusion is that for $^1G_4$ (Tm^{3+}) emission at 480 nm, the $Y_3Sc_2Ga_3O_{12}$ host would be better than the $LiYF_4$ one.

Because of their inherent small core diameter, glass fibers easily allow one to obtain high pumping density over long lengths. Such high densities over long lengths cannot be provided by any lens focusing system. Ground-state depletion of any doped fiber can be easily reached with less than 100 mW pumping.[227] In particular, fluoride fibers favor anti-Stokes lasers for three reasons:

(i) the existence of long-lived metastable states linked with the low-energy phonons of the fluoride matrix;

(ii) ground-state saturation allowing a CW laser functioning even in a three-level laser energy scheme;

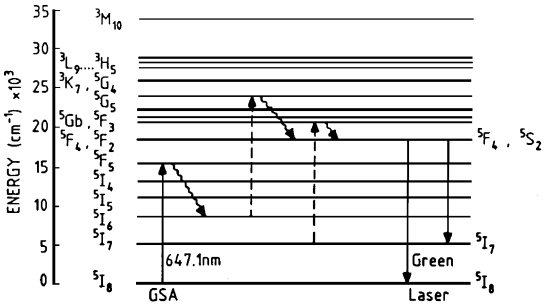

Figure 22. Energy scheme for the first visible CW upconversion Ho-doped fiber laser. (Reprinted with permission from ref 230. Copyright 1991 Institute of Electrical and Electronic Engineers.)

(iii) the advantage of a nonlinear pumping linked again with the optical confinement of the fiber medium.

Since the first demonstration in 1986[228] of the feasibility of CW room-temperature three-level lasers in the Er^{3+}-doped glass fibers, one could think that an upconversion-pumped three-level scheme could also be used in CW operation at room temperature for Er^{3+} emission at 540 nm.[132] After preliminary results, obtained first at 77 K with Tm^{3+}-doped fluorozirconate fiber, lasing at 455 and 480 nm,[229] the very first CW, room-temperature upconversion laser was demonstrated at CNET by Allain et al.[230] in a three-level scheme of the Ho^{3+}-doped fluoride fiber laser (Figure 22). Because of the weak Ho^{3+} concentration (1200 ppm), it was believed that within the single-ion level system ESA was taking place. However, since clustering with subsequent APTE (ETU) effect may sometimes occur at much lower concentration (70 ppm in ref 71), some doubt is cast about the effective pumping process, as in many of the subsequent upconversion-pumped fiber lasers.

Er^{3+}-doped glass fibers have also shown CW room-temperature three-level laser emission at 540 nm when pumped at 801 nm.[231] Because the pumping wavelength is in the diode laser range, there was some hope that a compact fiber laser could be obtained.

Besides these two-photon upconversion-pumped lasers, a three-photon pumped one has been demonstrated in a Tm^{3+}-doped ZBLAN fiber:[232] pumping at 1.12 μm, a room-temperature CW laser emitting at 480 nm, with a differential efficiency of 18%, has been obtained with the rather low threshold of 30 mW.

Pr^{3+}-doped fluoride fibers, because of their low phonon energy with respect to Pr^{3+}-emitting level energy differences, have allowed CW room-temperature anti-Stokes lasers at blue, green, and red wavelengths in a single fiber.[233] More detailed results on such upconversion laser recent evolution may be found in ref 234.

However, before closing this section, it is worth mentioning the possibility of upconversion laser with multiphonon pumping in the electronic rare-earth ion sideband transitions mentioned in section 3. It presents the advantage of the self-adaptation of the ESA absorption to a single pump wavelength. Upconversion pumping is successful through multiphonon sideband pumping with energy mismatches as large

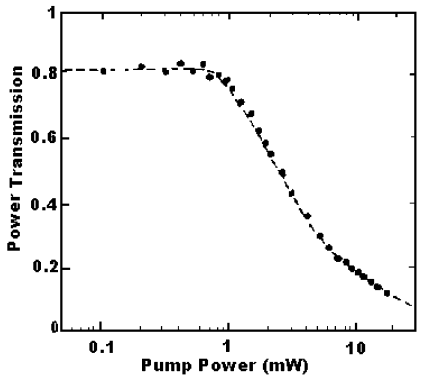

Figure 23. Decrease of transmission in a Pr^{3+}:$LaCl_3$ sample under $^3H_5-^3P_1$ pumping. (Reprinted with permission from ref 12. Copyright 1990 Elsevier.)

as 1000 cm^{-1}. This is the case for the Tm^{3+} fluoride fiber laser pumped at 1.06 μm in a three-photon ESA process and lasing at 1.47 μm.[235] This provides an efficient four-level scheme laser that allows CW oscillation with a differential efficiency of 27% at room temperature. On the other hand, this opens the door to long (kilometer) distributed amplifiers where the losses per unit length would be compensated at each point by the gain; the transmission line would then be turned into a lossless line.

Multiphonon pumping is also one of the processes involved in the avalanche upconversion process described in the next section.

5. Cross-Relaxation and the Photon Avalanche Effect

The most recently discovered upconversion process is the photon avalanche effect.[11] Since it has not been considered in the review of 1973,[2] more detailed attention will be paid to it here.

While looking for two-step absorption (ESA) in Pr^{3+}-doped $LaCl_3$ and $LaBr_3$ at low temperature (<40 K) as a means to detect an IR photon by its energy summation with a more energetic photon (IRQC) so performing excited-state absorption (ESA), it was found that the higher energy photon alone could, in the same time, give rise to upconversion and reduce the transmission of the sample above a given intensity threshold;[11] see Figure 23. The effect was attributed to an increase of population of an excited state resulting from a cross-relaxation process. The starting process was initially not completely determined. In the Pr^{3+} case, the $^3H_5$ $^3P_1$ absorption is initially very weak at low temperature because $^3H_5$ is about 2000 cm^{-1} above the ground state (see Figure 24); however, above about 1 mW of excitation, this transition is increased; the cross-relaxation process ($^3H_6$, $^3H_4$) ($^3H_5$, $^3H_5$) increases the $^3H_5$ population which in turn reduces the transparency of the sample at the ($^3P_1-^3H_5$) energy. Since the more the ($^3P_1-^3H_5$) energy is absorbed the more the $^3H_5$ population is increased, the process was termed photon avalanche.[11] It is clearly a way to increase ESA in a sample.

Afterward, similar effects have been observed in Sm^{3+}-, Nd^{3+}-, Ni^{2+}-, and Tm^{3+}-doped halide crystals.[236−239] Recently the photon avalanche effect has been obtained at room temperature for the Er^{3+} ion in a ZBLAN glass both in bulk and in fiber form[240−243] and in a $LiYF_4$ crystal.[244]

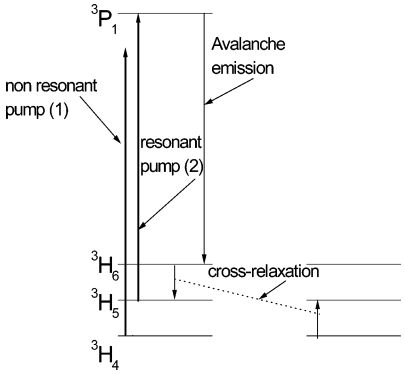

Figure 24. Simplified $LaCl_3$:Pr^{3+} energy scheme for the avalanche mechanism.

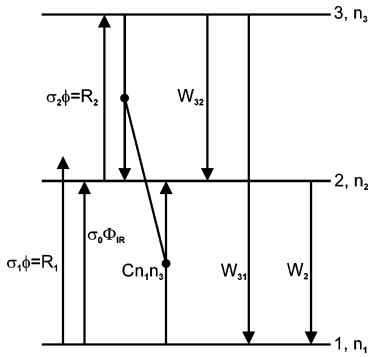

Figure 25. Avalanche simplified three-level scheme; C is the cross-relaxation coefficient; W_{ij} are the spontaneous emission terms.

The photon avalanche process is characterized by three distinct nonlinear behaviors:

(i) transmission, (ii) emission, and (iii) rise time on the pump power intensity with generally the existence of a critical pump threshold.

Particularly long rise times, from seconds to minutes,[244,245] have been observed.

At this point it is worth discussing the notion of threshold for avalanche. Because of the complexity of the phenomenon, it has been usually modeled by a simplified three-level system.[246−248]

5.1. Avalanche Process as a Positive Feedback System[244]

Using the three-level simplified model of ref 246 or 247 and adding to the initial ground-state absorption ($\sigma_1\Phi = R_1$) an auxiliary direct feeding into the metastable state ($\sigma_0\Phi_{IR}$) we may write the following set of equations (see Figure 25 for explanation of symbols which except for the trigger $\sigma_0\Phi_{IR}$ are the same as in ref 246).

Being interested in the steady-state initial step of avalanche, we assume

$$\text{(i)}\ \frac{dn_1}{dt} = \frac{dn_2}{dt} = \frac{dn_3}{dt} = 0$$

$$\text{(ii)}\ n_1 = 1 - n_2 - n_3 \approx 1$$

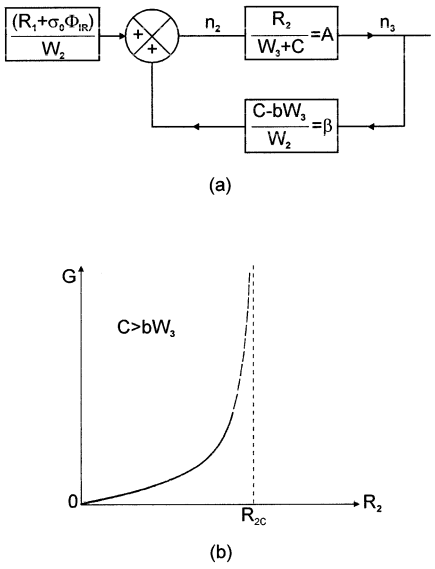

Figure 26. (a) Positive feedback model for avalanche. (b) Gain behavior of the model versus R_2; positive feedback condition is $b > CW_3$; the asymptote R_{2c} corresponds to the avalanche threshold.

Then the rate equations are simplified to

$$0 = -R_1 - \sigma_0\Phi_{IR} + bW_3n_3 + W_2n_2 - Cn_3 \quad (27)$$

$$0 = (1-b)W_3n_3 - W_2n_2 + 2Cn_3 + R_1 + \sigma_0\Phi_{IR} - R_2n_2 \quad (28)$$

$$0 = R_2n_2 - W_3n_3 - Cn_3 \quad (29)$$

with C being the cross-relaxation parameter and b the branching ratio, the following relationships exist between the transition probabilities

$$(1-b)W_3 = W_{32};\ bW_3 = W_{31};\ W_3 = W_{32} + W_{31}$$

Equation 29 can be written as

$$n_2\frac{R_2}{W_3 + C} = n_3 \quad (30)$$

Considering amplitude and using the symbolic representation for feedback systems, eq 30 gives block A of Figure 26a.

In the same way, eq 27 is written

$$n_2 = \frac{R_1 + \sigma_0\Phi_{IR}}{W_2} + \frac{C - bW_3}{W_2}n_3 \quad (31)$$

which can be symbolized in Figure 26a by block β and an adder with input source

$$(R_1 + \sigma_0\Phi_{IR})/W_2$$

Combining eqs 31 and 30 gives the classical feedback systems scheme of Figure 26a.

Such a system is known to be unstable for $A\beta = 1$. One can define a gain of the closed loop feedback system, G, by the ratio between the green output to a pump related input signal (R_1) plus an eventual external trigger (Φ_{IR})

$$G = \frac{n_3}{(R_1 + \sigma_0\Phi_{IR})/W_2} \quad (32)$$

It is well-known that in terms of the A and β of Figure 26a, one has

$$G = \frac{A}{1 - A\beta} \quad (33)$$

The stability condition is then written as

$$\frac{R_2}{W_3 + C}\frac{C - bW_3}{W_2} < 1 \quad (34)$$

Its limit is just the threshold condition given by Joubert et al.[246] obtained here in a simplified way as

$$R_{2C} = \frac{W_2(W_3 + C)}{C - bW_3} \quad (35)$$

with $C > bW_3$ for a positive feedback.

The behavior of our feedback system below threshold can be described by the behavior of $G(R_2)$, Figure 26b.

The feedback black box approach has also been considered in studying the dynamics of the above three-level system.[249] It is based on the fact that the general feedback linear theory may solve algebraically time variable differential equation systems by using the Laplace transform of the time-dependent functions.

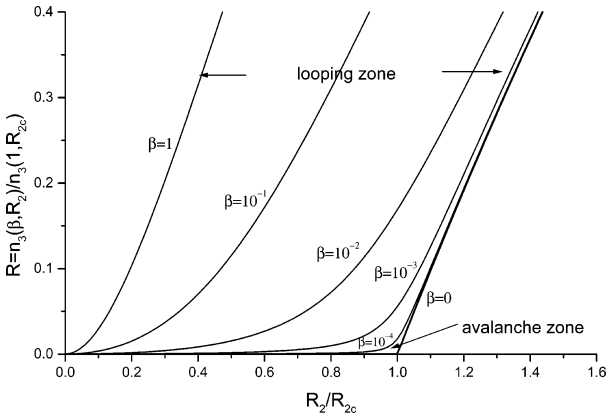

Figure 27. Third-level normalized population, $R = n_3(\beta,R_2)/n_3(\beta = 1,R_2 = R_{2c})$, versus pumping term ($R_2$) with β as a parameter. (Reprinted with permission from ref 248. Copyright 1995 Elsevier.)

5.2. Conditions in Order To Observe an Avalanche Threshold[248,250]

Neglecting the first nonresonant absorption step (R_1) and taking into account only the second resonant absorption step (R_2) when calculating the population of the third level (n_3) versus R_2 (the pumping excitation) leads to a well-defined nonlinearity in n_3 for the asymptotic curve ($R_1/R_2 = 0$), as shown in Figure 27.

When the first step (R_1) is explicitly taken into account,[248] the threshold nonlinearity is progressively smoothed out while increasing the ratio R_1/R_2 as

shown in Figure 24. This corresponds to a progressively more resonant first step. As shown by Goldner and Pellé,[248] practically a clear avalanche threshold can be expected only for $R_1/R_2 \leq 10^{-4}$

Some of the features of the avalanche effect have been observed at room temperature in Tm^{3+}:$YAlO_3$[239] and in Pr^{3+} in silica glass fibers.[251] The lack of a clear threshold in these two systems can certainly be related to the above prediction.

The region in Figure 24, where $10^{-4} < R_1/R_2 < 1$, corresponds to cases for which the losses in the feedback loop may exceed the loop gain for R_2 values below R_{2C}, so that after a number of loopings of the excited population between level 3 and the metastable level 2, the system would neither diverge nor maintain n_3 independently of R_1. Such cases have been called a looping mechanism.[252] We believe that some of the reported cases of quasi-zero threshold avalanche cases in the literature[251,253] belong to large $10^{-3} < R_1/R_2 < 1$ cases for which, as shown in Figure 24, it is very difficult to distinguish between avalanche and sequential two-photon absorption (ESA) which occurs strictly for $\beta = 1$. Sometimes such cases have been termed quasi-avalanche.[248] This intermediate behavior has been well studied in $YAlO_3$:Er^{3+} under 790−810 nm excitation.[254] The three kinds of upconversion, ESA, APTE(ETU), and quasi-avalanche, are simultaneously found to exist according to the precise excitation wavelength. For a 796 nm excitation, the blue-green upconversion is attributed for 23% to ESA and for 77% to the looping effect (quasi-avalanche).

Er^{3+}, with $(R_1/R_2) \cong 10^{-6}$, has shown at room temperature all three characteristic features of avalanche when doping a $LiYF_4$ crystal or a ZBLAN fluoride glass both in bulk and in a fiber shape (see sections 5.3 and 5.4); even a long delay of several seconds to a minute was observed.[242−244] For comparison, the following values for the critical parameter ($\beta = R_1/R_2$) have been found for Nd^{3+}−$LiYF_4$, $(R_1/R_2) = 1.7 \times 10^{-4}$ for avalanche at $T = 40$ K;[237,246] for Tm^{3+}−Ho^{3+}−$Gd_2Ga_5O_{12}$, $(R_1/R_2) = 3.6 \times 10^{-2}$ for the two-ion looping process;[255] for a Tm^{3+}−BIGaZYTZr glass, $(R_1/R_2) = 1.2 \times 10^{-2}$ [256] for what was claimed to be avalanche at 100 K.[257] In this last case since the delay reaches only 16 times the metastable state lifetime (W_2^{-1}), it looks more like a looping process case. In Er^{3+}, as can be seen from sections 5.3 and 5.4, the avalanche delay reaches 6×10^2 to 10^4 times W_2^{-1}, respectively, for Er-doped fluoride glass and crystal.

For Tm^{3+} ions, in divalent fluorides, SrF_2, CaF_2, BaF_2, and CdF_2, avalanche has been studied[258] in a red to blue upconversion scheme. Avalanche is characterized by the slow build-up of the signal and the spatial spreading. In Y_2SiO_5:Tm^{3+},[259] avalanche, as shown by a kick in the output slope, n, for 100 mW excitation, is believed to explain $^1G_4$ emission, whereas upconversion from $^1D_4$ is attributed to ESA and APTE (ETU).

In a ZBLAN glass, doped either with (0.1−5%)Ho^{3+} alone or with Ho^{3+} and (3%)Tm^{3+},[260] clear avalanche threshold is obtained at about 140 W/cm^2 of 585 nm laser excitation for the codoped sample, at both 77 and 300 K. Establishing times, which are the signatures for avalanche, are, respectively, 250 and 30 ms. Upconverted emission from Ho^{3+} is at 545 nm from $^5S_2/^3F_4$. The nonresonant first step is in a multiphonon sideband and for the second resonant step in static pair levels induced on Ho^{3+} by Tm^{3+} as reveled by the excitation spectrum.

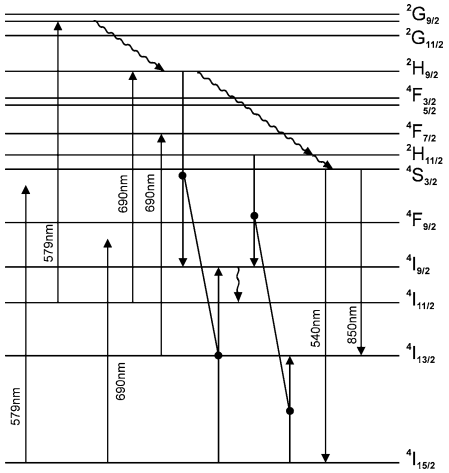

Figure 28. Energy scheme of Er^{3+}, and principal mechanisms responsible for photon avalanche cycles under excitation at 579 and 690 nm.

As for other types of upconversion, the advent of research with d ion-doped crystal has shown that avalanche could also be obtained with such ions. Cs_2ZrBr_6:Os^{4+} [187,188, 261] has shown clear signs of an avalanche process: slowing of the upconversion establishment from a few milliseconds up to 1.5 s at a threshold of 3.8 mW and nonlinearity (higher slope) in the slope 2 line of the two-photon upconversion process when excited aside the resonant ground-state absorption. From the information given, one can estimate the R_1/R_2 ratio to be in that case 5×10^{-3}. This is weak in principle to show a marked threshold, yet one can compute that the number of feedback loops is about $1.2/1.6 \times 10^{-3} = 750$, which is as large as in an Er-doped ZNLAN glass (see above). In Cs_2ZrCl_6:(1%)Os^{4+},[189] signs of avalanche with a weak threshold of 2.6 mW have also been found from 15 to 50 K. The fitted R_1/R_2 ratio is given to be 3.3×10^{-3}, which also is weak for a marked threshold. Here the number of looping cycles is only about $0.5/20 \times 10^{-3} = 25$. This is a quasi-avalanche or looping effect.

5.3. Er^{3+}–$LiYF_4$ as an Avalanche Model Experiment

In the case of Er^{3+}, the first step for photon avalanche has been clearly identified and attributed to anti-Stokes multiphonon sideband absorption[240,241] (see Figure 28). Calculating the R_1/R_2 ratio from mutiphonon absorption allows one to estimate a value of 5×10^{-6},[243,244] as shown in Figure 29, which displays the multiphonon sideband absorption in the avalanche excitation region. As observed, this experimental situation provides a marked threshold behavior in the erbium case.[240]

The simple theory of section 5.1 has been verified by experimentally measuring $G(R_2)$. This was done using the following method (see the experimental

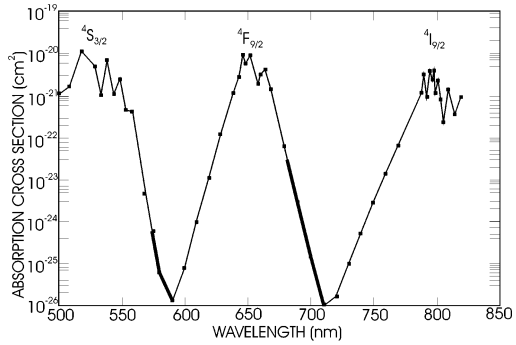

Figure 29. Absorption cross section for $Er^{3+}-LiYF_4$ taking into account the multiphonon contribution; the heavier lines show the anti-Stokes zones which contribute to W_1 for the avalanche processes in erbium.

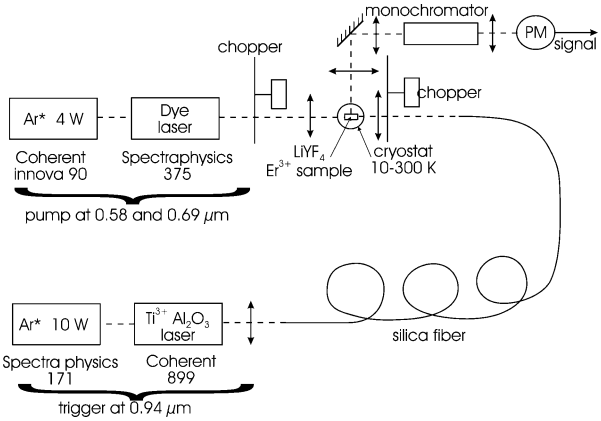

Figure 30. Experimental scheme for measuring the positive feedback gain and for an external triggering.

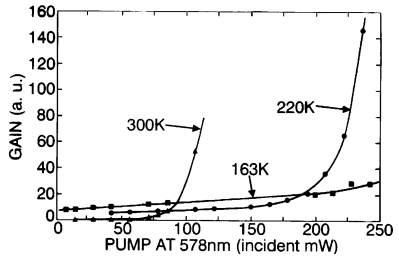

Figure 31. Experimental $G(R_2)$ for three temperatures: 30, 220, and 163 K; residual signal near $R_2 = 0$ comes from direct upconversion under 0.94 μm excitation.

setup in Figure 30): having obtained a given green output for a pump R_2 with $\Phi_{IR} = 0$, R_2 is reduced while increasing Φ_{IR} in order to maintain a constant green output. Φ_{IR} is an infrared signal at 0.94 μm in resonance with the metastable state 2 (here $^4I_{11/2}$) absorbing with a cross-section σ_0.

Each point is obtained after waiting for a steady state. Because of the large ratio for σ_0/σ_1, this experiment provides a good description of $G(R_2)$, as shown by the results in Figure 31 for three temperatures. One can define an R_{2C} asymptote only at 300 and 220 K, respectively, 120 and 240 mw. At 163 K one cannot reach an asymptote (threshold) in that experiment at the maximum available power of 250 mw. Thus, the effect of lowering temperature is essentially to increase R_{2C}.

The part in R_{2C} which is most sensitive to temperature is C because it is related to the phonon energy of only 100 cm^{-1}, whereas W_2 and W_3 are related to phonons covering the energy gap below levels 3 and 2, that is energies >2000 cm^{-1}. However, this requires C to be of the same order as W_3 or bW_3; otherwise, as long as $C \gg W_3, bW_3$, one has $R_{2C} \cong W_2$ and its temperature dependence is just the same as W_2.

Comparing the theoretical threshold as given by eq 35 with experimental conditions, one can verify the simple feedback model.

Assuming level 1 to be $^4I_{15/2}$, level 2 to be $^4I_{11/2}$, and level 3 to be the aggregation of levels between $^2G_{9/2}$ and $^4S_{3/2}$ with the emission properties of $^4S_{3/2}$ (see Figure 28) and taking the room-temperature data given by ref 256 and 257, the following parameters are found: $W_3 = 2500\ s^{-1}$; $b = 0.5$; $C = 0.5 \times 10^6\ s^{-1}$; $W_2 = 140\ s^{-1}$, because corresponding oscillator strengths are about equal (0.4×10^{-6}),[262] one can also assume $\sigma_2 = \sigma_0 = 4 \times 10^{-21}\ cm^2$.

Using reduced population units (pure number), it becomes $R_{2C} = 140(2500 + 510^5)/(510^5 - 1250) = 141\ s^{-1} \cong W_2$ (at room temperature) from which it can be estimated

$$\Phi_{threshold} = 141/4 \times 10^{-21} = 3.5 \times 10^{22}\ s^{-1}\ cm^{-2}$$

At 0.578 μm it gives, for a 50 μm diameter spot, a threshold power of $P_{th} = 222$ mW; this value is of the same order as threshold values observed for 0.578 μm pumping.

$G(R_2)$ shows (Figure 26b) that the Er^{3+}-doped solid constitutes a marginally stable positive feedback system: even below the R_{2C} asymptote, it is known from feedback theory that a strong input signal can drive a system that is otherwise stable into its instability state (existence of a gain stability margin).

To experimentally verify this behavior, a pulsed trigger of amplitude $\sigma_0\Phi_{IR}/W_2$ is added to the input signal R_1/W_2 given by the pump; the experimental setup is again the same as that presented in Figure 30.

The results at room temperature are given in Figure 32a−c. In the absence of a trigger, with $Pp =$ 114 mW at 578 nm incident on sample, the threshold is reached after a very long time (>50 s) (Figure 32a). With the same pump intensity ($Pp = 114$ mW) and with a short trigger of 0.6 s, the avalanche state is obtained quickly and maintained after trigger extinction (Figure 32b). With the same trigger but with a reduced pump ($Pp = 99$ mW), the avalanche state cannot be reached. This behavior, as depicted in Figure 32a−c, is obtained down to 180 K.

Below 180 K, the observed threshold increases as shown in Figure 31. However, due to the temperature scan cycles relatively short time constant (3 s/K from 10 to 50 K, then 21 s/K from 50 to 150 K), it is not sure whether or not the threshold could be reached for an avalanche delay time >50s.

From this experiment, it is understood that measuring an avalanche threshold depends on the time one is ready to wait before its observation. This time depends not only on the excited-state pumping but also on the ground-state absorption conditions. In any

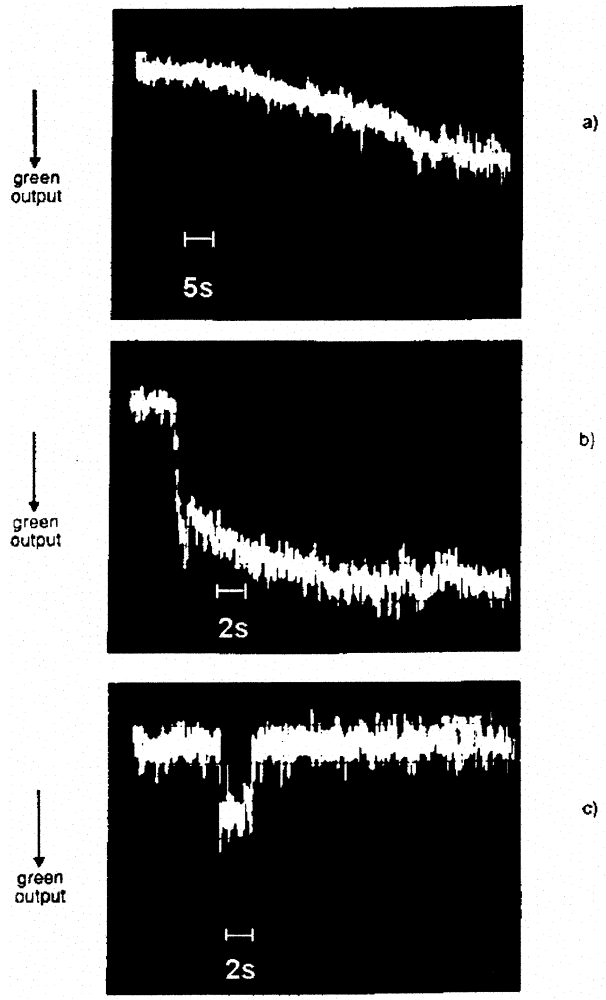

Figure 32. Avalanche behavior just below threshold without (a) and with (b) a trigger feeding the metastable state and (c) much below threshold.

case, below 180 K, being then limited by the pump laser at a much lower power than the threshold, the result of Figure 32c is obtained. This triggering effect constitutes an optical analogue of a thyratron providing an intrinsic material-based optical bistability.

The time delay behavior of the avalanche process has been studied theoretically quite recently within the general model of Landau for phase transition.[256] The time delay at threshold, in fact a critical slowing time, t_c, proved itself to be the most sensitive experimental data when looping or avalanche takes place. It has been shown to be given by[256,263]

$$t_c = K\sqrt{\sigma_2/\sigma_1} \qquad (36)$$

where K depends on other spectroscopic parameters. Equation 36 is rather well verified in the above experiments for which avalanche delay times have been determined for two different excitation wavelengths of known multiphonon anti-Stokes cross sections: at $\lambda = 688$ nm, with $\sigma_1 = 10^{-24}$ cm^2, delay is found to be 0.4 s; whereas at $\lambda = 579$ nm, with $\sigma_1 = 2 \times 10^{-26}$ cm^2, the observed delay is 4 s. Assuming for σ_2 the same value in both cases of excitation, the ratio of the delays is 0.1, which is in agreement with the value of 0.14 as given by eq 36.

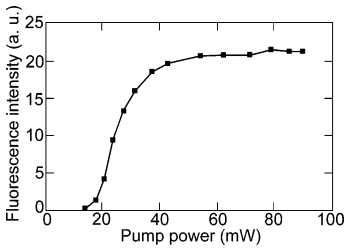

Figure 33. Upconversion emission at 550 nm showing the existence of the avalanche threshold in a ZBLAN:Er^{3+} fiber observed from its extremity.

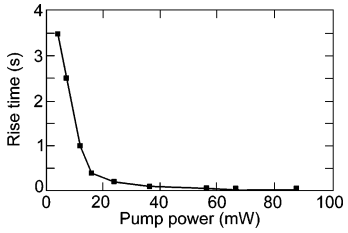

Figure 34. Time delay for the avalanche establishment versus incident pump power at 579 nm in a ZBLAN:Er^{3+} fiber.

Above the threshold, the delay for avalanche has been given by ref 264 as

$$t_c = kW_2^{-1}/(\Phi/\Phi_c - 1) \qquad (37)$$

with $k = W_3^{-1}/(1 + b)(2C + W_3)$ and where $\Phi_c = R_c/2$ is the pumping flux at threshold and Φ the effective pumping flux.

5.4. Photon Avalanche in Er^{3+}–Fluoride Glasses in Fiber and Bulk Shape

Recently, the photon avalanche effect has been observed at room temperature in a Pr^{3+}-doped silica fiber[251] and in an Er^{3+}-doped fluoride glass fiber.[241,243] In the first case, only a nonlinearity of the transmission is observed and not the upconversion emission threshold. It was believed that the threshold was so low that it could not be observed.We think that this is explained by the too large nonresonant to resonant absorption ratio as mentioned in section 5.2. On the other hand, in the second case, clear thresholds at 5 and 4 mW of incident power at, respectively, 579 and 690 nm[243] are observed because in these last two cases the first step is a weak anti-Stokes multiphonon absorption giving again a R_1/R_2 ratio of about 10^{-6}, much below the critical value of 10^{-4}. The involved energy scheme for both excitations is essentially the same as that in Figure 28; it shows both pumping routes and the two types of involved cross-relaxations. In Figure 33, the typical threshold behavior for the avalanche upconversion emission is presented. The long delay behavior is displayed in Figure 34, showing, near threshold, the very long time (3.5 s), widely in excess of any of the lifetimes of the metastable states of erbium. The observed delay follows rather well the behavior predicted by eq 37.

As for glass fibers, the same results can be obtained in bulk samples.[240,241] Because the first absorption step, being of a multiphonon nature, is featureless, the excitation spectrum for avalanche directly pro-

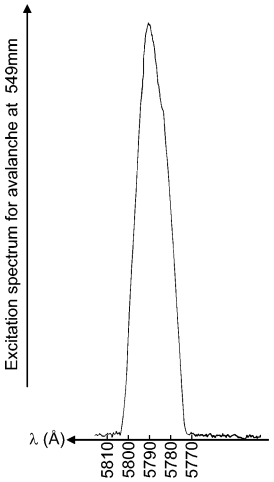

Figure 35. Excitation spectrum for the avalanche emission at 549 nm in a ZBLAN:Er^{3+} glass showing the spectrum for the $^4I_{11/2}-^2G_{9/2}$ ESA transition.

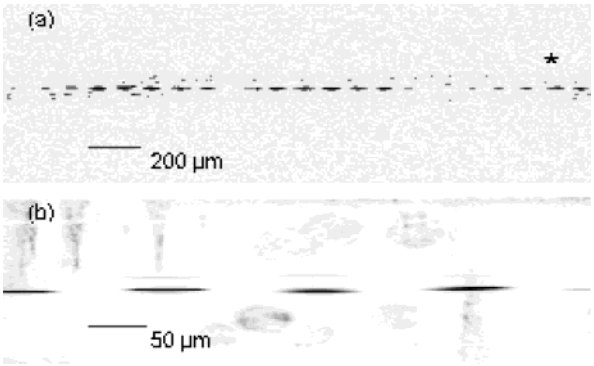

Figure 36. Spatial domains observed along the fiber above the photon avalanche threshold: (a) dot separation about 1 mm. (b) Microscope view of a 1 mm avalanche dot. The scale is 100 μm per division.

vides the ESA spectrum of the resonant second absorption with a single excitation beam as shown in Figure 35 for the $^4I_{11/2}-^2G_{9/2}$ transition of Er^{3+}; this gives a new method[242] to reach ESA spectra otherwise difficult to obtain without a double-beam excitation.

The main difference with a bulk sample is that in the fluoride fiber case upconversion spatial domains appear with periodic structures with periods ranging from a few centimeters to millimeters themselves containing substructures with a period of about 100 μm,[241,243] as shown in Figure 36. This behavior has been explained by the high contrast provided by the avalanche effect; it then optically reveals the internal electric field mode structure of the fiber waveguide.[241,265]

5.5. Avalanche in Codoped Systems

Up to this point, avalanche has been described within a single type of ions. As far as energy transfers in general are considered, the sensitizers and the acceptors may be either of the same or of a different nature. Thus, in the avalanche process, instead of having two ions of the same nature participating in the cross-relaxation step, as described to date, the cross relaxation has also been considered between two ions of a different type. This was the case of the first study by Brenier et al. of the avalanche involving

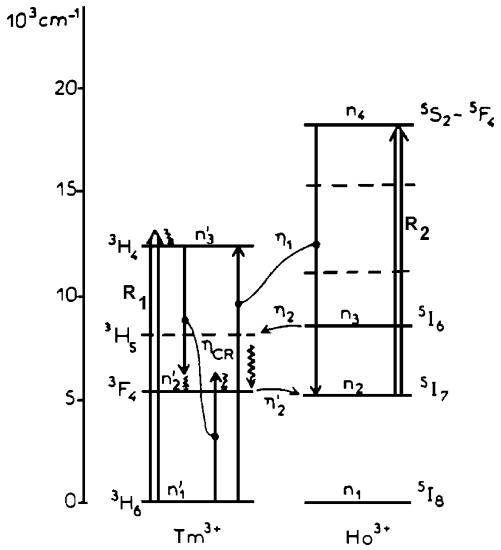

Figure 37. Energy scheme and mechanism for looping effect in the $Ho^{3+}-Tm^{3+}$ codoped system. (Reprinted with permission from ref 255. Copyright 1994 Elsevier.)

$Tm^{3+}-Ho^{3+}$.[255] A complex process of cross-relaxation within two Tm^{3+} ions together with a back transfer from Ho^{3+} to Tm^{3+} has been proposed. The first excitation step is out of resonance with the $^3H_6-^3H_4$ absorption of Tm^{3+}; it is followed by a cross-relaxation within two Tm^{3+} ions; which populates the $^3F_4(Tm^{3+})$ state, itself transferring its energy to the $^5I_7(Ho^{3+})$ state from which the resonant second step of excitation toward $^5S_2(Ho^{3+})$ takes place. Then another cross-relaxation (energy back-transfer) between Ho^{3+} and Tm^{3+} of the type $^3H_6(Tm^{3+}) + {}^5S_2(Ho^{3+}) \Rightarrow {}^3H_4(Tm^{3+}) + {}^5I_7(Ho^{3+})$ provides the feedback loop, see Figure 37. However, the avalanche threshold is not reached, and calculating the R_1/R_2 ratio from the data in ref 255, the critical parameter

$$\beta = 6.16 \times 10^{-22}/1.73 \times 10^{-20} = 3.6 \times 10^{-2}$$

is determined. This clearly confirms, what the authors have found, that the behavior of this system is in the looping region of Figure 27. The looping process is different from avalanche in the sense that it has a reversible character that real avalanche does not have. In the case of the codoped Yb−Pr system, real avalanche has been reached.[266] In this system, see Figure 38, the first nonresonant excitation step is in the Yb^{3+} ion, which transfers to the metastable state $^1G_4(Pr^{3+})$ from which the resonant second step up to $^3P_0(Pr^{3+})$ takes place. The cross-relaxation step within two Pr^{3+} ions feeds the metastable state $^1G_4(Pr^{3+})$ and the back transfer to Yb^{3+} again feeds the $^1G_4(Pr^{3+})$ metastable state. The ratio β from the nonresonant to resonant pumping was estimated to be from 10^{-6} to 10^{-8} [266], well within the condition to observe a real avalanche threshold.

In $YalO_3$:(10%)Yb, (1%)Ho,[267] a green emission from $^5S_2$(Ho) is obtained under 750 and 840 nm excitation. Yb plays a role in the back transfer which helps to populate the metastable state $^5I_6$ (Ho). A slight nonlinearity found in the output signal slope is an indication of a looping mechanism.

The Ho−Tm codoped ZBLAN glass system[260] observed in section 5.2 does not seem to enter into the

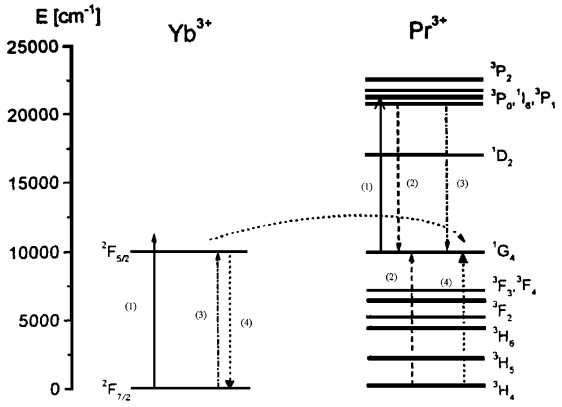

Figure 38. Energy scheme and mechanisms for the codoped $Yb^{3+}-Pr^{3+}$ avalanche system: pumping at 0.85 μm into Yb^{3+} sideband and in resonance by ESA into Pr^{3+}; cross-relaxation within Pr^{3+}; $Yb^{3+}-Pr^{3+}$ cross-relaxation; $Pr^{3+}-Yb^{3+}$ back-transfer. (Reprinted with permission from ref 266. Copyright 2000 Elsevier.)

avalanche codoped category since the Tm ion does not seem to play a role in the feedback loop but only in the R_2 excitation term.

In analogy with the previous case, avalanche in $La_{1-x}Ce_xCl_3:Nd^{3+}$ [268] shows that for $x > 0.1$, Ce plays a role in increasing the avalanche output signal. This effect is attributed to the presence of undefined pair states in clusters.

Other systems with codoping with 4f and 5f ions have been investigated: In $LaCl_3$:(1%)Pr^{3+}, (0.1%)-U^{3+},[269] under a dye laser excitation between 615 and 617 nm, the blue emission from $^3P_0$ to $^3H_4$ in Pr^{3+} is observed at the very low level of 2 mW and is ascribed to a double excitation: the first one from the ground state in U^{3+} and the second one between excited states in Pr^{3+}; cross relaxation between U^{3+} and Pr^{3+} provides the population of the metastable level $^3H_6$-(Pr^{3+}) from which takes place the resonant ESA to $^3P_0$(Pr^{3+}). However, because the matching is probably too good between excitation and ground-state absorption, no real threshold is observed and a looping mechanism is advocated to explain that the presence of U^{3+} increases the blue output of Pr^{3+} by 3 orders of magnitude.

5.6. Upconversion Laser with Multiphonon-Assisted Pumping Scheme and Photon Avalanche

Besides pumping in the electronic RE ions transitions, we have also seen that upconversion laser pumping could be attempted in multiphonon sidebands with energy mismatch as large as 1000 cm^{-1};[235] see section 4.5.

Of course, most of the avalanche-pumped lasers also enter this category because of the required weak first step absorption. It is worth mentioning the first avalanche laser in $LaCl_3:Pr^{3+}$.[270] A CW emission in a four-level scheme was obtained at 0.644 μm through an upconversion avalanche process under 0.677 μm pumping which corresponds to an ESA pumping for the second step and probably to multiphonon absorption for the first step, as recently observed for amplified spontaneous emission at 0.850 μm in a ZBLAN:Er^{3+} fiber in an avalanche-pumped regime.[271] Powerful avalanche-pumped upconversion lasers have been obtained in a CW regime, first at low temperature (7 K) in YAlO:Er^{3+};[272,273] 33 mW of output at 0.549 μm has been reached with an optical efficiency of 3.5%. Interestingly, the same crystal system may provide laser under APTE (ETU) upconversion pumping simply by tuning-in the first excitation step (0.8069 μm). The laser threshold is then lowered (~100 mW) in comparison with the avalanche regime (~380 mW at 0.7913 μm); the output law is quadratic versus pumping in the APTE (ETU) regime, while for the avalanche regime it has a much higher power law above threshold saturating toward a square law at about 1 W of incident pump power. In the APTE (ETU) regime, the laser output is 166 mW with an optical conversion efficiency of 17%.

As already mentioned in section 4.5, fiber optical confinement may allow one to obtain CW three-level lasers even at room temperature. This has also been the case for avalanche-pumped lasers. A high-power upconversion laser has been demonstrated in a ZBLAN:Pr,Yb double-clad fiber under avalanche pumping.[274] The energy scheme and avalanche processes, which are involved, are the ones described in the previous subsection for the avalanche process with Yb−Pr codoping.[266] Laser emission is from the $^3P_0-^3F_2$ transition of Pr^{3+} at 0.635 μm with a record output of 1020 mW. The pumping is from two Ti−sapphire lasers providing 5.51 W at 0.850 μm. This last wavelength, being detuned from the maximum Yb^{3+} absorption at 0.96 μm but tuned with the $^1G_4-^1I_6$ Pr^{3+} absorption, provides the condition for the avalanche regime of a weak β (10^{-6} to 10^{-8}) as seen above.

6. Perspectives and Future Advances

From the most recent studies and their respective aims as described in the above sections and from some emerging new research, one can try to derive some future trends and perspectives to better understand some of the observed features. In the following they will be divided into the five main directions that can be anticipated:

(i) upconversion pumped lasers;
(ii) new materials for low-level IR visualization;
(iii) intrinsic material optical bistability;
(iv) hot emission and avalanche-like codoped system; and
(v) biological applications.

6.1. Upconversion UV-Tunable Lasers

Because optically pumped lasers are originally based on a Stokes pumping process, one basic problem is to obtain a high-density pumping source at a shorter wavelength than their emitting wavelength. With the tendency to go all solid state, there will be a continuous race between the shortest wavelength of the pumping semiconductor-based source and the shortest solid-state laser-emitting wavelength.

Few years ago the anticipated pumping diode emitted only in the near-IR; now that blue semiconductor lasers have begun to appear, one can theoreti-

cally anticipate that, sometimes, blue diodes could pump visible solid-state lasers. However, because powerful red semiconductor lasers do not exist yet that could be used for solid-state laser pumping, one can also anticipate that for many years to come no UV CW semiconductor or even frequency-multiplied semiconductor laser will not exist that will be powerful enough to usefully pump tunable a CW UV solid-state laser.

Clearly, upconversion pumping of a tunable UV solid-state laser has a role to play. So much the better that presently available gas UV laser are not tunable. Recent results give hints for that. As already shown in section 4.5, UV emission has been obtained from LaF_3:Nd^{3+} at 380 nm through a somewhat complicated anti-Stokes pumping scheme.[223] On the other hand, a very efficient tunable UV laser from $LiLuF_4$:Ce^{3+} has recently been obtained from 305 to 333 nm under Stokes pumping provided by a frequency-doubled copper vapor laser;[275] the slope efficiency was 51%. This particular result has to be connected to other recent results[276] on upconversion and energy transfers from Pr^{3+} (4f−5d) to Ce^{3+}(5d) to see that a tunable UV laser by anti-Stokes pumping can be imagined. The recently issued collection of selected papers on upconversion lasers[232] certainly comforts this trend.

6.2. New Materials for Low-Intensity IR Imaging

As pointed out in section 4.3, an interesting point of view is the IR−IR upconversion for low-intensity IR viewing. Though it is basically the old IRQC concept to upconvert IR out of the photocathode range to the photocathode detection range (GaAs and S1, from 760 to 1200 nm), little research has used the more recent understanding of RE-doped materials for this application. It has been recently proposed to use low-phonon energy glasses such as chalcogenide glasses (GeS_2−Ga_3S_3) as 1500−1000 nm converters, with most of the upconverted energy at the latter wavelength.[277] Of course, other low-phonon energy materials such as the stable $CsCdBr_3$ which is well-known in this respect together with strong RE−RE pair coupling could be designed for still farther IR ranges.

6.3. Upconversion Material Intrinsic Bistability

This is certainly the most recent fundamental subject in the upconversion field. A few years ago it was found in Güdel's group[278,57] that the cooperative luminescence (see section 3) of Yb^{3+}:$Cs_3Y_2Br_9$ and $Cs_3Yb_2Br_9$ in the visible as well as the usual Stokes emission in the IR clearly displayed an hysteresis loop under variable excitation density and fixed temperature between 11 and 31 K. Correlatively a hysteresis loop was also observed when excitation was kept constant and the temperature was varied as shown in Figure 39. The physical explanation was given in the framework of the optical coherent field coupling between two ions in a solid that had been theoretically proposed[279,280] by Heber. The problem with this model is to what extent it can describe a RE-doped system physical reality. This can be questioned.

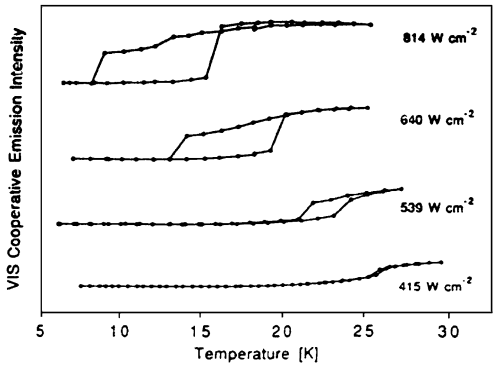

Figure 39. Thermal hysteresis loop for cooperative luminescence in $Cs_3Y_2Br_9$:Yb^{3+}. (Reprinted with permission from ref 284. Copyright 1996 American Institute of Physics.)

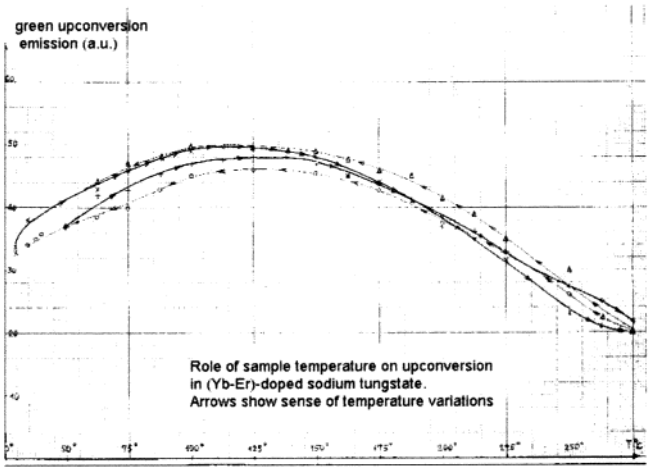

Figure 40. First observation (from 1967 unpublished original document) of a thermal hysteresis loop for APTE upconversion in $WO_4Na_{0.5}Yb_{0.5}$:2%Er^{3+}. Arrows show direction of the temperature variations for two sets of experiments.

It has been recognized for a long time now that optical bistability within a cavity could originate from optical cooperative coupling between cavity modes and the atomic system in a way similar to the optical cooperative coupling between atomic systems giving rise to superfluorescence.[281] However, superfluorescence in RE-doped systems is very difficult to observe because it requires long dephasing times (T_2) which are impossible to obtain in a solid at high doping concentration due to ion−ion and ion−phonon dephasing. Observation of superfluorescence in $LiYF_4$:Er requires both low T (<30 K) and very weak concentration (<0.3%)[282] and a threshold of 842 W cm^{-2}. The rather high concentration used here in the Yb^{3+} experiment certainly imposes that the Rabi frequency be less than the ion line width at the considered excitation density of 800 W cm^{-2}, which is also about the threshold for the observed hysteresis loop.[278] This forbids any sizable coherent field coupling.

Interestingly, in the very first experiment on APTE upconversion, thermal hysteresis loops were observed at high temperature,[283] see Figure 40. Clearly, at such high temperatures it has nothing to do with coherent field coupling. Also, the bistability observed

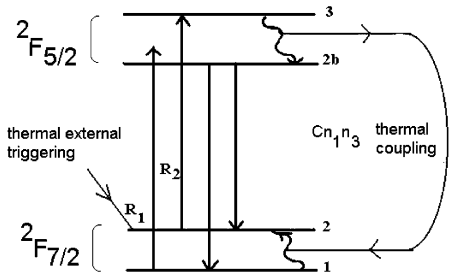

Figure 41. Yb^{3+} simplified energy scheme according to the simplified three-level energy scheme of Figure 25 for avalanche with a thermal cross-relaxation process explaining the thermal hysteresis loop of 285. The external triggering term corresponds to the temperature variable of the experiment.

in avalanche systems (see section 5.3) has been described within the framework of population rate equations. Then it appears more in accordance with physical reality not to consider coherent field coupling as the root of observed bistability. This is implicitly recognized for $Cs_3Y_2Br_9$:Yb in a later paper[284] pointing out the analogy with avalanche bistability and describing the effect through population rate equations. As the temperature changes, so do the overlap integrals ruling the RE−RE energy transfers, which provide the necessary nonlinear feedback effect. Clearly, it can also be the only explanation for the high-temperature (430 K) hysteresis loops that had been initially observed in $WO_4Na_{0.5}Yb_{0.5}$:2%Er.[283] From this result and the fact that the hysteresis behavior is produced at the Yb^{3+} ion, it can be predicted that all upconversion systems with Yb as a sensitizer could show thermal hysteresis. For the last 2 years, the thermal explanation has clearly been retained as explained by Gamelin et al. [285] and said to be due to the variable thermal absorption properties of Yb^{3+}. It is described as a thermal avalanche with a thermal cross-relaxation in analogy with the photon avalanche described above in section 5.1. According to Figure 41, the equivalent of R_1, the weak ground-state absorption, is a nonresonant absorption between $^2F_{7/2}$ to $^2F_{5/2}$. The resonant absorption term R_2 is from a Stark level of $^2F_{7/2}$ to a Stark level of $^2F_{5/2}$; the cross-relaxation term, Cn_1n_3 of Figure 25, is produced by the heat released within the Stark levels of $^2F_{5/2}$ by the phonon emission, which in turn, by absorption of phonons, populates a higher Stark excited state of $^2F_{7/2}$. This is the loop of this thermal avalanche. An external thermal triggering term, equivalent to $\sigma_0\Phi_{IR}$ of Figure 25, is provided by the external temperature variable T of the experiment.

As seen in section 5.1, one can predict that the threshold and the hysteresis will be steeper and the time constant longer for weaker R_1/R_2 ratios. Consequently, we can propose here that a large crystal field should be better for higher temperature observations and that it should be the case for hard oxides and YAG in particular.[286]

At any rate, the thermal avalanche convincing explanation certainly describes in a correct way the published observations including the one of 1967,[283] which was was thought to be due to the thermal behavior of the overlap integral between coupled Yb−Er ions and had been unexplained until now!

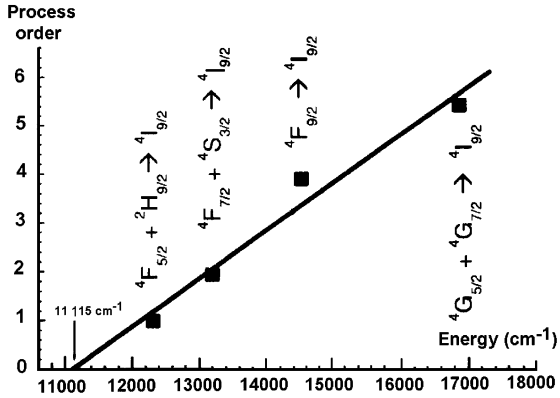

Figure 42. Upconversion power law indexes versus energy gap between emitting states and $^4F_{3/2}$ (Nd^{3+}) in Yb,Nd:YAG. (Reprinted with permission from ref 287. Copyright 2002 Institute of Physics Publishing.)

6.4. Hot Emission and Avalanche Like Co-Doped Systems

Here, it is interesting to discuss a not yet completely elucidated new phenomena recently observed by Bednarkiewicz and Strek[287] in an upconversion study of Nd^{3+}−Yb^{3+} codoped YAG nanocrystallite ceramics. Under laser diode pumping at 976 nm into the Yb absorption, visible orange antiStokes emission is observed at 300 K with broadened features at 579 nm from $^4G_{5/2}$−$^4G_{7/2}$, 690 nm from $^4F_{9/2}$, 757 nm from $^4F_{7/2}$−$^4S_{3/2}$, and 813 nm from $^4F_{5/2}$−$^2H_{9/2}$, all transitions to the Nd^{3+} $4I_{9/2}$ ground state. These emissions decrease with decreasing temperature. Those visible emissions are described by a, P^n, law for output versus excitation with, n linearly depending on the energy gap above $^4F_{3/2}$ as shown in Figure 42 There is also an establishing time constant increasing with the order parameter, n, reaching 1.5 s for $n = 4$. It was recognized that because the metastable character of $^4F_{3/2}$ is reduced by back transfer to Yb, the multiphonon process shown which could have explained the result of Figure 42 cannot be retained; moreover, dividing the energy gap between $^4F_{3/2}$ and emitting states by n provides virtual phonon energies not existing in YAG.

No real explanation is presented in ref 287, and this result is still a question. Though not mentioned by the authors, we think, however, that the long time transient is the clear signature of avalanche processes which have yet to be analyzed in detail.

6.5. Biological Applications

Very recently upconversion applications of the APTE (ETU) systems Yb−Er and Yb−Tm have been devised by Zilmans et al.[288] for detection of cell and tissue surface antigens as luminescent bioassays. Submicrometer-sized phosphor crystals (200−400 nm) of the usual oxysulfide, fluoride, gallate, and silicate types doped with Yb−Er and Yb−Tm couples are considered. The main advantage is that IR-upconverting phosphors are excited by wavelengths that cannot excite the natural biological materials, so providing a better detection contrast with respect to autofluorescence than the more usual luminescent bioassays working in the Stokes emission mode. The

upconversion method overcomes many of the limitations of the common reporters used in immunocytochemical applications.

A still more recent result that could be connected to previous application is the dissolution of nanoparticles (6−8 nm) of Yb−Er- and Yb−Tm-doped $LuPO_4$ as colloids in chloroform solutions.[289] Because of the inherent high efficiency of the APTE (ETU) effect, such colloids can show green, red, and blue upconversion in the liquid phase for the first time.

7. Conclusion

The general principles of upconversion have been presented in a self-contained way together with typical examples. Because these effects are now so generally observed with the general use of laser excitations, it was thought to be important to distinguish them in precise ways in order for future researchers to start from well-established definitions and to speak a common language.

Besides a didactical approach, I tried to present most of all the recent important results if not in an exhaustive way at least in a complete way for all important turning points.

If there was some general philosophy to derive from this review, it would be that upconversion is an endless field and that some features are becoming as common as plain Stokes luminescence. Some aspects of this reviewed field though not really exploited at some time may become important with more refined experiments and availability of new technologies. Also, the implied processes may help understand other aspects of optical processes in RE-doped solids.

An example could be the presently considered photon-cutting effect,[84−88] just the opposite of APTE (ETU) upconversion, which may open the way to new efficient lighting systems. The opposite of cooperative luminescence, cooperative quenching, recently discovered, may explain some of the yet not understood features of concentration quenching.[83]

From an applied point of view, it is observed that with the general use of lasers and the easiness in observing visible to the naked eye upconversion, too few people have found it necessary to measure efficiencies in order to be able to compare quantitatively the various proposed upconversion systems. This should be done to push upconversion beyond the qualitative approach that still too often characterizes it. Most of the recently proposed systems can be observed only at low temperature and no efficiency values are provided. One can also verify through this review that, as is often in science, the most efficient systems are the ones discovered at first, here the Yb−Er and the Yb−Tm systems.[7]

8. Acknowledgments

It is a pleasure to acknowledge a number of researchers who have kindly sent me their reprints and have so helped me in writing this review. I would like to mentioned particularly Dr. Junichi Owaki (NTT), Pr. Günter Huber (Hambourg University), Pr. Johann Heber (Darmstadt University of Technology), Drs.Valery Smirnov and Alina Man'shina (Russian Center for Laser Physics), Pr. Georges Boulon and Dr. Marie-France Joubert (Université de Lyon), Pr. Hans Güdel (Bern University), Dr. Markus Pollnau (Lausanne University), Pr. Wieslaw Srek (Low Temperature Physic Institute, Wrawclaw), and Pr. Joaquim Fernandez (Universidad del Pais Vasco, Bilbao). I would like to thank also Dr. Marco Bettinelli (University di Verona, Italy) for kindly pointing to me the bioassay application and Pascal Gerner (Bern University) for providing me with the very recent last reference. Many thanks also for my good friend Peter Lewis for reading over the whole text. Last but not least, thanks are due to my wife, Odile, for having accepted that I divert a lot of leisure time for that work.

9. References

(1) Leverenz, H. W. *Introduction to Luminescence of Solids*; Dover Publications: New York, 1968.
(2) Auzel, F. *Proc. IEEE* **1973**, *61*, 758.
(3) Wright, J. Up-conversion and excited-state energy transfer in rare-earth doped materials. In *Radiationless Processes in Molecules and Condensed Phases*; Fong, F. K., Ed.; Topics in Applied Physics; Springer: New York, 1976; Volume 15, p 239.
(4) Bloembergen, N. *Phys. Rev. Lett.* **1959**, *2*, 84.
(5) Brown, M. R.; Thomas, H.; Williams, J. M.; Woodwards, R. J. *J. Chem. Phys.* **1969**, *51*, 3321.
(6) Auzel, F. *J. Lumin.* **1984**, *31/32*, 759.
(7) Auzel, F. *C. R. Acad. Sci. (Paris)* **1966**, *262*, 1016. Auzel, F. *C. R. Acad. Sci. (Paris)* **1966**, *263*, 819.
(8) Van Uitert, L. G.; Johnson, L. F. *J. Chem. Phys.* **1966**, *44*, 3514.
(9) Mita, Y.; Nagasawa, E. *NEC Res. Dev.* **1974**, *33*, 61.
(10) Garlick, G. F. J. *Contemp. Phys.* **1976**, *17*, 127.
(11) Chivian, J. S.; Case W. E.; Eden, D. D. *Appl. Phys. Lett.* **1979**, *35*, 124.
(12) Case, W. E.; Koch, M. E.; Kueny, A. W. *J. Lumin.* **1990**, *45*, 351.
(13) Auzel, F. *Semiconductor Optoelectronics*; Wiley and PWN: New York and Warszawa, 1980; Chapter 10, p 233. Auzel, F. *J. Lumin.* **1990**, *45*, 341. Auzel, F. In *Luminescence: Phenomena, Materials and Devices;* Rao, R. P., Ed.; Nova Science Pub.: New York, 1992; p 33. Auzel, F. In *Nonlinear Spectroscopy of Solids; Advances and Applications;* DiBartolo, B., Bowlby, B., Eds.; Plenum Press: New York, 1994; p 531.
(14) Huber, G.; Heumann, E.; Sandrok, T.; Petermann, K. *J. Lumin.* **1997**, *72/74*, 1.
(15) Gamelin, D. R.; Güdel, H. U. *Acc. Chem. Res.* **2000**, *33*, 235.
(16) Hehlen, M. P.; Phillips, M. L. F.; Cockroft, N. J.; Güdel, H. U. *Encyclopedia of Materials; Science and Technology;* Elsevier Science Ltd.: New York, 2001; p 9956.
(17) Gamelin, D. R.; Güdel, H. U. *Top. Curr. Chem.* **2001**, *214*, 1.
(18) Auzel, F. *SPIE* **2001**, *4766*, 179. Auzel, F. In *Spectroscopic properties of rare-earths in optical materials*; Liu, G. K., Jacquier, B., Eds.; Springer-Verlag: New York, 2003; Chapter 5.
(19) *Selected papers on Photoluminescence of Inorganic Solids;* Weber, M., Ed.; SPIE Milestone Series, Vol. MS150; SPIE: Bellingham, WA, 1998.
(20) Auzel, F. Multiphonon processes, cross-relaxation and upconversion in ion activated solids, exemplified by minilaser materials. In *Radiationless Processes*; DiBartolo, B., Goldberg, V., Eds.; Plenum Publishing Co.: New York, 1980; p 213.
(21) Henderson, B.; Imbusch, G. F. *Optical Spectroscopy of Inorganic Solids*; Clarendon Press: Oxford, 1989; p 445.
(22) Milne, E. A. *J. London Math. Soc.* **1926**, *1*, 1.
(23) Varsanyi, F.; Wood, D. L.; Schawlow, A. L. *Phys. Rev. Lett.* **1959**, *3*, 544.
(24) Auzel, F. *Ann. Telecom. (France)* **1969**, *24*, 363.
(25) Auzel, F.; Bonfigli, F.; Gagliari, S.; Baldacchini, G. *J. Lumin.* **2001**, *94/95*, 293.
(26) Förster, T. *Ann. Phys.* **1948**, *2*, 55.
(27) Dexter, D. L. *J. Chem. Phys.* **1953**, *21*, 836.
(28) Kushida, T. *J. Phys. Soc. Jpn.* **1973**, *34*, 1318.
(29) Pouradier, J. F.; Auzel, F. *J. Phys. (France)* **1978**, *39*, 825.
(30) Axe, J. D.; Weller, P. F. *J. Chem. Phys.* **1964**, *40*, 3066.
(31) Orbach, R. *Optical Properties of Ions in Solids;* DiBartolo, B., Ed.; Plenum Press: New York, 1975; p 445.
(32) Miyakawa, T.; Dexter, D. L. *Phys. Rev.* **1971**, *B1*, 70.
(33) Auzel, F. *Phys. Rev.* **1976**, *B13*, 2809.
(34) Yamada, N.; Shionoya, S.; Kushida, T. *J. Phys. Soc. Jpn.* **1972**, *32*, 1577.
(35) Inokuti, M.; Hirayama, F. *J. Chem. Phys.* **1965**, *43*, 1978.

(36) Barthem, R. B.; Buisson, R.; Vial, J. C. *J. Phys.* **1985**, *46*, C7−483.
(37) Yokota, M.; Tanimoto, O. *J. Phys. Soc. Jpn.* **1967**, *22*, 779.
(38) Weber, M. J. *Phys. Rev.* **1971**, *B4*, 2932.
(39) Grant, W. J. C. *Phys. Rev.* **1958**, *109*, 648.
(40) Auzel, F. *Mater. Res. Bull.* **1979**, *14*, 223.
(41) Snitzer, E.; Woocock, R. *Appl. Phys. Lett.* **1965**, 6, 5.
(42) Auzel, F.; Deuschbein, O. *Z. Naturfosch.* **1969**, *24a*, 1562.
(43) Ovsyankin, V. V.; Feofilov, P. P. *Sov. Phys. JETP Lett.* **1966**, *4*, 317.
(44) Hewes, R. A.; Sarver, J. F. *Phys. Rev.* **1969**, *182*, 427.
(45) Pollnau, M.; Gamelin, D. R.; Lüthi, S. R.; Güdel, M. *Phys. Rev.* **2000**, *B61*, 3337.
(46) Rios Leite, J. R.; de Araujo, C. B. *Chem. Phys. Lett.* **1980**, *73*, 71.
(47) Bonneville, R.; Auzel, F. *Opt. Commun.* **1976**, *18*, 51.
(48) Ovsyankin, V. V.; Fedorov, A. A. *Opt. Spectrosc.* **1981**, *50*, 565.
(49) Mita, Y.; Ide, T.; Katase, T.; Yamamoto, H. *J. Lumin.* **1997**, *72/74*, 959.
(50) Goldner, P.; Pellé, F. *J. Lumin.* **1994**, *60/61*, 651.
(51) Auzel, F.; Pecile, D.; Morin, D. *J. Electrochem. Soc.* **1975**, *122*, 101.
(52) Auzel, F.; Pecile, D. *C. R. Acad. Sci. Paris* **1973**, *277B*, 155.
(53) Silver, J.; Martinez-Rubio, M. I.; Ireland, T.G.; Fern, G. R.; Withnall, R. *J. Phys. Chem.* **2001**, *B105*, 948.
(54) Silver, J.; Martinez-Rubio, M. I.; Ireland G. R.; Withnall, R. *J. Phys. Chem.* **2001**, *B105*, 7200.
(55) Ovsyankin, V. V. *Spectroscopy of Solids Containing Rare-Earth Ions*; Kaplyanskii, A. A., MacFarlane, R. M., Eds.; North-Holland: Amsterdam, 1987; p 405.
(56) Orlovskii, Y. U.; Basiev, T. T.; Papashvili, A. G.; Voroev, I. N.; Alimov, O. K.; Osiko, V. V.; Heber, J. *SPIE* **2001**, *4766*, 204.
(57) Gamelin, D. R.; Lüthi, S. R.; Güdel, H. U. *J. Phys. Chem.* **2000**, *B104*, 11045. Lüthi, S. R.; Hehlen, M. P.; Riedener, T.; Güdel, H. U. *J. Lumin.* **1998**, *76/77*, 447.
(58) Auzel, F.; Dexpert-Ghys, J.; Gauthier, C. *J. Lumin.* **1982**, *27*, 1.
(59) Vial, J. C.; Buisson, R.; Madeore, F.; Poirier, M. *J. Phys. (France)* **1979**, *40*, 913.
(60) Dexpert-Ghys, J.; Auzel, F. *J. Chem. Phys.* **1984**, *80*, 4003.
(61) Nakazawa, E.; Shionoya, S. *Phys. Rev. Lett.* **1970**, *25*, 1710.
(62) Cockroft, N. J.; Jones, G. D.; Syme, R. W. G. *J. Lumin.* **1989**, *43*, 275.
(63) Varsanyi, F; Dieke, G. H. *Phys. Rev. Lett.* **1961**, *7*, 442.
(64) Van der Ziel, J. P.; Van Uitert, L. G. *Phys. Rev.* **1969**, *180*, 343.
(65) Stavola, M.; Dexter, D. L. *Phys. Rev.* **1979**, *B20*, 1867.
(66) Livanova, L. D.; Saitkulov, I. G.; Stolov, A. L. *Sov. Phys. Solid State* **1969**, *11*, 750.
(67) Ostermayer, F. W., Jr.; Van Uitert, L. G. *Phys. Rev.* **1970**, *B1*, 4208.
(68) Auzel, F.; Meichenin, D.; Pellé, F.; Goldner, P. *Opt. Mater.* **1994**, *4*, 35.
(69) Heber, J.; Nikitin, S. I.; Demirbilek, R.; Papashvili, A. G.; Vorobev, I. N.; Alimov, O. K.; Orlovskii, Y. V.; Orlovskaya, E. O. *SPIE* **2001**, *4766*, 218. Schäfer, U.; Neukum, J.; Bodenschatz, N.; Heber, J. *J. Lumin.* **1994**, *60/61*, 633.
(70) Noginov, M. A.; Loutts, G. B.; Steward, C. S.; Lucas, B. D.; Fider, D.; Peters, V.; Mix, E.; Huber, G. *J. Lumin.* **2002**, *96*, 129.
(71) Blixt, P.; Nilsson, J.; Carlknäs, J.; Jaskorzynska, B. *IEEE Trans. Photon Techn.* **1991**, *3*, 996.
(72) Auzel, F. *J. Lumin.* **1984**, *31/32*, 759.
(73) Auzel, F. In *Rare-Earth Spectroscopy*; Trzebiatowska, B., Legendziewicz, J., Strek, W., Eds.; World Scientific: Singapore, 1985; p 502.
(74) Rand, S. C.; Lee, L. S.; Schawlow, A. L. *Opt. Commun.* **1982**, *42*, 179.
(75) Lee, L. S.; Rand, S. C.; Schawlow, A. L. *Phys. Rev.* **1984**, *B29*, 6901.
(76) Valiente, R.; Wenger, O.; Güdel, H. *Chem. Phys. Lett.* **2000**, *320*, 639.
(77) Valiente, R.; Wenger, O.; Güdel, H. *Phys. Rev.* **2001**, *B63*, 165102−1.
(78) Gerner, P.; Wenger, O.; Valiente, R.; Güdel, H. *Inorg. Chem.* **2001**, *40*, 4534.
(79) Valiente, R.; Wenger, O.; Güdel, H. *J. Chem. Phys.* **2002**, *116*, 5196.
(80) Salley, G. M.; Valiente, R.; Güdel, H. *J. Lumin.* **2001**, *94/95*, 305.
(81) Salley, G. M.; Valiente, R.; Güdel, H. *J. Phys.: Condens. Matter* **2002**, *14*, 5461.
(82) Strek, W.; Bednarkiewicz, A.; Deren, P. J. *J. Lumin.* **2001**, *92*, 229.
(83) Dexter, D. L. *Phys. Rev.* **1957**, *108*, 630. Dexter, D. L. *Phys. Rev.* **1962**, *126*, 1962.
(84) Basiev, T.T.; Dorochenko, M. E.; Osiko, V. V. *JETP Lett.* **2000**, *71*, 8.
(85) Vegh, R. T.; Donker, H.; van Loef, E. V. D.; Oskam, K. D.; Meijerink, A. *J. Lumin.* **2000**, *87/89*, 1017.
(86) Wegh, T. T.; Donker, H.; Meijerink, A.; Lamminmäki, R. J.; Hölsa, J. *Phys. Rev.* **1997**, *B56*, 13841.
(87) Wegh, R. T.; Donker, H.; Oskam, K. D.; Meijerink, A. *J. Lumin.* **1999**, *82*, 93.
(88) Wegh, R. T.; Meijerink, A. *Acta Phys. Pol.* **1996**, *A90*, 333.
(89) Weegh, R. T.; Donker, H.; Oskam, K. D.; Meijerink, A. *Science* **1999**, *283*, 663.
(90) Strek, W.; Deren, P.; Bednarkiewicz, A. *J. Lumin.* **2000**, *87/89*, 999.
(91) Strek, W.; Deren, P. J.; Bednarkiewicz, A.; Kalisky, Y., Boulanger, P. *J. Alloys Compd.* **2000**, *300/301*, 180.
(92) Orlovskii, Y. V.; Basiev, T. T.; Papashvili, A. G.; Vorobev, I. N.; Alimov, O. K.; Osiko, V. V.; Heber, J. *J. Lumin.* **2002**, *99*, 223.
(93) Delevaque, E.; Georges, T.; Monerie, M.; Lamouler, P.; Bayon, J. F. *IEEE Photon Techn. Lett.* **1993**, *5*, 73.
(94) Maurice, E.; Monnom, G.; Dussardier, B.; Ostrowsky, D. B. *Opt. Lett.* **1995**, *20*, 2487.
(95) Auzel, F. *J. Lumin.* **1990**, *45*, 341.
(96) Goldner, P.; Pellé, F.; Meichenin, D.; Auzel, F. *J. Lumin.* **1997**, *71*, 137.
(97) Goldner, P.; Pellé, F.; Auzel, F. *J. Lumin.* **1997**, *72/74*, 901.
(98) Auzel, F.; Goldner, P. *Opt. Mater.* **2001**, *16*, 93.
(99) Schaudel, B.; Goldner, P.; Prassas, M.; Auzel, F. *J. Alloys Compd.* **2000**, *300/301*, 443.
(100) Remillieux, A.; Jacquier, B. *J. Lumin.* **1996**, *68*, 279.
(101) Balda, R.; Fernandez, J.; Saez de Ocariz, I.; Voda, M.; Garcia, A. J. *Phys. Rev.* **1999**, *B59*, 9972.
(102) Fernandez, J.; Balda, R.; Mendorioz, A; Garcia-Adeva, A. J. *J. Phys. Condens. Matter* **2001**, *13*, 10347. Balda, R.; Saez de Ocariz, I.; Fernandez, J.; Fdez-Navarro, J. M.; Arriandaga, M. A. *J. Phys. Condens. Matter* **2000**, *12*, 10623.
(103) Ju, J. J.; Ro, J. H.; Cha, M. *J. Lumin.* **2000**, *87/89*, 1045.
(104) Kim, S. I.; Yun, S. I. *J. Lumin.* **1994**, *60/61*, 233.
(105) Malinovski, M.; Joubert, M. F.; Jacquier, B. *J. Lumin.* **1994**, *60/61*, 179.
(106) Hirao, K.; Higuchi, M.; Soga, N. *J. Lumin.* **1994**, *60/61*, 115.
(107) Deren, P. J.; Mahiou, R.; Strek, W.; Bednarkiewicz, A.; Bertrand, G. *Opt. Mater.* **2002**, *19*, 145.
(108) Balda, R.; Sanz, M.; Fernandez, J.; Fdez-Navarro, J. M. *J. Opt. Soc. Am.* **2000**, *B17*, 1671.
(109) Fernandez, J.; Balda, R.; Mendorioz, A.; Sanz, M.; Adam, J. L. *J. Non-Cryst. Solids* **2001**, *287*, 437.
(110) Fernandez, J.; Balda, R.; Sanz, M.; Lacha, L. M.; Oleaga, A.; Adam, J. L. *J. Lumin.* **2001**, *94/95*, 325.
(111) Acioli, L. H.; Guo, J. T.; de Araujo, C. B.; Messaddeq, T.; Aegerter, M. A. *J. Lumin.* **1997**, *72/74*, 68.
(112) Balda, R.; Sanz, M.; Mendorioz, A.; Fernandez, J.; Griscom, L. S.; Adam, J. L. *Phys. Rev.* **2001**, *B64*, 144101.
(113) Fernandez, J.; Sanz, M.; Mendorioz, A.; Balda, R.; Chaminade, J. P.; Ravez, J.; Lacha, L. M.; Voda, M.; Arriandiaga, M. A. *J. Alloys Compd.* **2001**, *323/324*, 267.
(114) Iparraguirra, I.; Al-Saleh, M.; Balda, R.; Voda, M.; Fernandez, J. *J. Opt. Soc. Am.* **2002**, *B19*, 1.
(115) Malinovski, M.; Jacquier, B.; Bouazaoui, M.; Joubert, M. F., Linares, C. *Phys. Rev.* **1990**, *B41*, 31.
(116) Pollnau, M.; Hardman, P. J.; Kern, M. A.; Clarkson, W. A.; Hanna, D. C. *Phys. Rev.* **1998**, *B58*, 16070.
(117) Pollnau, M.; Hardman, P. J.; Clarkson, W. A.; Hanna, D. C. *Opt. Commun.* **1998**, *147*, 203.
(118) Blätte, M.; Danielmeyer, H. G.; Verich, R. *Appl. Phys. (Germany)* **1973**, *1*, 275.
(119) Wenger, O. S.; Gamelin, D. R., Güdel, H. U. *Phys. Rev.* **2000**, *B61*, 16530.
(120) Holliday, K.; Russell, D. L.; Henderson, B. *J. Lumin.* **1997**, *72/74*, 927.
(121) Zhang, X; Daran, E.; Serrano, C.; Lahoz, F. *J. Lumin.* **2000**, *87/89*, 1011.
(122) Deren, P. J.; Strek, W.; Krupa, J. C. *Chem. Phys. Lett.* **1998**, *298*, 217.
(123) Mahiou, R.; Metin, J.; Cousseins, J. C. *J. Lumin.* **1990**, *45*, 363.
(124) Wermuth, M.; Riedener, T.; Güdel, H. U. *Phys. Rev.* **1998**, *B57*, 4369.
(125) Pouradier, J. F.; Auzel, F. *J. Phys.* **1976**, *37*, 421.
(126) Müller, P.; Wermuth, M.; Güdel, H. *Chem. Phys. Lett.* **1998**, *290*, 105.
(127) Ryba-Romanovski, W.; Deren, P. J.; Golab, S.; Dominiak-Dzik, G. *J. Appl. Phys.* **2000**, *88*, 6078.
(128) Ryba-Romanovski, W.; Golab, S.; Dominiak-Dzik, G.; Solarz, P. *Appl. Phys. Lett.* **2001**, *79*, 3026.
(129) Chamarro, M. A.; Cases, R. *J. Lumin.* **1988**, *42*, 267.
(130) Auzel, F.; Hubert, S.; Meichenin, D. *Appl. Phys. Lett.* **1989**, *54*, 681.
(131) Ronac'h, D.; Guibert, M.; Auzel, F.; Meichenin, D.; Allain, J. Y.; Poignant, H. *Electron. Lett.* **1991**, *27*, 511.
(132) Monerie, M.; Allain, J.-Y.; Poignant, H.; Auzel, F. In *Fluorescence, Up-conversion, and lasing in Er-doped quasi-single mode fluorozirconate fibres*, Proceedings of ECOC'89, Gothenburg, Sweden, Sept 1989; paper TuB12−6.
(133) Pollnau, M.; Ghisler, C.; Bunea, G.; Lüthy, W., Weber, H. P. *Appl. Phys. Lett.* **1995**, *66*, 3564.

(134) Golding, P. S.; Jackson, S. D.; King, T. A.; Pollnau, M. *Phys. Rev*. **2000**, *B62*, 856.
(135) Silversmith, A. *J. Lumin*. **1994**, *60/61*, 636.
(136) Chen, X.; Nguyen, T.; Qui, L.; DiBartolo, B. *J. Lumin*. **1999**, *83/84*, 471.
(137) Pollnau, M.; Heumann, E.; Huber, G. *Appl. Phys*. **1992**, *A54*, 404.
(138) Lüthi, S. R.; Pollnau, M.; Güdel, H.; Hehlen, M. P. *Phys. Rev*. **1999**, *60*, 162.
(139) Hehlen, M. P.; Krämer, K.; Güdel, H.; McFarlane, R. A.; Schartz, R. N. *Phys. Rev*. **1994**, *B49*, 12475.
(140) Wenger, O; Gamelin, D. R., Güdel, H. U.; Butashin, A. V.; Kaminskii, A. *Phys. Rev*. **1999**, *B60*, 5312.
(141) Riedener, T.; Egger, P.; Hulliger, J.; Güdel, H. *Phys. Rev*. **1997**, *B56*, 18000.
(142) Riedener, T.; Güdel, H. *J. Chem. Phys*. **1997**, *107*, 2169.
(143) Pollnau, M.; Lüthy, W.; Weber, H. P.; Krämer, K.; Güdel, H.; McFarlane, R. A. *OSA Topics on Advanced Solid State Lasers*; Payne, A., Polock, C., Eds.; OSA: Washington, DC, 1996; Vol. 1, p 493.
(144) Hehlen, M. P.; Frei, G.; Güdel, H. *Phys. Rev*. **1994**, *B50*, 16264.
(145) Zhang, X.; Jouart, J. P.; Mary, G.; Liu, X; Yuan, J. *J. Lumin*. **1997**, *72/74*, 983.
(146) Spinger, B.; Danilov, V. P.; Prokhorov, A. M.; Schwan, L. O.; Schmid, D. *SPIE* **2001**, *4766*, 191.
(147) Felix, S. F.; Gouveia, E. A.; de Araujo, M. T.; Sombra, A. S. B.; Gouveia-Neto, A. S. *J. Lumin*. **2000**, *87/89*, 1020.
(148) Tkachuk, A. M.; Razumova, I. K.; Malyshev, A. V.; Gapontsev, V. P. *J. Lumin*. **2001**, *94/95*, 317.
(149) Dierolf, V.; Kutsenko, A. B.; von der Hosten, W. *J. Lumin*. **1999**, *83/84*, 487.
(150) Nunez, L.; Herreros, B.; Duchowicz, R.; Lifante, G.; Tocho, J. O.; Cusso, F. *J. Lumin*. **1994**, *60/61*, 81.
(151) Herreros, B.; Lifante, G.; Cusso, F.; Towsend, P. D.; Chandler, P. J. *J. Lumin*. **1997**, *72/74*, 198.
(152) Cokcroft, N. J.; Murdoch, K. M. *J. Lumin*. **1994**, *60/61*, 891.
(153) Chen, X. B.; Zhang, G. Y.; Mao, Y. H.; Hou, Y. B.; Feng, Y.; Hao, Z. *J Lumin*. **1996**, *69*, 151.
(154) Wyss, C. P.; Kehrli, M.; Huber, T.; Morris, P. J.; Lüthy, W.; Weber, H. P.; Zagumennyi, A. I.; Zavartsev, Y. D.; Studenikin, P. A.; Shcherbakov, I. A.; Zerrouk, A. F. *J. Lumin*. **1999**, *82*, 137.
(155) Riedener, T.; Güdel, H.; Valley, G. C.; McFarlane, R. A. *J. Lumin*. **1995**, *63*, 327.
(156) Gomes, A. S. L.; de Araujo, C. B. *J. Lumin*. **1991**, *48/49*, 876.
(157) Wu, X.; Denis, J. P.; Özen, G.; Pellé, F. *J. Lumin*. **1994**, *60/61*, 212.
(158) Auzel, F.; Pecile, D. *J. Lumin*. **1976**, 11, 321. Pecile, D. *De l'influence de la matrice sur l'addition de photons par transferts d'energie (APTE) dans les couples* $Yb^{3+}-Er^{3+}$ *et* $Yb^{3+}-Tm^{3+}$; Thèse, Université P.et M.Curie, Paris, 1976.
(159) Jacquier, *J. Lumin*. **1994**, *60/61*, 175.
(160) Wenger, O. S.; Wickleder, C.; Krämer, K.; Güdel, H. *J. Lumin*. **2001**, *94/95*, 101.
(161) Hubert, S.; Song, C. L.; Genet, M.; Auzel, F. *J. Solid State Chem*. **1986**, *61*, 252.
(162) Auzel, F.; Hubert, S., Delamoye, P. *J. Lumin*. **1982**, *26*, 251.
(163) Deren, P. J.; Karbowiak, M.; Krupa, J. C.; Drozdzynski, J. *J. Alloys Compd*. **1998**, *275/277*, 393.
(164) Stump, N. A.; Murray, G. M.; Del Cul, G. D.; Haire, R. G.; Peterson, J. R. *Radiochim. Acta* **1993**, *61*, 129.
(165) Deren, P. J.; Krupa, J. C.; Strek, W. *J. Lumin*. **1997**, *72/74*, 655.
(166) Deren, P. J.; Feries, J.; Krupa, J. C.; Strek, W. *Chem. Phys. Lett*. **1997**, *264*, 614.
(167) Deren, P. J.; Krupa, J. C.; Yin, M.; Joubert-, M. F.; Strek, W. *Spectrochem. Acta (A)* **1998**, *A54*, 2105.
(168) Deren, P. J.; Joubert, M. F.; Krupa, J. C.; Mahiou, R.; Yin, M. *J. Alloys Compd*. **2002**, *341*, 134.
(169) Deren, P. J.; Strek, W.; Zych, E.; Drozdzynski, J. *Chem. Phys. Lett*. **2000**, *332*, 308.
(170) Cresswell, P. J.; Robbins, D. J.; Thomson, A. J. *J. Lumin*. **1978**, *17*, 311.
(171) Moncorgé, R.; Breteau, J. M.; Auzel, F. *Philos. Mag*. **1985**, *B51*, 489.
(172) Wenger, O. S.; Güdel, H. U. *Inorg. Chem*. **2001**, *40*, 5747. Jacobsen, S. M.; Güdel, H. U. *J. Lumin*. **1989**, *43*, 125.
(173) Heer, S.; Wermuth, M.; Krämer, K.; Ehrentraut, D.; Güdel, H. U. *J. Lumin*. **2001**, *94/95*, 337.
(174) Heer, S.; Wermuth, M.; Krämer, K.; Güdel, H. U. *Phys. Rev*. **2002**, *65*, 125112.
(175) Heer, S.; Wermuth, M.; Krämer, K.; Güdel, H. U. *Chem. Phys. Lett*. **2001**, *334*, 293.
(176) Lim, K., S; Lee, C. W.; Kim, S. T.; Seo, H. J.; Kim, C. D. *J. Lumin*. **2000**, *85/89*, 1008.
(177) Wenger, O. S.; Valiente, R.; Güdel, H. U. *High-Press. Res*. **2002**, *22*, 57.
(178) Wenger, O. S.; Güdel, H. U. *Inorg. Chem*. **2001**, *40*, 157.
(179) Wenger, O. S.; Valiente, R.; Güdel, H. U. *Phys. Rev*. **2001**, *B64*, 235116.
(180) Wenger, O. S.; Gamelin, D. R.; Güdel, H. U. *J. Am. Chem. Soc*. **2000**, *122*, 7408.
(181) Gamelin, D. R.; Güdel, H. U. *J. Am. Chem. Soc*. **1998**, *120*, 12143.
(182) Gamelin, D. R.; Güdel, H. U. *J. Phys. Chem*. **2000**, *B104*, 10222.
(183) Sugano, S.; Tanabe, Y.; Kaminura, H. *Multiplets of Transition-Metal Ions in Crystals*; Academic Press: New York, 1970; p 109.
(184) Gamelin, D. R.; Güdel, H. U. *Inorg. Chem*. **1999**, *38*, 5154.
(185) Wermuth, M.; Güdel, H. U. *J. Phys.: Condens. Matter* **2001**, *13*, 9583.
(186) Wermuth, M.; Güdel, H. U. *Chem. Phys. Lett*. **1997**, *281*, 81.
(187) Wermuth, Güdel, H. U. *J. Lumin*. **2000**, *87*, 1014.
(188) Wermuth, M.; Güdel, H. U. *J. Am. Chem. Soc*. **1999**, *121*, 10102.
(189) Wermuth, M.; Güdel, H. U. *J. Chem. Phys*. **2001**, *114*, 1393.
(190) Wermuth, M.; Güdel, H. U. *Phys. Rev*. **2001**, *B63*, 245118.
(191) Page, R. H.; Schaffers, K. I.; Waide, P. A.; Tassano, J. B.; Payne, S. A.; Krupke, W. F.; Bischel, W. K. *J. Opt. Soc. Am*. **1998**, *B15*, 996.
(192) Mita, Y.; Yamamoto, H.; Katayanagi, K.; Shionoya, S. *J. Appl. Phys*. **1995**, *78*, 1219.
(193) Chamaro, M. A.; Cases, R. *J. Lumin*. **1990**, *46*, 59.
(194) Yeh, D. C.; Sibley, W. A.; Suscavage, M. J. *J. Appl. Phys*. **1988**, *63*, 4644.
(195) Kermaoui, A.; Özen, G.; Goldner, P.; Denis, J. P.; Pellé, F. *J. Phys. Chem. Solids* **1994**, *55*, 677.
(196) Auzel, F. French Patent No. 1.532.609, 1968.
(197) *Tokin IR Catcher;* Tokin America (155 Nicholson Lane, San Jose, CA, 95134), 1987.
(198) *Photo-Turkey-1;* Sumita Optical Glass Inc. (4−7−25 Harigaya, Urawa-City, Saitama, Japan), 1994.
(199) Breteau, J. M.; Ayral, J. L.; Micheron, F.; Auzel, F. *J. Appl. Phys*. **1990**, *67*, 1102.
(200) Downing, E.; Hesselink, L.; Ralston, J.; Macfarlane, R. *Science* **1996**, *273*, 1185.
(201) Auzel F.; Pecile, D. *J. Lumin*. **1973**, *8*, 32.
(202) Bril, A.; Sommerdijk, J. L.; de Jager, A. W. *J. Electrochem. Soc*. **1974**, *121*, 660.
(203) Quimby, R. S.; Drexhage, M. G.; Suscavage, M. J. *Electron. Lett*. **1987**, *23*, 32.
(204) Malta, O. L.; Santa-Cruz, P. A.; de Sa, G. F.; Auzel, F. *J. Solid State Chem*. **1987**, *68*, 314.
(205) Malta, O. L.; Santa-Cruz, P. A.; de Sa, G. F.; Auzel, F. *J. Lumin*. **1985**, *33*, 261.
(206) Wang, Y.; Ohwaki, J. *Appl. Phys. Lett*. **1993**, *63*, 3268.
(207) Wang, Y.; Ohwaki, J. *J. Appl. Phys*. **1993**, *74*, 1272. Ohwaki, J.; Wang, Y. *Jpn. J. Appl. Phys*. **1994**, *33*, L334.
(208) Ohwaki, J.; Wang, Y. *Appl. Phys. Lett*. **1994**, *65*, 129.
(209) Auzel, F.; Santa-Cruz, P. A.; de Sa, G. F. *Rev. Phys Appl. (France)* **1985**, *20*, 273.
(210) Kurochkin, A. V.; Mailibaeva, L. M.; Manashirov, O. Y.; Sattarov, D. K.; Smirnov, V. B. Part 1. *Opt. Spectrosc*. **1992**, *73*, 442. Kurochkin, A. V.; Mailibaeva, L. M.; Manashirov, O. Y.; Sattarov, D. K.; Smirnov, V. B. Part 2. *Opt. Spectrosc*. **1992**, *73*, 447.
(211) Kurochkin, A. V.; Manshisrov, O. Ya.; Sattarov, D. K.; Smirnov, V. B.; Tsyurupa, O. V. *Svetotekhnika* **1992**, *5*, 4 (Translated by Allerton Press Inc., 1993).
(212) Danielmeyer, H. G.; Blätte, M. *Appl. Phys. (Germany)* **1973**, *1*, 269.
(213) Deutschbein, O.; Auzel, F. In *Quantum Electronics*; Grivet, P., Bloembergen, N., Eds.; Dunod and Columbia University Press: Paris and New York, 1963; p 851.
(214) Bagdasarov, K. S.; Zhekov, V. I.; Lobachev, V. A. J; Murina, M.; Prokhorov, A. M. *Sov. J. Quantum Electron*. **1983**, *13*, 262.
(215) Van der Weg, W. F.; Van Tol, M. W. *Appl. Phys. Lett*. **1981**, *38*, 705.
(216) de Leeuward, D. M.; Hooft, G. W.'t. *J. Lumin*. **1983**, *28*, 275.
(217) Smith, D. *J. Lumin*. **1981**, *23*, 209.
(218) Johnson, L. F.; Guggenheim, H. J. *Appl. Phys. Lett*. **1971**, *19*, 44.
(219) Pollack, S. A.; Chang,D. B. *J. Appl. Phys*. **1988**, *64*, 2885.
(220) Tong, F.; Risk, W. P.; Macfarlane, R. M.; Lenth, W. *Electron. Lett*. **1989**, *25*, 1389.
(221) Lenth, W.; MacFarlane, R. M. *J. Lumin*. **1990**, *45*, 346.
(222) Hebert, T.; Wannemacher, R.; Lenth, W.; Macfarlane, R. M. *Appl. Phys. Lett*. **1990**, *57*, 1727.
(223) Macfarlane, R. M.; Tong, F.; Silversmith, A. J.; Lenth, W. *Appl. Phys. Lett*. **1988**, *52*, 1300.
(224) Brede, R.; Heumann, E.; Koltke, J.; Danger, T.; Huber, G. *Appl. Phys. Lett*. **1993**, *63*, 2030.
(225) Heine, F.; Heumann, E; Danger, T.; Schweizer, T.; Huber, G. *Appl. Phys. Lett*. **1994**, *65*, 383.
(226) Möbert, P. E.-A.; Heumann, E.; Huber, G. *Opt. Lett*. **1997**, *22*, 1412.
(227) Auzel, F. Amplifiers and Lasers with Optical Fibers. In *Defects in Insulating Materials*; Kanert, O., Spaeth, J.-M., Eds.; World Scientific: Singapore, 1993; p 43.
(228) Mears, R. J.; Reekie, L.; Poole, S. B.; Payne, D. N. *Electron. Lett*. **1986**, *22*, 159.

(229) Allain, J.-Y.; Monerie, M.; Poignant, H. *Electron. Lett.* **1990**, *26*, 166,.
(230) Allain, J.-Y.; Monerie, M.; Poignant, H. *Electron. Lett.* **1990**, *26*, 261.
(231) Whitley, T. J.; Millar, C. A.; Wyatt, R.; Brierley, M. C.; Szebesta, D. *Electron. Lett.* **1991**, *27*, 1785.
(232) Grubb, S. G.; Bennett, K. W.; Cannon, R. S.; Humer, W. F. *Electron. Lett.* **1992**, *28*, 1243.
(233) Smart, R. G.; Hanna, D. C.; Tropper, A. C.; Davey, S. T.; Carter, S. F.; Szebesta, D. *Electron. Lett.* **1991**, *27*, 1308.
(234) *Selected papers on Upconversion Lasers*; Gosnell, T. R., Ed.; SPIE Milestone Series MS 161; SPIE Optical Engineering Press: Bellingham, WA, 2000.
(235) Komukai, T.; Yamamoto, T.; Sugawa, T.; Miyajima, Y. *Electron. Lett.* **1992**, *28*, 830.
(236) Krasutsky, N. J. *J. Appl. Phys.* **1983**, *54*, 1261.
(237) Lenth, W.; Macfarlane, R. M. *J. Lumin.* **1990**, *45*, 346.
(238) Oetliker, U.; Riley, M. J.; May, P. S.; Güdel, H. U. *J. Lumin.* **1992**, *53*, 553.
(239) Ni, H.; Rand, S. C. *Opt. Lett.* **1992**, *17*, 1222.
(240) Auzel, F.; Chen, Y. H.; Meichenin, D., ICL'93, Storrs, CN, USA, 9−12 Aug 1993. Auzel, F.; Chen, Y. H.; Meichenin, D., *J. Lumin.* **1994**, *60/61*, 692.
(241) Chen, Y. H.; Auzel, F. *Electron. Lett.* **1994**, *30*, 323.
(242) Auzel, F.; Chen, Y. H. *J. Non-Cryst. Solids* **1995**, *184*, 57.
(243) Chen, Y. H.; Auzel, F. *J. Phys. D: Appl. Phys.* **1995**, *28*, 207.
(244) Auzel, F.; Chen, Y. H. *J. Lumin.* **1995**, *65*, 45.
(245) Pelletier-Allard, N.; Pelletier, R. *Phys. Rev.* **1987**, *B26*, 4425.
(246) Joubert, M. F.; Guy S.; Jacquier, B. *Phys. Rev.* **1993**, *B48*, 10031.
(247) Kueny, A. W.; Case, W. E.; Koch, M. E. *J. Opt. Soc. Am.* **1993**, *B10*, 1834.
(248) Goldner, P.; Pellé, F. *Opt. Mater.* **1995**, *5*, 239.
(249) Brenier, A.; Boulon, G.; Madej, C.; Pédrini, C.; Lou, L. *J. Lumin.* **1993**, *54*, 271.
(250) Auzel, F. *Acta Phys. Pol.* **1996**, *90*, 7.
(251) Gomes, A. S. L.; Maciel, G. S.; de Araujo, R. E.; Acioli, L. H.; de Araujo, C. B. *Opt. Commun.* **1993**, *103*, 361.
(252) Brenier, A.; Courrol, L. C.; Pédrini, C.; Madej, C.; Boulon, G. *J. Lumin.* **1994**, *58*, 285.
(253) Dyson, J. M.; Jaffe, S. M.; Eilers, H.; Jones, M. L.; Dennis, W. M.; Yen, W. M. *J. Lumin.* **1994**, *60/61*, 668.
(254) Brenier, A.; Jurdyc, A. M. *J. Lumin.* **1996**, *69*, 131.
(255) Brenier, A.; Courrol, L. C.; Pedrini, C.; Madej, C.; Boulon, G. *Opt. Mater.* **1994**, *3*, 25.
(256) Guy, S. L'avalanche de photons; application à l'ion Tm^{3+} dans differents matériaux. Thèse, Université Claude-Bernard-Lyon I, 1995. Guy, S. S.; Joubert, M. F.; Jacquier, B. *Phys. Rev.* **1997**, *B55*, 8240.
(257) Joubert, M. F.; Guy, B.; Linares, C.; Jacquier, B.; Adam, J. L. *J. Non-Cryst. Solids* **1995**, *184*, 98.
(258) Jouart, J. P.; Bouffard, M.; Klein, G.; Mary, G. *J. Lumin.* **1994**, *60/61*, 93.
(259) Bielejec, E.; Kisel, E.; Silversmith, A. *J. Lumin.* **1997**, *72/74*, 62.
(260) Liu, G. K.; Chen, Y. H.; Beitz, J. V. *J. Lumin.* **1999**, *81*, 7.
(261) Gamelin, D. R.; Wermuth, M.; Güdel, H. U. *J. Lumin.* **1994**, *83/84*, 405.
(262) Hubert, S.; Meichenin, D.; Zhou, B.; Auzel, F. *J. Lumin.* **1991**, *50*, 7.
(263) Guy, S.; Joubert, M. F.; Jacquier, B. *J. Lumin.* **1997**, *72/74*, 65.
(264) Case, W. E.; Koch M. E.; Kueny, A. W. *J. Lumin.* **1990**, *45*, 351.
(265) Goldner, P.; Fesquet, M.; Auzel, F. *J. Opt. Soc. Am.* **1998**, *B15*, 2688.
(266) Kük, S.; Diening, A.; Heumann, E.; Mix, E.; Sandrock, T.; Sebald, K.; Huber, G. *J. Alloys Compd.* **2000**, *300/301*, 65.
(267) Osiak, E.; Sokolska, I; Kük, S. *J. Lumin.* **2001**, *94/95*, 289.
(268) Pelletier-Allard, N.; Pelletier, R. *J. Lumin.* **1991**, *48/49*, 867.
(269) Deren, P. J.; Krupa, J. C.; Strek, W. *J. Alloys Compd.* **2000**, *300/301*, 18.
(270) Koch, M. E.; Kueny, A. W.; Case, W. E. *Appl. Phys. Lett.* **1990**, *56*, 1083.
(271) Chen, Y. H.; Auzel, F. *Electron. Lett.* **1994**, *30*, 1602.
(272) Scheps, R. *IEEE* **1994**, *QE30*, 2914.
(273) Scheps, R. *IEEE* **1995**, *QE31*, 309.
(274) Sandrock, T.; Scheife, H.; Heuman, E.; Huber, G. *Opt. Lett.* **1997**, *22*, 808.
(275) McGonigle, A. J. S.; Girard, S.; Coutts, D. W.; Moncorgé, R. *Electron. Lett.* **1999**, *35*, 1640.
(276) Nicolas, S.; Descroix, E.; Guyot, Y.; Joubert, M.-F.; Abdulsabirov, R. Yu.; Korableva, S. L.; Naumov, A. K.; and Semashko, V. V. *Opt. Mater.* **2001**, *16*, 233.
(277) Tverjanovich, A.; Grioriev, Y. G.; Degtyarev, S. V.; Kurochkin, A. V.; Man'shina, A. A.; Tver'yanovich, Yu. S. *J. Non-Cryst. Solids* **2001**, *286*, 89.
(278) Hehlen, M. P.; Güdel, H. U.; Shu, Q.; Rai, S.; Rand, S. C. *Phys. Rev. Lett.* **1994**, *73*, 1103.
(279) Heber, J. *Z. Phys. B: Condens. Matter* **1987**, *68*, 115.
(280) Heber, J. *J. Alloys Compd.* **2000**, *300/301*, 32.
(281) Bonifacio, R.; Lugiato, L. A. In *Dissipative Systems in Quatum Optics*; Bonifacio, R., Ed.; Springer-Verlag: Berlin, 1982; p 2.
(282) Auzel, F.; Hubert S.; Meichenin, D. *Europhys. Lett.* **1988**, *7*, 459.
(283) Auzel, F. Document de Travail PCM.171, *Utilisation du transfert d'energie entre ions de terres-rares pour leur application eventuelles aux compteurs quantiques; addition de deux et trois photons*; CNET, Issy-les −Moulineaux (France), 1967; unpublished.
(284) Hehlen, M. P.; Güdel, H. U.; Shu, Q.; Rand, S. C. *J. Chem. Phys.* **1996**, *104*, 1232.
(285) Gamelin, *J. Chem. Phys.* **2000**, *B104*, 11045.
(286) Auzel, F. *J. Lumin.* **2001**, *93*, 129.
(287) Bednarkiewicz, A.; Strek, W. *J. Phys D. Appl. Phys.* **2002**, *35*, 2503.
(288) Zijlmans, H. J. M. A. A.; Bonnet, J.; Burton, J.; Kardos, K.; Vail, T.; Niedbala, R. S.; Tanke, H. J. *Anal. Biochem.* **1999**, *267*, 30.
(289) Heer, S.; Lehman, O.; Haase, M.; Güdel, H. U. *Angew. Chem., Int. Ed.* **2003**, *42*, 3179.

CR020357G